Structural and Functional Changes in the Cerebellum in Sporadic Ataxias

Dissertation
zur Erlangung des Doktorgrades (PhD)
der Medizinischen Fakultät
der Rheinischen Friedrich-Wilhelms-Universität
Bonn

Xueyan Jiang
aus JIANGSU, CHINA
2021

Angefertigt mit der Genehmigung
der Medizinischen Fakultät der Universität Bonn

1. Gutachter: Prof. Dr. Lukas Scheef
2. Gutachter: Prof. Dr. Thomas Klockgether

Tag der Mündlichen Prüfung: 22.01.2021

Aus der Klinik für Neurologie
Direktor: Prof. Dr. Thomas Klockgether

Table of Contents

List of abbreviations

ALFF	Amplitude of Low-Frequency Fluctuation
ANCOVA	Analysis of Covariance
ANOVA	Analysis of Variance
ASL	Arterial Spin Labelling
AUC	Area under curve
BOLD	Blood oxygen level-dependent
ccFC	cerebellar-cerebral Functional Connectivity
CBF	Cerebral Blood Flow
CSF	Cerebrospinal Fluid
DARTEL	Diffeomorphic Anatomical Registration using Exponentiated Lie Algebra
DTI	Diffusion Tensor Imaging
DWI	Diffusion-weighted Imaging
DZNE	Deutsches Zentrum für Neurodegenerative Erkrankungen (German Center for Neurodegenerative Diseases)
FA	Fractional Anisotropy
FC	Functional Connectivity
FD	Framewise Displacement
fMRI	functional Magnetic Resonance Imaging
FWE	Family-Wise Error
FWHM	Full Width at Half Maximum
GM	Gray Matter
HC	Healthy control
ICV	Intracranial Volume
ILOCA	Idiopathic Late-Onset Cerebellar Ataxia

INAS	Inventory of Non-Ataxia Signs
MPRAGE	Magnetization-Prepared Rapid Gradient Echo
MRI	Magnetic Resonance Imaging
MSA-C	Cerebellar Variant of Multiple System Atrophy
MSA-P	Parkinsonian type of Multiple System Atrophy
ROC	Receiver Operating Characteristic
ROI	Region of Interest
rs-fMRI	resting-state functional Magnetic Resonance Imaging
SAOA	Sporadic Adult Onset Ataxia of Unknown Etiology
SARA	Scale for the Assessment and Rating of Ataxia
SCA7	Spinocerebellar Ataxia type 7
SnPM	Statistical non-Parametric Mapping
SPORTAX-NHS	Sporadic Degenerative Ataxia with Adult Onset: Natural History Study
SUIT	Spatially Unbiased Infratentorial Template
UMSARS	Unified Multiple System Atrophy Rating Scale
VBM	Voxel-Based Morphometry
WM	White matter

1. Introduction

Ataxia literally means ‘absence of order’ and denotes clinical syndromes that are characterized by a lack of motor coordination (Harding, 1983; Klockgether, 2010). For most patients with ataxia, loss of control over voluntary body movements is the initial main symptom, manifesting for instance as unstable gait, impaired stance, dysarthric disturbances of motor-speech execution, dysmetria (i.e. missing of targeted objects owing to over- or undershooting movements), oculomotor abnormalities (e.g. nystagmus, or over- or undershooting saccades), or tremor (Ashizawa & Xia, 2016). The individual symptomatology can vary, depending on the location of the underlying pathological changes within the neuroanatomical circuitries that are normally implicated in the respective forms of fine-motor control.

Ataxia is not a single disease but rather can reflect a heterogeneous group of etiologies, the precise number of which is unknown, but at least 50 different subtypes have been classified to date (Klockgether, 2010). According to current etiology-based classifications they can be subdivided into three major groups (Lin *et al*, 2016): (1) acquired ataxias, due to a wide variety of potential causes, such as chronic alcohol abuse and other toxins, viral infections, or tumors (Brusse *et al*, 2007; Fogel & Perlman, 2006); (2) hereditary ataxias, which show early onset and familial clustering as typical features, and whose underlying mutational mechanisms are increasingly identified by genetic and biochemical tests (Fogel & Perlman, 2006; Klockgether, 2008; Schols *et al*, 2004); and (3) sporadic degenerative ataxias, in where neither specific nor genetic causes can be identified and which will represent the main topic of the present thesis.

There are different forms of sporadic degenerative ataxias, which can be linked with neurodegeneration in overlapping brain regions, and this can result in substantial symptomatic overlap on the clinical level, especially in early disease stages. Here, differential diagnosis often remains a clinical challenge. This is especially true for two major forms of sporadic degenerative ataxia that are both characterized by prominent patterns of cerebellar neurodegeneration. The cerebellar variant of multiple system atrophy (MSA-C) is a pathologically and clinically well-defined entity (Quinn, 1989), but in the early course of the disease, when the full clinical symptomatology and brain atrophy patterns have not evolved completely, MSA-C may be mistakenly diagnosed initially as

sporadic adult onset ataxia of unknown etiology (SAOA) initially (Klockgether, 2010). In fact, the certainty of an SAOA diagnosis increases with disease duration, since clinical progression is faster and more severe in MSA-C than in other variants (Abele *et al*, 2002; Giordano *et al*, 2017).

Therefore, it is of interest to study early neuroimaging features that may help to better understand the commonalities and differential features of MSA-C and SAOA. To date, the neuroimaging literature on SAOA, including direct comparisons with MSA-C populations, is rather limited, making conclusions about potential SAOA-specific alterations in brain structure and/or function difficult. Moreover, many studies cannot rule out the possibility that their SAOA samples also contained unidentified MSA-C patients, i.e. that they actually examined “mixed” MSA-C/SAOA samples. Accordingly, it is of special interest to look for specific neuroimaging features, e.g. structural MRI changes in specific cerebellar subregions, or altered organization of cerebellar functional connectivity, in SAOA patients where prolonged disease duration makes future conversion to MSA-C unlikely.

This thesis is organized into four main sections, as follows. The first introductory section provides a general orientation about the main issues discussed and the overall aims of the thesis. The second section includes a short description of the ‘Sporadic Degenerative Ataxia with Adult Onset: Natural History Study (SPORTAX-NHS)’ project and all data used in the following studies. The third section reviews four different studies that form the basis of this dissertation. Among the four studies, the results of the first two studies relating to the SAOA group were recently published (Jiang *et al*, 2019), and parts of the first study are also contained in another recently published paper (Faber *et al*, 2020). Papers about the last two studies reported here are in preparation. In the final section, the main study findings are integrated, and possible research directions for future studies are suggested.

1.1 Sporadic degenerative ataxias

In contrast to acquired or hereditary forms of ataxia, a genetic or acquired cause of ataxia cannot be identified in sporadic degenerative ataxia patients (Klockgether, 2010). Sporadic ataxias can be subdivided into two major types, multiple system atrophy (which can be further subdivided into MSA-P with predominant Parkinsonian features and MSA-C with predominant cerebellar features) and SAOA. For the present studies, MSA-C and

SAOA diagnoses are of primary interest, owing to their overlapping clinical and neuroimaging features, and will be characterized further.

Diagnosis

Patients with MSA-C or SAOA exhibit common cerebellar features of motor presentation, comprising unstable gait and stance. Most patients with sporadic ataxias have slurred speech and problems with swallowing, trouble with decomposition of movement in the upper extremities, dysmetria, dysdiadochokinesis and action tremor (Abele *et al*, 2007; Ciolli *et al*, 2014; Klockgether, 2018; Krismer & Wenning, 2017). In particular, patients with MSA-C exhibit severe autonomic failure, which may be manifested in erectile dysfunction and urinary problems, such as incontinence and urinary retention (Ito *et al*, 2006; Jecmenica-Lukic *et al*, 2012; Kirchhof *et al*, 2003; Watanabe *et al*, 2002), whereas clinical examinations of patients with SAOA reveal no or only milder symptoms of autonomic dysfunction.

Frequent musculoskeletal pain (Tison *et al*, 1996), sleep behavior dysfunction (Gilman *et al*, 2008; Iranzo *et al*, 2005; Krismer & Wenning, 2017; Wenning *et al*, 2004a), cognitive impairment (e.g. executive functions and verbal learning (Balas *et al*, 2010; Burk *et al*, 2006; Chang *et al*, 2009; Kawai *et al*, 2008; Kitayama *et al*, 2009; Koga *et al*, 2017; Siri *et al*, 2013)), and psychiatric syndromes (e.g. depression (Siri *et al.*, 2013) and anxiety (Balas *et al.*, 2010)) appear frequently only in MSA-C patients.

Diagnosis of MSA-C is based on an expert consensus of diagnostic criteria, which specify three different levels of increasing diagnostic certainty, namely definite, probable and possible MSA-C (Gilman *et al.*, 2008). Definite MSA-C requires an autopsy examination to confirm the neuropathological demonstration of CNS -synuclein–positive glial cytoplasmic inclusions with neurodegenerative changes in striatonigral or olivopontocerebellar structures. However, the clinical presentation of a progressive adult-onset (>30 years) disease that is characterized by the presence of both autonomic failure and a cerebellar ataxia syndrome (see Table 1 for more detailed symptom descriptions) is thought to be sufficiently predictive for a probable MSA-C diagnosis. Meanwhile, patients will only receive an uncertain diagnosis of possible MSA-C if their cerebellar syndrome (and additional optional features of MSA-C) are combined with symptoms of autonomic dysfunction whose clinical severity does not yet qualify as autonomic failure.

Criteria for probable MSA-C:

- A cerebellar syndrome (gait ataxia with cerebellar dysarthria, limb ataxia, or cerebellar oculomotor dysfunction)

- Autonomic failure involving urinary incontinence (inability to control the release of urine from the bladder, with erectile dysfunction in males) or an orthostatic decrease of blood pressure within 3 min of standing by at least 30 mm Hg systolic or 15 mm Hg diastolic

Criteria for possible MSA-C (assigned as SAOA):

- A cerebellar syndrome (gait ataxia with cerebellar dysarthria, limb ataxia, or cerebellar oculomotor dysfunction)

- At least one feature suggesting autonomic dysfunction (otherwise unexplained urinary urgency, frequency or incomplete bladder emptying, erectile dysfunction in males, or significant orthostatic blood pressure decline that does not meet the level required in probable MSA)

- At least one of the additional features shown:
    - Babinski sign with hyperreflexia
    - Stridor
    - Parkinsonism (bradykinesia and rigidity)
    - Atrophy of putamen, middle cerebellar peduncle, or pons visible (MRI)
    - Hypometabolism of putamen (FDG-PET)
    - Presynaptic nigrostriatal dopaminergic denervation (SPECT or PET)

Criteria for probable MSA-C and possible MSA-C. Adapted from (Gilman *et al.*, 2008). *FDG, [^{18}F] fluorodeoxyglucose: PET, positron emission tomography; SPECT, single photon emission computed tomography.*

In contrast to MSA-C, no neuropathological features have been identified to date that could prove a definite diagnosis of SAOA. Indeed, it remains unclear whether SAOA describes a distinct disease entity or a collection of similar diseases (Klockgether, 2010). There are also alternative classification terms in the neurological literature that are used to refer to similar patient groups, e.g. idiopathic late-onset cerebellar ataxia (ILOCA (Harding, 1981)), idiopathic cerebellar ataxia (either as a purely cerebellar form (IDCA-C)

or with additional extra-cerebellar features (IDCA-P (Burk *et al*, 2004)), or cortical cerebellar atrophy (CCA (Fukui *et al*, 2016)). For the clinical diagnosis of SAOA, the following diagnostic criteria have been proposed (Klockgether, 2018): (1) progressive ataxia; (2) adult disease onset (while earlier studies suggested >20 years (Abele *et al.*, 2002), recent studies (Giordano *et al.*, 2017) adopt a more conservative threshold of age > 40 years); (3) no acute or subacute disease onset; (4) informative and negative family history; (5) no evidence of a causative gene mutation; (6) no established acquired cause; and (7) lack of severe autonomic failure.

Therefore, the presence of severe autonomic failure is a key clinical feature for distinguishing MSA-C from SAOA. In fact, some studies assign patients with possible MSA-C (i.e. symptoms of autonomic dysfunction, but not failure) to the SAOA group (Giordano *et al.*, 2017). Differential diagnosis is complicated by the fact that autonomic failure in MSA-C patients can evolve after the onset of ataxia symptoms (Gilman *et al.*, 2008). Thus, a patient with an initial diagnosis of SAOA may later turn out to have MSA-C. Previous studies observed this conversion in about 30% of patients (Abele *et al.*, 2002; Gilman *et al.*, 2008), although they become unlikely after disease durations of 10 years or longer (Giordano *et al.*, 2017). Accordingly, the certainty of an SAOA diagnosis improves with disease duration (Giordano *et al.*, 2017; Klockgether, 2010, 2012, 2018).

In general, MSA-C and SAOA cannot easily be distinguished by their usual age at onset, since both forms of ataxia frequently present in the mid-50s (Lin *et al.*, 2016), although it must be noted that the reported typical age at onset for SAOA patients varies across studies, a recent example finding a substantially earlier mean onset at 41.1 years (Lin *et al.*, 2016). There are also no pronounced sex differences: while MSA is generally considered to affect male and female patients similarly (Fanciulli & Wenning, 2015; Gebus *et al*, 2017), and SAOA is more frequently found in male patients (Gebus *et al.*, 2017; Harding, 1981; Klockgether, 2018), some recent studies report higher proportions of male patients in both MSA-C (Watanabe *et al.*, 2002) and SAOA populations (Giordano *et al.*, 2017; Lin *et al.*, 2016). Meanwhile, there are obvious differences in clinical progression, as demonstrated by a recent natural history cohort study (Giordano *et al.*, 2017), in which MSA-C patients showed a much steeper increase of ataxia symptom severity than SAOA patients. In fact, the disease severity of SAOA patients was milder, despite a substantially

longer disease duration. The mean survival for patients with MSA-C is only about 6 to 10 years (Fanciulli & Wenning, 2015; Klockgether, 2010; Lin *et al.*, 2016; Roncevic *et al*, 2014; Wenning *et al*, 1994), whereas the life span is not affected in SAOA (Klockgether, 2010, 2012; Klockgether *et al*, 1990).

Epidemiology

There are a few descriptive epidemiological data on MSA-C and SAOA. Descriptive epidemiology shows an estimated prevalence of 1.9-4.9 cases per 100,000 (Fanciulli & Wenning, 2015; Kollensperger *et al*, 2010; Watanabe *et al.*, 2002; Wenning *et al.*, 2004a) for MSA in general; with MSA-P predominating over MSA-C in a ratio of 2:1 to 4:1 in most populations, except for Japan, where the pattern is reversed (Tsuji *et al*, 2008). The estimated SAOA prevalence was 2.2-8.4 cases per 100,000 in European cohorts (Klockgether, 2018; Leone *et al*, 1995; Muzaimi *et al*, 2004; Polo *et al*, 1991).

Neuroimaging studies

The number of in vivo biomarkers evaluated so far to distinguish between different forms of sporadic degenerative ataxias is limited, and neuroimaging, particularly MR imaging, could play a central role. While there is a more extensive literature examining MSA (or MSA-C) specifically (for a recent review, see (Chelban *et al*, 2019)), a limited number of studies compared brain MR imaging in MSA-C or SAOA directly (Burk *et al.*, 2004; Carre *et al*, 2020; Faber *et al.*, 2020; Fukui *et al.*, 2016), but some had small patient sizes and yielded conflicting results. Although various methodologies were applied with multiple analytical approaches, it is still unknown whether there are patterns of neuroimaging abnormalities that are specific for MSA-C or SAOA, respectively, and whether there are anatomical regions that are most appropriate as reliable biomarkers for distinguishing between them.

Structural MRI

MRI is the most common method for investigating the structural changes in sporadic ataxias. Qualitative visual reading of conventional clinical MR sequences (e.g. T2-weighted/ proton density-weighted images) shows a variety of signal abnormalities that are suggested to carry diagnostic information for the presence of MSA, for example middle cerebellar peduncle hyperintensity, putaminal hypointensity, hyperintense putaminal rim,

and, especially, the ‘hot cross bun’ sign, a radiological finding describing a cruciform hyperintensity signal on axial images through the pons visible in T2-weighted and proton density-weighted MRI (Carre *et al.*, 2020; Lin *et al.*, 2016). However, some authors claim that (a) these qualitative findings are not disease-specific and may only emerge after clinical symptom onset (thus reducing their value for early diagnosis), and (b), considering the differential diagnosis between MSA-C and SAOA, available data are limited, as many early studies did not explicitly distinguish between MSA-P and MSA-C, or focus on comparison with Parkinsonian syndromes (Lin *et al.*, 2016); see also: (Chelban *et al.*, 2019). An earlier study considered that, among other features, the presence of middle cerebellar peduncle hyperintensity and the ‘hot cross bun’ sign can help to differentiate between SAOA (here: IDCA-P, idiopathic cerebellar ataxia with extra-cerebellar features) and MSA-C patients (Burk *et al*, 2005); see also: (Fukui *et al.*, 2016). This was confirmed by a recent study (Carre *et al.*, 2020).

Beyond signal abnormalities, the main focus is the diagnostic specificity of regional atrophic changes, especially in the brainstem (pons) and middle cerebellar peduncles, which are currently included as diagnostic criteria in the ‘possible MSA’ criteria (Gilman *et al.*, 2008). Based on semi-automated volumetric analyses, brainstem atrophy was reported in both MSA-C and SAOA patients, although these changes were more pronounced in MSA-C (Burk *et al.*, 2005; Burk *et al.*, 2004). This finding converges with automated voxel-based morphometry (VBM) studies that observed white matter (WM) reductions in the middle cerebellar peduncles and brainstem, both in MSA-C (Minnerop *et al*, 2007) and (at least in an outer pontine rim) in SAOA patients (Abele *et al.*, 2007). Further support was provided by Faber et al.(Faber *et al.*, 2020), whose VBM analysis showed significant WM volume reductions in the brainstem of MSA-C, but not SAOA patients, compared with healthy controls, but no significant differences between the patient groups. Moreover, a higher frequency of atrophic changes in the brainstem and middle cerebellar peduncles in MSA-C than in SAOA patients was confirmed by Carre et al. (Carre *et al.*, 2020), although they also admitted that these radiological features may not be optimal for early MSA-C diagnosis.

Of central relevance for the present studies are radiological findings of cerebellar cortical atrophy, which are regularly observed in both MSA-C, e.g. (Dash *et al*, 2019; Minnerop *et*

al., 2007; Yang *et al*, 2019) and SAOA, e.g. (Abele *et al.*, 2007). While some studies that directly compared the two patient groups suggested more pronounced atrophic changes in MSA-C patients, this trend was not significant in direct statistical comparisons (Burk *et al.*, 2005; Burk *et al.*, 2004).

Several of the abovementioned studies used VBM (Ashburner & Friston, 2000) to measure structural brain changes, e.g. (Abele *et al.*, 2007; Minnerop *et al.*, 2007). These measures have practical advantages over traditional manual or semi-automated segmentation methods, including reduced workload (thanks to the automated tissue segmentation process), and the possibility of assessing potential local differences in an unbiased, hypothesis-free manner, since statistical analyses are conducted on a voxel-by-voxel level, without the need to outline predefined anatomical structures. Therefore, VBM may also detect change patterns in subregions of broader anatomical structures. Meanwhile, the quality of VBM data depends on the quality of the brain templates used during VBM data preprocessing. The default brain templates were primarily developed for the analysis of cerebral differences, with no specific focus on the cerebellum. The organization of the cerebellum, with tightly folded gray matter (GM) layers of cerebellar cortex, and only thin layers of WM between them, makes automated data segmentation and normalization (i.e. voxel-by-voxel mapping to a common anatomical standard space) more difficult. This may reduce the spatial fidelity of voxel mappings from subject to subject, and, because of the increased error, reduce the chance of detecting existing differences in small brain areas. To overcome these limitations, Diedrichsen (Diedrichsen, 2006) developed a specific high-resolution brain atlas for the cerebellum and brainstem (SUIT – *Spatially Unbiased Infratentorial Template*). Yang et al. (Yang *et al.*, 2019) used this improved template to examine GM volume differences between MSA patients and healthy controls, observing spatially distinct patterns of GM volume reductions in MSA-P and MSA-C patients. Specifically, MSA-C cases showed significantly lower GM volume than healthy controls in bilateral lobules IV-V, VIII, IX, and crus I/II, and, for a region in the right cerebellar crus, this atrophy was also significantly different from MSA-P patients. Crucially, the study did not examine SAOA patients, leaving open the question whether the use of SUIT also provides a more specific topography of cerebellar GM alterations in this patient group.

Diffusion MRI

Diffusion-weighted Imaging (DWI) is an advanced MRI technique that helps to characterize brain tissue microstructure by quantifying the diffusion properties of tissue water (Conturo *et al*, 1999), and the anisotropy of water diffusion on the voxel level, Diffusion tensor imaging (DTI) (Le Bihan *et al*, 2001) can be used to make additional inferences about the integrity and preferred direction of the large WM fiber bundles in specific brain regions. Previous DWI studies have reported abnormal diffusion parameters in the cerebellum and brainstem of patients with MSA-C (Blain *et al*, 2006; Dash *et al.*, 2019; Jao *et al*, 2019; Nicoletti *et al*, 2013; Shiga *et al*, 2005; Wang *et al*, 2011; Zanigni *et al*, 2017) or SAOA (Della Nave *et al*, 2004). Direct DTI comparisons between MSA-C and SAOA (CCA, cortical cerebellar atrophy) patients were firstly performed by Fukui and colleagues (Fukui *et al.*, 2016), who observed reduced fractional anisotropy (FA) values of the olivocerebellar and pontocerebellar tracts in MSA-C patients when compared with SAOA patients, and receiver operator characteristic curve analysis showed the FA values of the olivocerebellar tract to have good discrimination in distinguishing MSA-C from SAOA. Recently, widespread WM reduction in MSA-C but not in SAOA were also confirmed by Faber and colleagues (Faber *et al.*, 2020).

Functional MRI

Functional MRI (fMRI) is a class of imaging techniques used to measure brain activity or brain activity fluctuations. While arterial spin labelling (ASL) fMRI sequences can be used to quantify regional cerebral blood flow (CBF, e.g. (Liu & Brown, 2007)), most fMRI applications use MRI sequences that are sensitive to the blood oxygen level-dependent (BOLD) contrast (Ogawa *et al*, 1990), i.e. they measure MRI signal changes that depend on brain activity-induced changes in the local concentration of oxygen-rich blood.

While BOLD fMRI methods were originally used to measure brain activity changes that are induced by task stimulation (e.g. (Amaro & Barker, 2006)), more recently developed resting-state fMRI (rs-fMRI) techniques (Fox & Raichle, 2007; Raichle *et al*, 2001) make use of the fact that brain areas show spontaneous fluctuations of their brain activity level (and, therefore, variations of the measured BOLD signal) over time, even during ‘rest’, i.e. without engaging in tasks. Based on the observation that the fluctuation patterns of different brain areas show temporal correlations, which suggests functional connectivity

(FC) between these brain regions, rs-fMRI can be used to make inferences about the functional brain networks that specific brain structures are involved in or the degradation of these functional brain networks in psychiatric and neurological disease (e.g. (Hohenfeld *et al*, 2018)). There is a broad variety of rs-fMRI metrics that measure different characteristics, ranging from local measures such as amplitude of low-frequency fluctuation (ALFF), which measures the strength of spontaneous BOLD fluctuations on the voxel level (Zang *et al*, 2007), to graph-theoretical network measures of whole-brain connectivity (Sporns, 2013).

As far as is known, task fMRI data are not available, either for MSA-C patients or for SAOA patients. Only a few papers have been published reporting resting-state FC data in MSA-C patients. There is initial evidence that MSA patients show reduced FC in the default mode network (Rosskopf *et al*, 2018; You *et al*, 2011), which is linked with introspective awareness and task-independent thought (Raichle *et al.*, 2001) (Buckner *et al*, 2008). By contrast, there is also evidence for increased connectivity within the sensorimotor circuit (You *et al.*, 2011) and the ponto-cerebellar circuit (Rosskopf *et al.*, 2018). In addition, some studies in MSA-C patients observed functional impairments in cerebellar regions, which were linked to reduced intra-cerebellar and cerebellar-cerebral connectivity (Ren *et al*, 2018; Zheng *et al*, 2019). At the same time, no study has been published to date that examined FC changes in SAOA using rs-fMRI. Hence, the preliminary results in MSA-C patients require further replication, and there is a lack of research comparing MSA-C and SAOA, leaving substantial room for further research.

Conclusions

Compared with MSA-C, the neuroimaging literature on SAOA is generally limited, and there are few studies directly comparing these patient groups. While there is preliminary evidence that DWI of the brainstem provides relevant information for differential diagnosis, the potential of improved VBM routines and rs-fMRI methods in SAOA remains unclear. In general, the reliability of quantitative analyses in revealing dissimilarities between MSA-C and SAOA could be limited for studies that include SAOA patients with relatively short disease duration, since at least some of these cases may develop MSA-C later (Burk *et al.*, 2004; Faber *et al.*, 2020).

1.2 Objectives

In the first years after ataxia onset, a reliable distinction between MSA-C and SAOA is often not possible. With increasing disease duration, some SAOA patients may convert to MSA-C, and it is unknown at what time after onset of ataxia this conversion happens, and which factors could predict this development. Currently, there are only a few studies with considerable patient size comparing the phenotype of MSA-C and SAOA. Disease-specific structural change patterns that distinguish MSA-C from SAOA patients remain unknown, and systematical evaluations focusing on the functional differences between MSA-C vs. SAOA, as measured by rs-fMRI, are completely lacking. In particular, characterizations on those SAOA patients with a low risk to convert to MSA-C as a result of a long disease duration (>10 years) have not yet been investigated.

In this thesis, the cerebellum was chosen as the main region of interest because of its intense involvement in both forms of sporadic ataxias. A high-resolution cerebellar template, as provided by the software package SUIT (Diedrichsen, 2006), was applied to establish a more accurate delineation of the disease-related atrophy pattern. It is noteworthy that only SAOA patient with a disease duration longer than 10 years were included in the thesis studies. These patients were classified as $SAOA_{>10y}$, following Giordano and colleagues (Giordano *et al.*, 2017), who suggested that the conversion from SAOA to MSA-C becomes very unlikely after this extended disease duration. Therefore, in this thesis, the objective was to identify the essential differences between MSA-C and SAOA by comparing MSA-C with $SAOA_{>10y}$.

The overall target of this dissertation was to characterize local cerebellar neurodegeneration and global network organization in two sporadic ataxia groups based on structural and functional models. To examine these research questions, four associated studies were conducted based on high-resolution T1- weighted MRI as well as resting-state fMRI data sets from MSA-C and $SAOA_{>10y}$ patient groups. **Study 1** examined the structural changes of the cerebellum in both MSA-C and $SAOA_{>10y}$, ataxia groups, while **Study 2** explored how the local atrophy patterns detected in Study 1 impact the intra-cerebellar functional connectivity in these patients. Beyond these local cerebellar features, the network level functional communication within the cerebellum was assessed

in **Study 3.** In **Study 4**, the communication between cerebellar and cerebral circuits was explored in the healthy group and in the two ataxia groups.

2. Materials and methods

The patient data presented in this thesis are taken from a study named 'Sporadic Degenerative Ataxia with Adult Onset: Natural History Study (SPORTAX-NHS)'. This project is a multi-center project including Bonn, Magdeburg and Rostock, enrolling patients with sporadic degenerative ataxia of adult onset in European countries. In this thesis, we analyzed data from Bonn and Magdeburg only, owing to the limited number of patients and quality issues in the Rostock datasets. The key goals were to compare the phenotype of MSA-C vs. SAOA.

The data of the control group were taken from the DZNE Longitudinal Cognitive Impairment and Dementia (DELCODE) study (Jessen *et al*, 2018), an ongoing multicenter study with a special focus on subjective cognitive decline (SCD) in the context of Alzheimer dementia which also collects data from healthy individuals. Because the centers involved in SPORTAX-NHS were also participating in the DELCODE project and both studies used the same harmonized MR protocol, the data collected from the healthy control population in DELCODE could be used as a healthy control group (HC) for this project.

Both study protocols were approved by the institutional review boards of all participating sites. All investigations were performed in accordance with the relevant guidelines and regulations. All participants provided written informed consent in accordance with the Declaration of Helsinki.

2.1 Participants

Patient groups

Initially, 46 SAOA patients and 16 MSA-C patients were included in this study. For technical reasons, 9 participants had to be excluded and the exclusion due to 4 incomplete MRI data sets, 3 incomplete clinical characterizations and 3 insufficient data quality, i.e., motion artifacts (movement by the patient during image acquisition). As described below in detail, the SAOA group was additionally divided into two subgroups: 13 $SAOA_{>10y}$, and 23 SAOA-mixed patients (defined by SAOA patients with disease duration of less than 10yrs who had the potential to convert to the MSA-C type). The final sample consisted of 13 SAOA patients and 16 MSA-C patients.

The main inclusion criteria were:

1) progressive ataxia

2) disease onset after the age of 40 years

3) informative and negative family history

4) no established acquired cause of ataxia.

All participants were genetically screened to exclude the most common spinocerebellar ataxias (SCA1, 2, 3 and 6) or Friedreich's Ataxia. In addition, FMR1 pre-mutation was tested to exclude fragile X-associated tremor/ataxia syndrome (FXTAS) if the clinical phenotype was suspicious, and when the MRI showed the signal abnormality of the middle cerebellar peduncles.

Participants were classified as MSA-C if they fulfilled the criteria for clinically probable MSA-C according to the criteria summarized in Table 1. Participants were classified as SAOA if they fulfilled the criteria of clinically possible MSA-C. Within the SAOA group, a subgroup named $SAOA_{>10y}$ was created to denote patients whose symptoms lasted for more than 10 years. This approach was taken because it was recently shown that, after this time, a 'conversion' into MSA-C is very unlikely (Giordano *et al.*, 2017).

The primary clinical assessment of the SAOA/MSA-C patients was based on the Scale for the Assessment and Rating of Ataxia (SARA). The SARA score comprises eight items, including tests of gait, stance, sitting and speech, as well as the finger-chase test, finger-nose test, fast alternating movements and heel-shin test (Schmitz-Hubsch *et al*, 2006). The scores range from 0 to 40, higher scores indicating more serious impairment. The SPORTAX assessment protocol additionally includes the Unified Multiple System Atrophy Rating Scale (UMSARS) (Wenning *et al*, 2004b) and the Inventory of Non-Ataxia Signs (INAS) (Jacobi *et al*, 2013).

Control group

In addition, 51 age and gender matched controls (HC) were taken from the healthy population of the DELCODE project. From this cohort, one HC had to be excluded because of incomplete MR data, and one data set had to be dismissed owing to severe head motions. Thus, 49 HC were finally included.

Detailed inclusion and exclusion criteria and group definitions for the participants of the DELCODE study can be found elsewhere (Jessen et al., 2018). Within DELCODE the HC participants were recruited by local newspaper advertisements seeking for healthy people without relevant cognitive problems. The main exclusion criteria were: major psychiatric disorders, a current major depressive episode, a neurodegenerative disorder, a history of stroke with residual clinical symptoms, history of malignant disease or a severe or unstable medical condition. The control group had to achieve unimpaired cognitive performance, which was accessed using the neuropsychological CERAD test battery. A test performance better than 1.5 standard deviations (SD) below the age-, sex-, and education-adjusted normal performance on all subtests of the CERAD was considered as 'cognitive normal'.

2.2 MRI acquisition

All sites were equipped with 3T Tim Trio MR systems (Siemens Medical Systems, Erlangen, Germany) running the identical software release and MR-protocols. In order to eliminate several sources of variance between sites even before starting the study, the imaging methods were harmonized across the participating sites. For quality assurance and assessment, the following steps were taken. The DZNE imaging network qualified each MRI site with a traveling head measurement prior to the start of the study. DZNE iNET then provided every site with detailed standard operating procedures (SOPs) for the implementation of each protocol. All radiographers who operate MRIs in the study underwent centralized training to implement the SOPs (i.e., subjects' positioning in the MRI scanner, sequence preparation steps, image angulation, participant instruction, and testing). A small MRI-phantom built and designed by the American College of Radiology was used to monitor the performance of the MR systems every week.

Structural MRI

Isotropic high-resolution T1-weighted images were acquired using a magnetization-prepared rapid gradient echo sequence. The scan parameters were as follows: repetition time = 2500 msec, echo time = 4.37 msec, inversion time = 1100 msec, flip angle = 7˚, GRAPPA acceleration R = 2, field of view = 256 mm, acquisition matrix = 256 × 256, 176 sagittal slices, slice thickness = 1 mm).

Resting-state functional MRI (rs-fMRI)

The rs-fMRI was acquired using a standard T2*-weighted gradient echo-planar imaging sequence. The scan parameters were chosen as follows: repetition time = 2580 msec, echo time = 30 msec, flip angle = 80˚, GRAPPA acceleration R = 2, field of view = 224 mm, acquisition matrix = 64 × 64, 47 slices and slice thickness = 3.5 mm. A total of 180 volumes were acquired within one run. Subjects were instructed to lay still with their eyes closed in the scanner and not to fall asleep during resting-state scans. All lights within the MR-room were switched off during the rs-fMRI acquisition.

2.3 Data preprocessing

2.3.1 Preprocessing of structural MRI data

The structural MRI data were preprocessed and analyzed using the SUIT[1] toolbox, as outlined in Figure 1 (Diedrichsen, 2006). In a first step, the images were cropped to isolate the cerebellum. After that, they were segmented into their gray matter (GM), white matter (WM), and cerebrospinal fluid (CSF) partitions. This step was based on probabilistic tissue maps, which are a part of the SPM-toolbox. The method of partitioning brain images using tissue probabilistic maps is described in Ashburner and Friston's paper (Ashburner & Friston, 2000). The values in the tissue probability maps represent the prior probability that any voxel belongs to a particular tissue class. For each subject, a cerebellum mask was automatically generated in its individual image space. Any misclassifications of the cerebellar boundaries were than manually corrected using FSLView (Smith *et al*, 2004). This leads to a 'clean' binary cerebellar mask. By projecting this individual mask on to the individual MR-data sets, the cerebellum can be isolated for each participant. The normalization of the isolated cerebellum into the cerebellar standard template space was achieved using the diffeomorphic anatomical registration using exponentiated lie algebra (DARTEL) algorithm (Ashburner, 2007). The normalization template was contained in the SUIT toolbox.

[1] http://www.diedrichsenlab.org/imaging/suit.htm

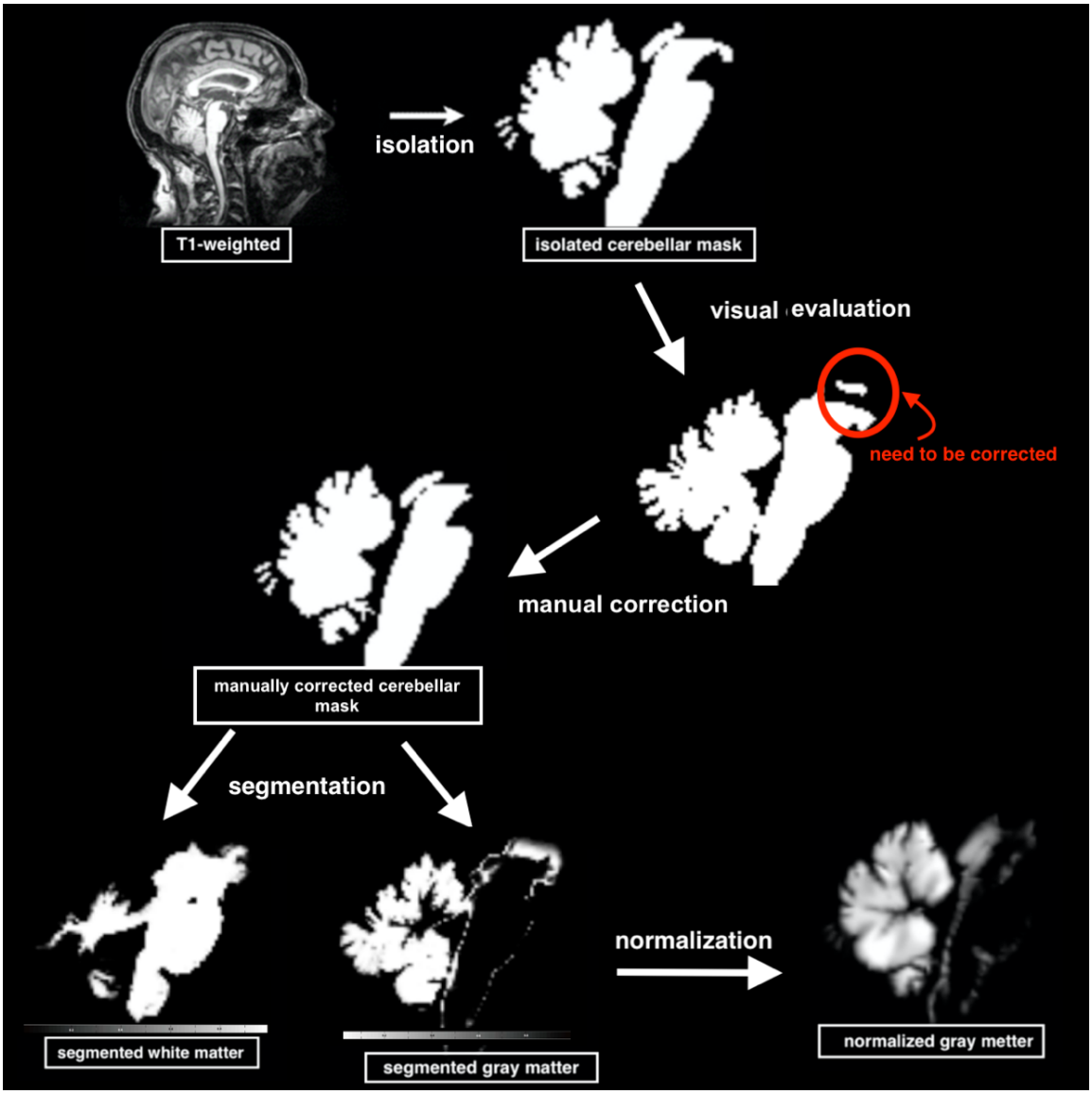

Figure 1. **Flowchart of the structural preprocessing stream**. The T1 images were cropped to isolate the cerebellum. After that, visual evaluation was needed to manually correct the cerebellar mask to exclude the misclassification. Within the corrected mask, the cerebellum was segmented into gray matter and white matter based on the tissue probability maps. The segmented gray matter was then normalized into SUIT space by the DARTEL algorithm.

2.3.2 Preprocessing of resting state fMRI data

The rs-fMRI data sets were preprocessed using the GRETNA[2] toolbox as outlined in Figure 2 (Wang *et al*, 2015) which is based on the SPM12[3] toolbox. For each subject, the first five volumes were discarded to ensure a steady-state longitudinal magnetization. The

[2] https://www.nitrc.org/projects/gretna/
[3] https://www.fil.ion.ucl.ac.uk/spm/software/spm12/

preprocessing pipeline contained slice timing correction, realignment (= head motion correction) and normalization. The derived head motion parameters of (x-, y-, z-) translations and rotations (pitch, yaw, roll) were used to access the amount of head motion during the fMRI exam. Excessive motion (criterion: frame-to-frame translation >3mm and/or frame-to-frame rotation >3° in any direction) led to the exclusion of an exam. In addition, root mean squared (RMS) value and framewise displacement (FD) were considered as data control measures. The RMS was calculated by the root mean square values of the realignment estimates and their derivatives across all time points, while the FD indexed the movement from one volume to the next volume and the sum across all timepoints (Power *et al*, 2012). Data sets were further excluded if the RMS and mean FD exceeded 0.5mm (Power *et al.*, 2012).

The normalization of the data sets into standard space was performed for the whole brain and the cerebellum separately. In order to normalize the rs-fMRI time series of the cerebellum the realigned functional images were co-registered to the cerebellar structural data set using the temporal mean image of the individual data sets. The transformation into SUIT space used the non-linear deformation derived during the normalization of the structural data. The whole-brain data were processed similarly. After slice-timing correction and realignment, the fMRI time series were co-registered to the individual structural T1 data set using the individual functional mean image across time. The structural data were normalized into the standard MNI-space realigned using a non-linear deformation algorithm (Ashburner, 2007). The derived transformation was applied to the functional data sets. During this process, the whole brain functional data sets were resampled to an isotropic resolution of 3 x 3 x 3 mm^3 for the cerebrum and 2 x 2 x 2 mm^3 for the cerebellum. The normalized data subsequently underwent linear trend removal in order to remove signal drifts on a voxel level (Tanabe *et al*, 2002). To account for the expected frequency range reflecting spontaneous neural activity, the time series were temporally bandpass-filtered (passed frequency band 0.01-0.08 Hz) (Fox *et al*, 2005). In order to reduce the effect of physiological noise components, the mean WM and mean CSF signal were regressed. Then, to remove unwanted signal components related to residual motion components, the 24 motion parameters derived above (absolute motion (6x), frame-to-frame motion (6x), and the corresponding squared parameters (2x6x) were

used to further clear the data from unspecific noise sources using a linear regression approach (Friston *et al*, 1996).

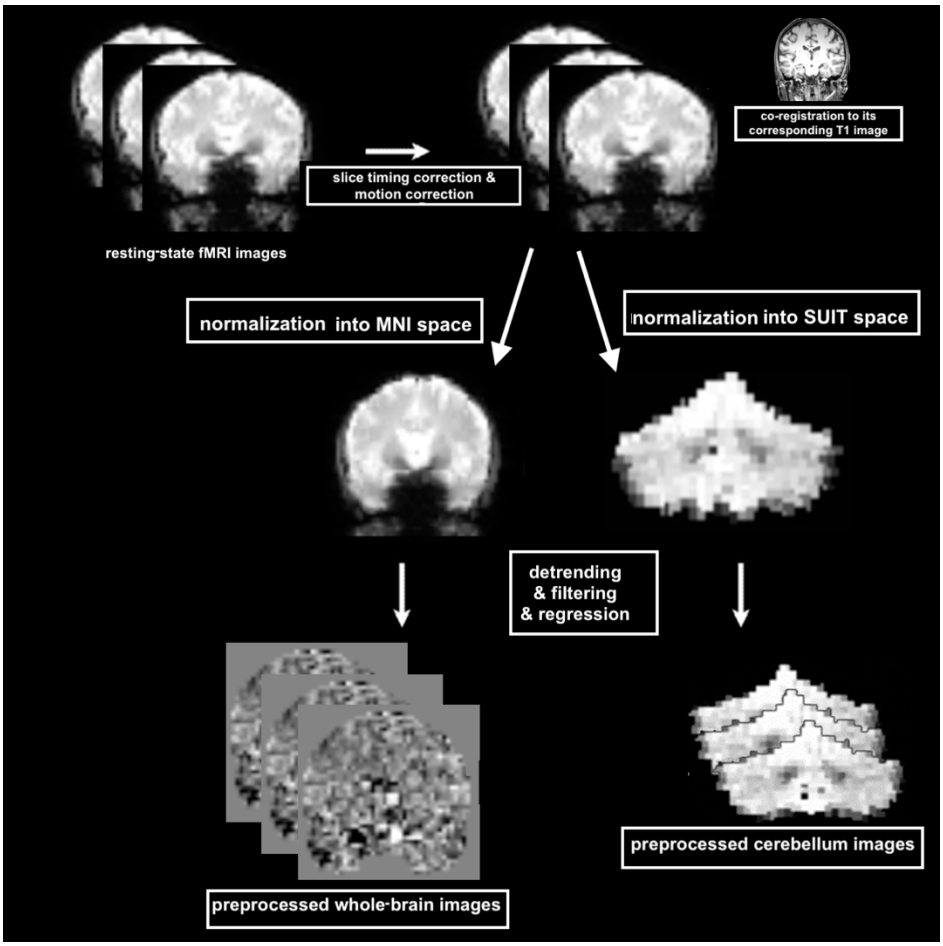

Figure 2. **Flowchart of rs-fMRI preprocessing pipeline by SPM and SUIT**. Resting state fMRI images were acquired, preprocessed to slice timing correction and motion correction. The corrected fMRI images were co-registered to corresponding T1 images. The fMRI images were normalized into MNI space for the whole brain analysis and resliced into SUIT space for cerebellar analysis as well. Then, further detrending, filtering and regression were applied on the whole-brain images and cerebellum images separately.

3. Results

3.1 Study 1: Analysis of morphological changes in the cerebellum in MSA-C and SAOA

3.1.1 Introduction

Neuroimaging studies in sporadic ataxias have observed a prominent volume loss in the cerebellum (Abele *et al.*, 2007; Baloh *et al*, 1986; Burk *et al.*, 2004). However, owing to the lack of a high-resolution human cerebellar atlas template, it has not been possible to date to establish specific spatial patterns for either MSA-C or SAOA. Hence, it is unknown if any structural pattern exists that may be related to any clinical feature. To investigate disease-related structural changes of the cerebellum in more detail, the high-resolution T1- weighted MRI data sets were analyzed within the high-resolution cerebellar standard space as defined by SUIT (Diedrichsen, 2006). The goal of this investigation was to characterize disease-related gray matter abnormalities in the cerebellum in MSA-C and $SAOA_{>10y}$ patients and to determine the relationship of local cerebellar neurodegeneration with clinical variables.

3.1.2 Study specific methods

Voxel-based morphometry analysis of the cerebellum

Voxel-based morphometry (VBM) is a fully automated method to identify group differences in brain tissue such as gray matter (GM) on a voxel level. The technique typically uses T1-weighted structural MRI scans. In this study, the individual segmented cerebellar GM maps, extracted as described in chapter 2.3.1, were spatially normalized using the DARTEL algorithm. In order to make sure the total amount of GM remained the same as the original maps, the image intensities were modulated by scaling by the amount of contraction and extension. The resulting ‘modulated’ normalized GM maps were finally smoothed with a 4 mm Gaussian smoothing kernel (full width at half maximum, FWHM = 4 mm).

Flat-mapping

As a part of the SUIT toolbox, a flat-mapping representation of the cerebellum was provided to visualize the imaging data (Diedrichsen & Zotow, 2015). The flat-map was

generated in SUIT space based on the anatomical data from 20 subjects. At first, outer and inner cerebellar surface boundaries were constructed and inflated (Figure 3). The corresponding lobules' definition on each surface was marked by the connection by pre-selected and paired reference points on each surface. Cuts (thick black line in Figure 3C) were inserted to enable the surface to flatten out. This procedure allows visualization of any of the results in one concise view.

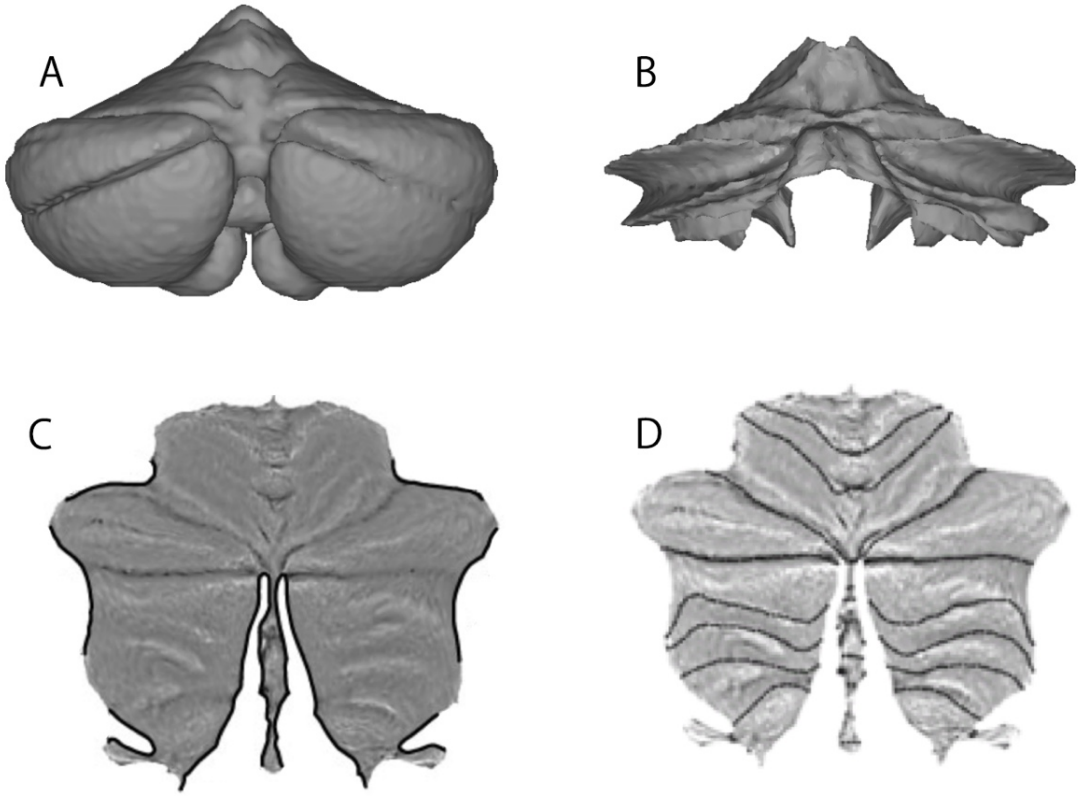

Figure 3. **Cerebellar surfaces and cerebellar flatmap representation**. A) outer (gray matter) surface construction; B) inner (white matter) surface; C) flat surface with outlined cuts (thick black line) in the horizontal fissure, the superior-posterior fissure, between the posterior vermis and VII-IX, and between the X and VIII; D) flat-map representation of cerebellum surfaces. Dotted lines indicate boundaries between lobules (Diedrichsen & Zotow, 2015).

Statistical analysis

Demographic and clinical data

Non-parametric Kruskal-Wallis one-way analysis of variance (ANOVA) was used to test for group differences in age. The χ^2 test was used to access group differences in gender and scanning site. Non-parametric Mann-Whitney U-tests were used to compare the differences in clinical variables, such as disease severity (SARA total score), disease

duration and disease onset age between the two ataxia patient groups (MSA-C group and $SAOA_{>10y}$ group). The statistical significance threshold was set to $p < 0.05$.

Structural imaging data

All imaging data were statistically analyzed using the Statistical non-Parametric Mapping toolbox (SnPM[4]).

Statistical analysis of the smoothed segmented GM images was performed with *a* non-parametric ANCOVA to test for voxel-level GM difference among the three groups, controlling for age, gender, site, and total intracranial volume.

The multiple comparison correction was applied by family-wise error (FWE) corrected $p < 0.01$. Significant results were displayed onto a flat-map that shows the complete cerebellar GM in one concise view.

Correlation analysis

To assess the relationship between altered GM with clinical parameters in the two ataxia groups, voxel-level linear regression models were generated between the regional GM volume with the clinical variables (SARA total sum score, disease duration, and disease onset) in the MSA-C and $SAOA_{>10y}$ group separately, parceling out the effect of age, gender, scanning site, and total intracranial volume.

To control for multiple statistical testing, FWE corrected $p < 0.05$ was considered significant.

3.1.3 Results

Demographic and clinical data

Table 1 summarizes the demographic and clinical characteristics of the cohorts. The three groups, 49 HC, 16 MSA-C and 13 $SAOA_{>10y}$ did not differ with respect to age ($F_{(77)} = 2.33$, $p = 0.10$) or gender ($\chi^2_{(1)} = 0.71$, $p = 0.70$). However, the distribution of scanning sites between two ataxia patients groups had marginal significance ($\chi^2_{(1)} = 6.11$, $p = 0.047$). There were no statistically significant differences in the SARA sum scores ($T_{(27)} = 0.84$, $p = 0.41$) or age at onset ($T_{(27)} = 1.22$, $p = 0.23$). As the $SAOA_{>10y}$ group included patients

[4] http://warwick.ac.uk/snpm

who had symptoms for more than 10 years, the two patient groups also differed significantly with regard to the average symptom duration (MSA-C group: 3.94 ± 2.02 years; $SAOA_{>10y}$ group: 14.00 ± 3.46 years, $T_{(27)} = 9.78$, $p < 0.001$). The mean age at disease onset was 53.46 ± 8.55 for $SAOA_{>10y}$ group and 57.38 ± 8.63 for the MSA-C group ($T_{(27)} = 1.22$, $p = 0.23$).

	HC (49)	**MSA-C (16)**	**$SAOA_{>10y}$ (13)**	**Statistics**
Age [years]	65.08 ± 6.85 (48 - 78)	61.31 ± 8.48 (47 - 75)	67.00 ± 8.39 (51 - 78)	F = 2.33, p = 0.10
Gender [M /F]	20 / 29	7 / 9	7 / 6	χ^2= 0.71, p = 0.70
Site [BN / MD]	23 / 26	12 / 4	4 / 9	χ^2= 6.11, p = 0.05
Age at onset [years]	/	57.38 ± 8.63 (43 - 72)	53.46 ± 8.55 (41 - 69)	T = 1.22, p = 0.23
Duration [years]	/	3.94 ± 2.02 (1 - 9)	14.00 ± 3.46 (10 - 23)	T = 9.78, p < **0.001****
SARA	/	15.75 ± 5.40 (5.5 - 25.5)	13.62 ± 8.25 (6 - 31)	T = 0.84, p = 0.41

Table 1. Demographic and clinical characteristics for HC group, MSA-C group and $SAOA_{>10y}$ group. Data are presented as mean ± SD. The intervals presented below the means refer to value range. *HC: healthy controls; MSA-C: multiple system ataxia cerebellar type; $SAOA_{>10y}$: SAOA with disease duration larger than 10 years; M, male; F, female; BN, Bonn; MD, Magdeburg. SARA, scale for the assessment and rating of ataxia. ** represent the significant difference (p < 0.01).*

Structural differences in the cerebellum

With respect to the HC group, the MSA-C group showed cerebellar atrophy in bilateral I-IV, V, VI and right crus I-crus II-VIIb-VIIIa-VIIIb (FWE corrected $p < 0.01$, Figure 4A). A similar atrophy pattern to the MSA-C group was observed in the $SAOA_{>10y}$ group, but with additional GM reduction in bilateral IX and vermis crus II-VIIb-VIIIa-VIIIb-IX (FWE corrected $p < 0.01$, Figure 4B).

A comparison between the MSA-C group and the $SAOA_{>10y}$ group did not reveal a significant GM difference (Figure 4C). However, applying a less strict threshold (FWE corrected $p < 0.05$), the $SAOA_{>10y}$ group showed a GM reduction in left VI and vermis VI (Figure 4D).

All cerebellar regions showing a significant GM reduction are listed in Table 2. An increased local GM volume was not observed in any group comparison. The results are summarized on the flat-maps provided by SUIT (Figure 4).

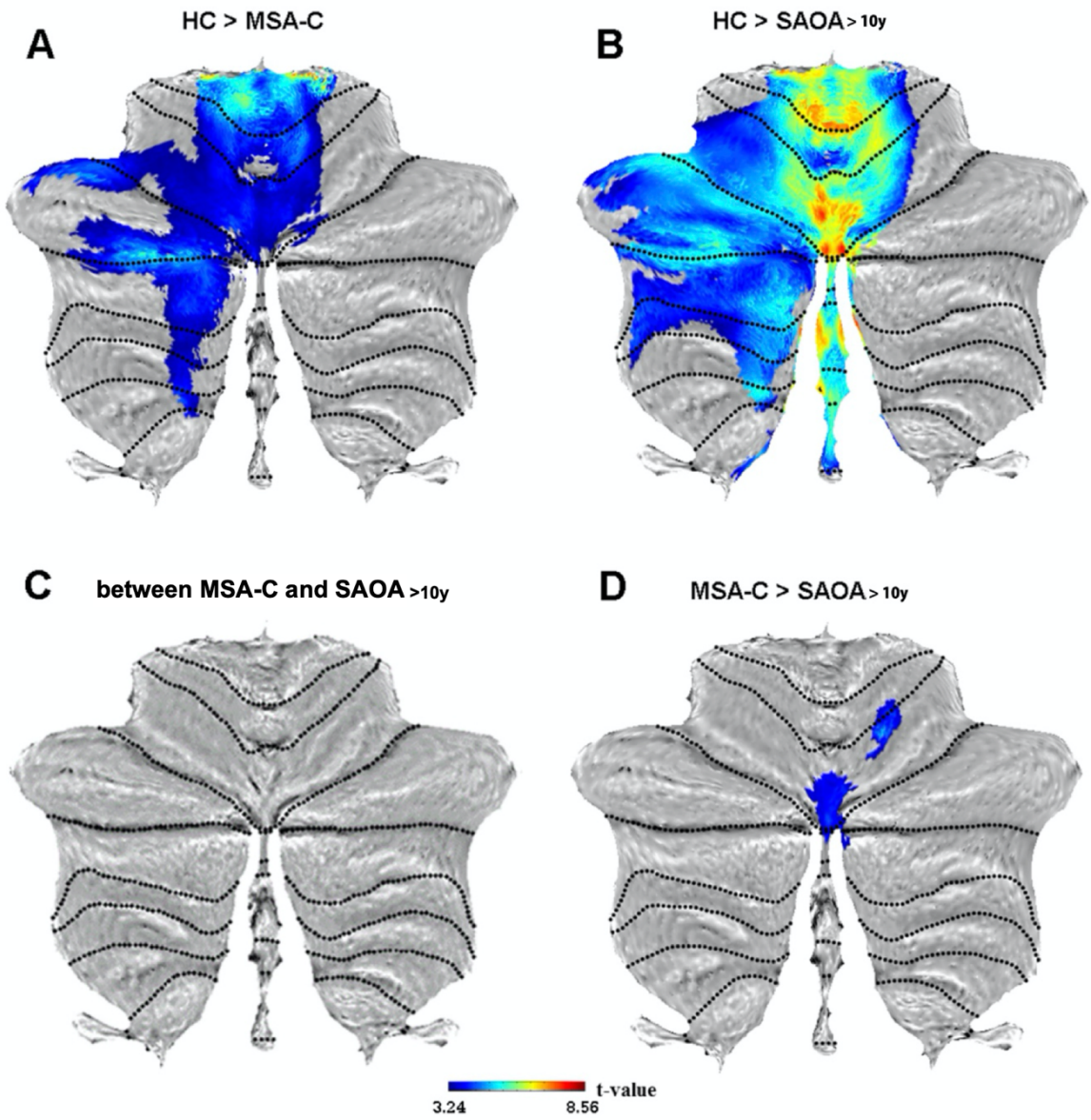

Figure 4. **Voxel-wise comparison of the local cerebellar GM volume between MSA-C and SAOA$_{>10y}$ and HC.** A) MSA-C vs. HC: reduced GM volume was found in bilateral I-IV, V, VI and right crus I-crus II-VIIb-VIIIa-VIIIb for the MSA-C group, FWE corrected $p < 0.01$; B) SAOA$_{>10y}$ vs. HC: reduced GM volume in bilateral I-IV, V, VI, IX, right crus I-crus II-VIIb-VIIIa-VIIIb and vermis crus II-VIIb-VIIIa-VIIIb-IX was found in the SAOA$_{>10y}$ group, FWE corrected $p < 0.01$; C) MSA-C vs. SAOA$_{>10y}$: no significant GM difference between the groups was detected, FWE corrected $p < 0.01$; D) however, with a less conservative threshold, atrophy in left VI and vermis VI was found in the SAOA$_{>10y}$ group, FWE corrected $p < 0.05$.

	Cerebellar region	side	Peak coordinate [mm]			T value	Cluster size, [mm^3]
			x	y	z		
Atrophy in MSA-C group	I-IV	R	-15	-36	-24	7.94	1446
	I-IV	L	5	-49	-17	6.85	1747
	V	R	-17	-40	-25	5.57	1223
	V	L	8	-56	-16	4.83	1621
	VI	R	-5	-65	-18	4.49	1065
	VI	V	4	-66	-24	4.52	1076
	VI	L	33	-50	-35	4.85	2121
	Crus I	L	30	-70	-37	5.73	1605
	Crus II	L	27	-70	-39	5.31	1838
	VIIb	L	20	-76	-49	3.91	301
	VIIIa	L	15	-64	-50	4.01	136
	VIIIb	L	13	-60	-52	4.32	102
Atrophy in SAOA$_{>10y}$ group	I-IV	R	-5	-50	-16	7.76	1897
	I-IV	L	5	-48	-18	8.06	2043
	V	R	-4	-57	-11	7.66	3085
	V	L	4	-67	-15	7.46	3344
	VI	R	-5	-68	-26	8.23	3944
	VI	V	5	-68	-25	8.51	1726
	VI	L	7	-68	-25	7.74	6807
	Crus I	L	30	-70	-36	6.30	4849
	CrusII	V	2	-75	-28	7.15	245
	CrusII	L	3	-74	-39	6.39	3803
	VIIb	V	1	-69	-29	6.96	123
	VIIb	L	11	-72	-47	5.33	1896
	VIIIa	V	3	-71	-38	7.72	636
	VIIIa	L	13	-64	-53	5.24	383
	VIIIb	V	1	-60	-36	7.47	437
	VIIIb	L	11	-63	-52	5.57	129
	IX	R	-4	-55	-37	5.55	312
	IX	V	1	-59	-36	7.55	548
	IX	L	1	-55	-49	4.95	227

Table 2. **Regions showing significant gray matter atrophy in MSA-C group and in SAOA$_{>10y}$ group when compared with HC group**. L, Left; R, Right; V, Vermis.

Correlation between altered GM volume and clinical parameters

After FWE was corrected with $p < 0.01$ (also for corrected $p < 0.05$), none of the altered GM volume voxels was correlated with clinical variables (SARA scores, disease duration and age at onset), neither in the MSA-C group nor in the SAOA$_{>10y}$ group.

3.1.4 Discussion

In the current study, the structural abnormalities in the cerebellum in MSA-C and $SAOA_{>10y}$ were investigated and further explored to determine whether the altered structure was associated with clinical assessment (duration, age at onset and severity). Compared with HC, a reduced GM volume was found mainly in bilateral I-IV, V, VI and right crus I-II-VIIb-VIIIa-IX for both ataxia groups. Atrophy in the vermal region VIIIa-VIIIb-IX was found in the $SAOA_{>10y}$ group only. However, a statistically significant correlation with any clinical parameter was not observed.

Using the cerebellar atlas provided by SUIT, its advanced preprocessing pipeline using DARTEL and the flat-mapping technique allowing for better visualization as compared with conventional whole brain analysis, enabled us to map morphological changes in the MSA-C and $SAOA_{>10y}$ groups in more detail than previous studies (Abele *et al.*, 2007; Burk *et al.*, 2004). The spatial distribution of the atrophy found in both ataxia groups corresponded well to the clinical presentation of the ataxia. A cluster with significant GM atrophy was found, including the anterior part of the cerebellum (bilateral I–IV, V, VI) and the right posterior cerebellum (right crus I -crus II-VIIb-VIIIa-IX). The anterior cerebellum is highly involved in motor and sensorimotor processing, e.g. motor dexterity, coordination, and complex movement integration (Samson & Claassen, 2017). For example, lobules V and VI have strong primary somatosensory representation (Buckner *et al*, 2011; Grodd *et al*, 2001; Reetz *et al*, 2012). Lobule V contains representation of upper-limb movements, while lobule VI is reported to be involved in lower-limb movements (Stoodley & Schmahmann, 2009; Timmann *et al*, 2008). Therefore, atrophy in lobule V-VI explains sufficiently the phenotype of MSA-C and SAOA as a cerebellar syndrome of limb coordination (Abele *et al.*, 2007; Burk *et al.*, 2004). In addition, posterior cerebellum atrophy exhibited clear hemispheric asymmetry. The right hemisphere of the posterior cerebellum was highly affected in both ataxia groups. This corresponds well with observed slurred speech and dysarthria in these ataxia patients (Abele *et al.*, 2007; Gilman *et al.*, 2008; Klockgether, 2018), because the right cerebellar hemisphere is reported to be more associated with language production than the left cerebellar hemisphere (Klein *et al*, 2016). Furthermore, the GM atrophy was interpreted as neuro-axonal loss (McEwen, 1997; Thompson *et al*, 2003); the loss found in these motor and sensorimotor regions could be

a major contributor to the motor dysfunction in the ataxia groups (Abele *et al.*, 2007; Burk *et al.*, 2004; Gilman *et al.*, 2008; Klockgether, 2018). Although the atrophic GM was not correlated with clinical assessments, one possible reason may be the small sample size, limiting the statistical power.

In addition, reduced GM volume in bilateral cerebellar lobules IX was observed in the $SAOA_{>10y}$ group. Impairments of lobule IX are frequently reported as being associated with abnormal eye movements (Beh *et al*, 2017). Previous lesions studies in lobule IX showed lobule IX lesions to cause nystagmus and impaired vestibular-ocular reflex suppression. Lobule IX has extensive connections with the vestibular nuclei (Barmack, 2003). As a consequence, an atrophy of lobule IX may lead to a dysfunction of visual and vestibular projections. Considering that lobule IX is also reported to be involved in cognitive performance, such as episodic memory, self-reflection, facial emotions and associated functions (Habas *et al*, 2009; Scharmuller *et al*, 2013), this observation of GM loss may also explain the mild and unspecific cognitive disturbances observed in SAOA such as verbal and visual learning deficits (Biswal *et al*, 1997; Klockgether, 2018).

The atrophy of the posterior vermis in the $SAOA_{>10y}$ group is interesting and has already been reported in two previous studies (Abele *et al.*, 2007; Baloh *et al.*, 1986). It may be related to the loss of Purkinje neurons of the cerebellar vermis (Klockgether, 2018). Considering the functional anatomy, it is known that the vermis participates in motion control (Gellersen *et al*, 2017; Shin *et al*, 2016). The posterior part in particular, i.e. the portion close to lobule VIII, plays a central role in locomotion (Kheradmand & Zee, 2011). Projections from the cerebral cortex to vermis VIII originate from arm, leg, and proximal body representations that are located within multiple cortical areas. Projections from the motor cortex to vermis VIII are likely to send signals related to force, speed, motor direction and movement execution (Morton & Bastian, 2004). These wide-range, motor-related connections to the vermis VIII lead to the assumption that the atrophy in vermis VIII may represent the morphological basis of SAOA-related movement disorder symptomatology. Despite the lack of direct evidence of clinical correlation, this speculation is plausible given the small sample size in the study.

The main limitation of the present work, as we mentioned above, is the sample sizes. Further studies with larger sample sizes are needed to explore the relationship between

the structural loss and the clinical assessments of the ataxia patients. Besides, the GM volume is one of the structural properties, and more studies using multiple modalities, such as WM tracts, should be applied to better describe the structural changes in the ataxia.

3.2 Study 2: Cerebellar functional connectivity in MSA-C and SAOA

3.2.1 Introduction

Previous neuroimaging studies have already revealed structural changes of the cerebellum in sporadic ataxias (Abele *et al.*, 2007; Baloh *et al.*, 1986; Burk *et al.*, 2004). However, it remains unknown whether the structural atrophy affects the functional intra-cerebellar communication. Two common parameters can be derived from rs-fMRI time series characterizing different aspects of this intra-cerebellar communication, namely i.e the amplitude of low-frequency fluctuation (ALFF), and the degree centrality (DC). ALLF reflects regional spontaneous synchronous neural activity (Zang *et al.*, 2007), whereas DC indicates how strongly a certain region is connected to other regions (Zuo *et al*, 2012).

The goal of this study was to discover if the functional connectivity is altered in those regions of the cerebellum that are found to be atrophic in SAOA and MSA-C. An addition goal was to investigated if these regions exhibit any distinct connectivity feature compared to the unaffected regions of the cerebellum.

3.2.2 Study specific methods

Amplitude of low-frequency fluctuation (ALFF), a voxel-level index, was applied to detect the regional intensity of the spontaneous fluctuations of the BOLD signal (Zang *et al.*, 2007). The voxel-level calculations were illustrated in Figure 5 were suggested by Zang and colleagues. Briefly, the voxel level resting-state time series were first transformed into the frequency domain using a fast Fourier transform. The square root of the power spectrum, which was obtained from a predefined frequency interval (0.01-0.08 HZ), was calculated voxel-wise and averaged across the frequency interval. This averaged square root is defined as ALFF. To reduce the global effects among all he participants, the ALFF of each voxel was divided by the global mean ALFF for each participant. The resulting maps were spatially smoothed before entering the statistical analysis (FWHM = 4 mm).

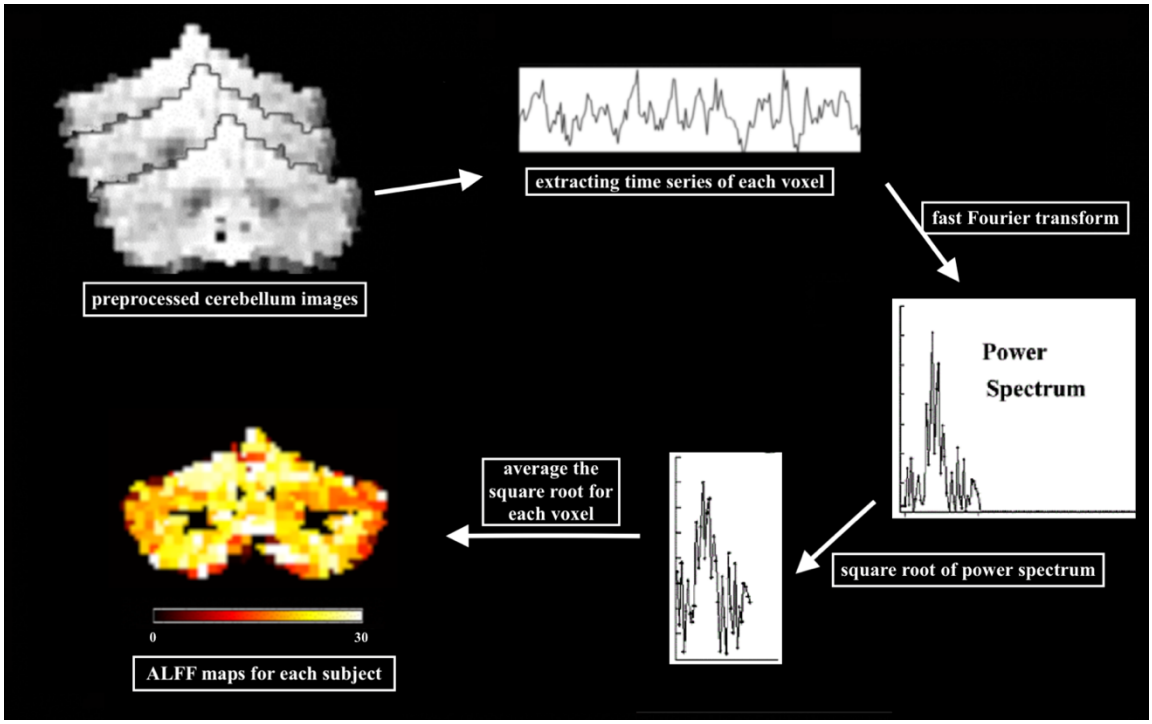

Figure 5. **Brief illustration of the voxel-level ALFF analysis pipeline**. The time series of each voxel were first extracted from the preprocessed cerebellum images. Every time series was Fourier transformed to obtain the power spectrum. The square root of the power spectrum was calculated and then averaged as the ALFF value.

Degree centrality (DC), a voxel-level measure as well, was assessed by how many voxels connected to a given voxel. The calculation followed the procedure suggested by Wang and colleagues outlined in Figure 6 (Wang *et al.*, 2015). In a first step, a cerebellar GM mask was constructed. This mask excluded all voxels that had a high probability of belonging to the WM or CSF partition. The cut-off was set to 0.8. Voxels with zero variance over time for all participants were also excluded. Within the resulting mask, a pairwise Pearson correlation between every two voxels was calculated and a correlation coefficient and a corresponding p value was obtained for each connection between every two voxels. In order to threshold the connection, a false discovery rate (FDR) corrected p value less than 0.0001 was defined and its corresponding correlation coefficient was 0.29 in this study (Zuo *et al.*, 2012). The DC of each voxel was calculated as the sum of all the meaningful coefficients connected to this voxel (Buckner *et al*, 2009; Zuo *et al.*, 2012). The resulting DC maps for each subject were converted into Fisher z -value maps and smoothed spatially with a Gaussian kernel (FWHM = 4 mm).

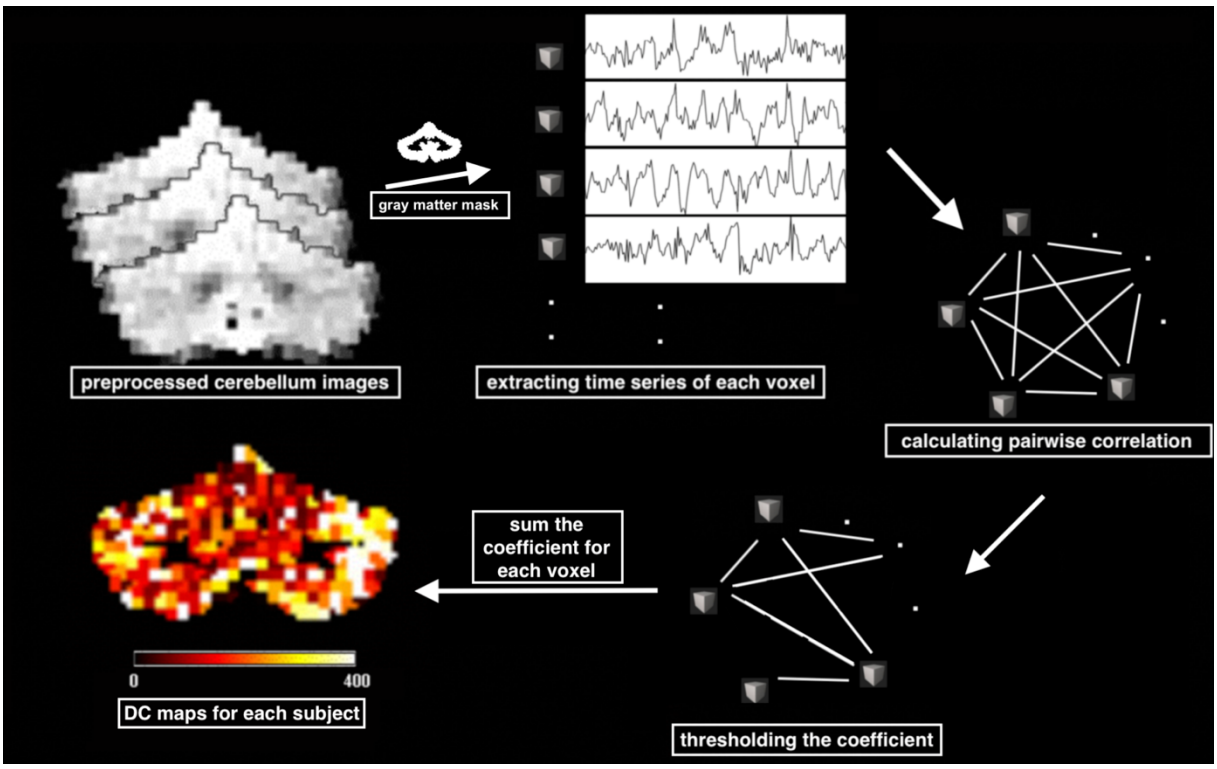

Figure 6. **Flowchart of the voxel-level DC calculation in the cerebellum**. The time series of each voxel within the predefined cerebellar mask were first extracted from the preprocessed cerebellum images. Pairwise Pearson correlation between every two voxels was then calculated and thresholded. The thresholded connections to each voxel were summed as the DC value of the voxel.

Quality assessment of rs-fMRI time series

The quality control measures employed here are largely based on the realignment estimate-derived calculations. The difference in the root mean squared (RMS) value and framewise displacement (FD) value were compared among three groups. A p value below 0.05 was considered as significant.

Statistical analysis

Quality assessment of rs-fMRI images

There was no significant difference in the quality control measures among the three groups (RMS: $F_{(77)} = 0.77$, $p = 0.47$; FD: $F_{(77)} = 1.49$, $p = 0.23$).

Voxel-level comparison in atrophic regions between ataxia groups and HC

The between-group comparisons were analyzed using the SnPM toolbox. Non-parametric, two samples t-tests were used to compare functional characteristics (ALFF and DC) of the

atrophic regions between MSA-C and HC. Therefore, a mask containing only those voxels showing atrophy in the structural analysis in the MSA-C group was generated (see **chapter 3.1.3**, Figure 4A, page 30). Age, gender, and imaging site were included in the model as covariates of no interest. The statistical significance threshold was set to $p < 0.01$, FWE-corrected.

The same approach was taken for the SAOA group. The cerebellar regions analyzed are outlined in Figure 4B (**chapter 3.1.3**, Figure 4B, page 30).

Cluster-level comparison within the ataxia groups

The within-group comparisons between atrophic regions and non-atrophic regions were statistically applied in the MSA-C group and the SAOA>10y group, respectively. Here, a permutation test rather than a t-test was chosen, because the unequal number of voxels between atrophic and non-atrophic regions may dramatically affect t-test statistical power. The permutation test generally quantifies the statistic based on randomly resampling with/without replacement. This is one of the non-parametric statistics and especially useful when the sampling distribution is not available or the sample size is un-matched in parameter statistics (e.g. one sample t-test and two samples t-test). The permutation test enabled us to see the range we obtained from re-using our dataset when we randomly performed it, for example, 10,000 times, and, when a numerical value was given, which position of this given value was within the range. The position was calculated by counting the number of permutated values that were larger/smaller than the given value, and then divided by the simulation times (10,000). In this study, the permutation test was performed 10,000 times and each permutation was performed by randomly extracting n1 voxels (n1, number of voxels in the atrophic regions) from the n2 voxels (n2, number of voxels in the non-atrophic regions). The extracted n1 voxels from every performance of the test were defined as a permutation sampling and 10,000 permutation samplings were ultimately obtained. This procedure is also known in the literature as ‘bootstrapping’ (Johnson, 2001).

To give an example of the procedure, the atrophic region of the MSA-C group consists of 14,281 voxels (n1) and the number of voxels in the non-atrophic region is 34,162 (n2). The permutation was performed on the mean ALFF (DC) maps across all MSA-C subjects 10,000 times. A permutation sampling was obtained after each permutation and each permutation sampling consisted of 14,281 voxels. The ALFF (DC) values in each

permutation sampling were averaged as a simulated data and the permutation dataset consisting of 10,000 simulated datasets was gathered. The statistical p value was further calculated by the percentage of 10, 000 simulated datasets that were larger/smaller than the real dataset. Here, the real dataset was the averaged ALFF (DC) value of the atrophic regions in the MSA-C group. A p value below 0.05 was considered as significant.

The same permutation test was applied in the healthy group as a control. The atrophic regions of the MSA-C group were defined as artificial atrophic regions of the HC group, and the same, the non-atrophic regions of the MSA-C group were defined as for artificial non-atrophic regions of the HC group. The aim was to investigate whether the functional difference between atrophic regions and non-atrophic regions was MSA-C specific or the same in the HC group.

The within-group comparisons of ALFF (DC) values between atrophic regions and non-atrophic regions were performed in the $SAOA_{>10y}$ group. As a control, the same comparison was repeated in the healthy group as well. For the HC group, the atrophic (non-atrophic) regions of the $SAOA_{>10y}$ group were defined as artificial atrophic (non-atrophic) regions.

3.2.3 Results

Demographic and clinical data

As described above (**chapter 3.1.3**, page 29), the three groups, 49 HC, 16 MSA-C and 13 $SAOA_{>10y}$, did not differ with respect to age or gender but displayed a marginal difference in site distribution. In addition, the two ataxia groups exhibited no difference in the SARA scores and age at onset, but the SAOA group had significantly longer disease duration than the MSA-C group.

Voxel-level between-group comparison of ALFF and DC of the atrophic regions between ataxia groups and HC

The analysis did not reveal any abnormalities in either ALFF or DC when comparing HC and MSA-C (FWE corrected $p < 0.01$).

The same result was found in the SAOA data. Both functional measures (ALFF and DC) failed to show any detectable difference when compared with HC (FWE corrected $p < 0.01$).

Cluster-level within-group comparison of ALFF between atrophic regions and non-atrophic regions within the ataxia groups

The averaged ALFF value of the real atrophic regions in the MSA-C group was 32.16 (± 5.37), while the range of the averaged ALFF values of the simulated datasets was 26.4 to 26.8 (26.57 ± 0.06). Statistically, none of the ALFF values of the simulated atrophic regions was larger than the ALFF value of the real atrophic regions ($p < 0.001$, Figure 7A: the red histogram illustrates the simulated values and the red dot represents the real value).

However, an opposite result was found when the same permutation test was performed in the HC group. The averaged ALFF value of the artificial atrophic regions in the HC group was 30.78 (± 7.33) and this value being totally out of the range of the averaged ALFF values of the simulated datasets, which was 35.0 - 38.0 (36.34 ± 0.42) ($p < 0.001$, Figure 7B).

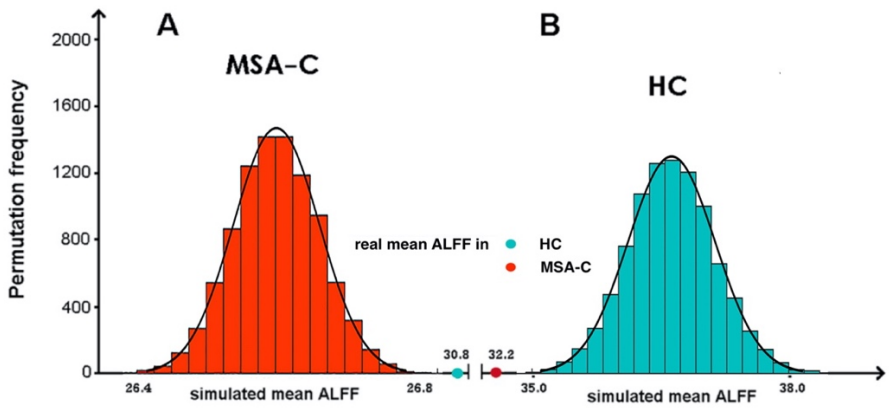

Figure 7. Comparison of the ALFF value between the atrophic regions and the simulated atrophic regions in A) the MSA-C group and B) the HC group. Dots represent the real ALFF values and histograms illustrate the simulated ALFF values.

For the within-group comparison in the $SAOA_{>10y}$ group, the averaged ALFF value of the real atrophic regions was 31.08 (± 11.32). The permutation test had created a simulated dataset with an ALFF value ranging from 26.6 to 27.0 (26.76 ± 0.05) and none of the simulated values was larger than the real value ($p < 0.001$, Figure 8A: the yellow histogram represents the simulated datasets and the yellow dot represents the real value). For the

control HC group, the averaged ALFF value of the invented atrophic regions was 28.94 (± 6.60) and was less than all the ALFF values (range from 35.6 to 37.2, 36.33 ± 0.24) of the simulated datasets, the statistical p value was less than 0.001 (Figure 8B).

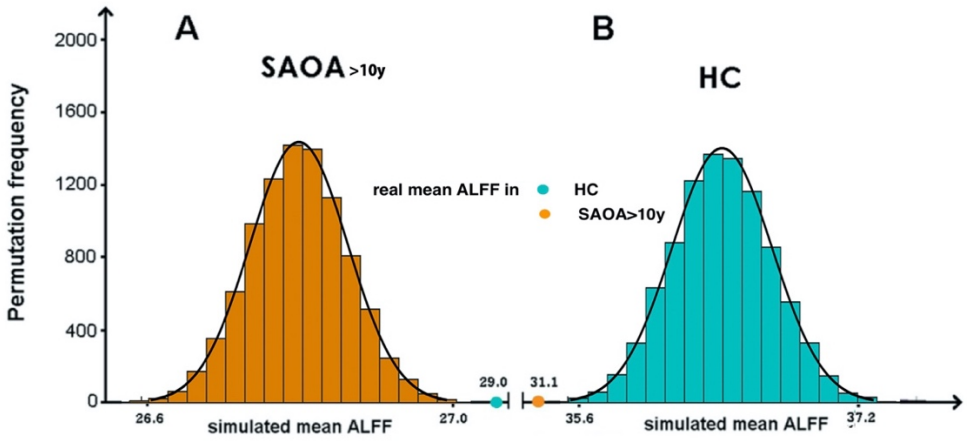

Figure 8. Comparison of the ALFF value between the atrophic regions and the simulated strophic regions in A) the SAOA$_{>10y}$ group and B) the HC group. Dots represent the real ALFF values and histograms plot the simulated ALFF values.

Cluster-level within-group comparison of DC between atrophic regions and non-atrophic regions within the ataxia groups

The same analyses were performed to explore the DC difference between atrophic regions and non-atrophic regions. In the MSA-C group, the averaged DC value of the real atrophic regions was 620.04 (± 109.32) and the DC values of the simulated datasets were between 524 and 532 (528.22 ± 1.27). The p value was below to 0.001 and none of the simulated DC values was larger than the real value (Figure 9B: Red histogram plots the simulated datasets and the red dot represents the real value).

For the control HC group, the averaged DC value of the artificial atrophic regions was 449.77 (± 112.07). Statistically, this value was not in the range of averaged DC values of the simulated datasets, which was from 441 to 447 (444.00 ± 0.67) ($p < 0.001$, Figure 9A).

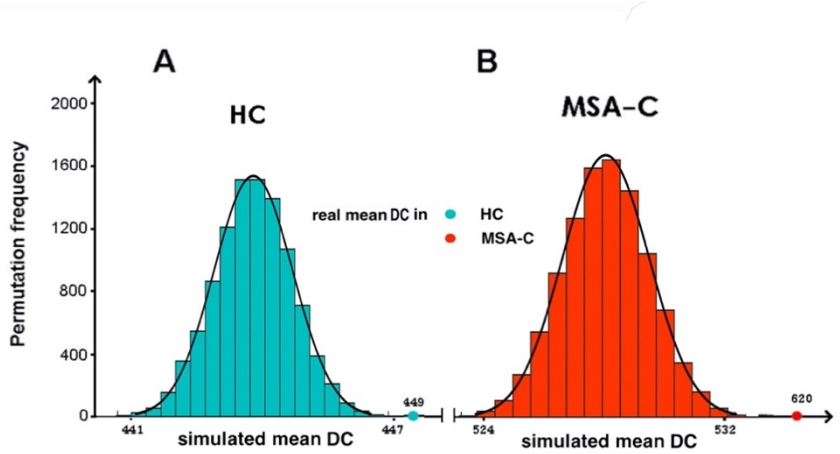

Figure 9. **Comparison of the DC value between the atrophic regions and the simulated strophic regions in A) the HC group and B) the MSA-C group**. Dots represent the real DC values and histograms visualized the simulated DC values.

In the $SAOA_{>10y}$ group, the averaged DC value of the real atrophic regions was 620.94(± 141.04). The statistical calculation revealed that none of the averaged DC values of the simulated datasets (range 564 to 569, 566.87 ± 0.74) was larger than the measured value ($p < 0.001$, Figure 10B: the yellow histogram displays the simulated datasets and the yellow dot represents the measured value). Similarly in the control group, none of the averaged DC values (range 442- 446, 444.00 ± 0.67)) of the simulated datasets was larger than the averaged DC of the artificial atrophic regions 450.22 (± 123.64). Likewise, the p value was below 0.001 as well (Figure 10A).

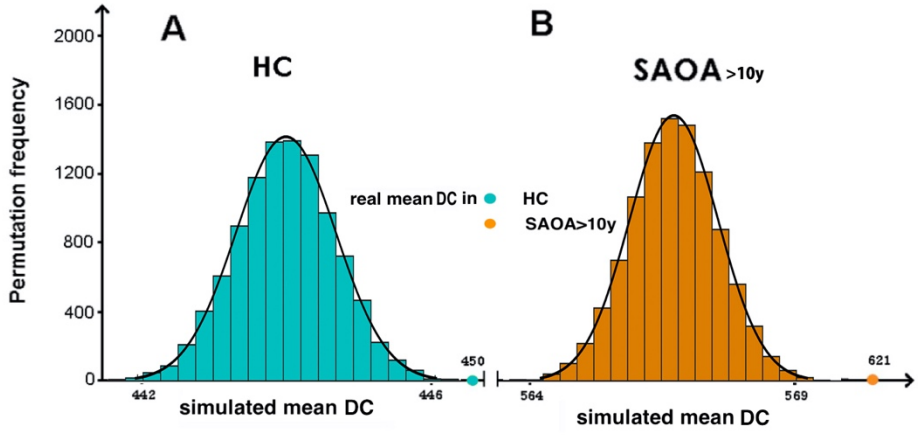

Figure 10. **Comparison of the DC value between the atrophic regions and the simulated atrophic regions in A) the HC group and B) the $SAOA_{>10y}$ group**. Dots represent the real DC values and histograms plot the simulated DC values.

3.2.4 Discussion

By applying voxel-level functional analysis to the structurally atrophic cerebellar regions, similar functional connectivity patterns were revealed in the MSA-C group and the SAOA group when compared with the healthy group. At the same time, within both ataxia groups, the structurally affected pattern was observed to show higher functional connectivity (ALFF and DC) than the structurally non-affected pattern.

As described in chapter 3.1.3 (page 30), the ataxia patients showed cerebellar atrophy in regions consistently involved in motor and somatosensory processing. Interestingly, none of these regions showed altered local ALFF or DC when compared with the healthy group. Even though the local GM volume is reduced in the ataxia groups, neither the local spontaneous activity (accessed by ALFF) nor the intra-cerebral functional connectivity characterized by DC seemed to be altered. These findings indicate a relatively normal neural activity and network integration despite the structural damage. One may speculate that functional changes seem less detectable than the structural changes. Although this finding may at first sight be unexpected, it confirms the general advantage of functional connectivity measurements. The functional connectivity system was assessed across the overall voxels, not only on a separated voxel. The functional connectivity was examined based on the intrinsic temporal correlation of the spontaneous BOLD signal among many regions (Fox & Raichle, 2007; Friston, 2011). One of the key features of this system is its stability against disturbances. It may be assumed that the cerebellar architecture has this ability to balance out the structural loss by functional compensation.

This raises the question whether any evidence can be found for a compensational mechanism. The approach to test this hypothesis is to compare the functional characteristics between the structurally atrophic and non-atrophic cerebellar regions. Using bootstrapping, it was shown that those cerebellar regions with structural atrophy had higher functional connectivity features than those regions without structural atrophy. This held true for the MSA-C group and the $SAOA_{>10y}$ group as well, indicating that these two subtype ataxias may have a shared mechanism with which to compensate neuronal loss.

Of the two functional connectivity measurements, ALFF showed the greater ability to reflect the voxel-wise strength of intrinsic neural activity (Biswal *et al*, 1995). It has been

shown that the high ALLF can be linked to high resting-state cerebral blood flow and glucose metabolic rate (Biswal *et al.*, 1997; Biswal *et al.*, 1995). The DC is a widely used voxel-level metric as well, representing the most local and direct measure in the rs-fMRI. It is a network centrality assessed by the number of connections of a given region (Zuo *et al.*, 2012). The region may be considered to be more important if it has a high DC value. Specifically, a region with a high DC value tends to take the responsibility for maintaining the network communication and stability (Liang *et al*, 2013; Zuo *et al.*, 2012).

In the study, it was found that the structurally atrophic regions showed higher ALFF and DC values than the non-atrophic regions in both ataxia groups. On the one hand, the structural atrophic regions with higher ALFF may have a high regional cerebral blood flow, as well as a high glucose metabolism rate (Biswal *et al.*, 1995). This phenomenon could make these regions more active and more effective when attacked by disease. It is not to be expected that the higher ALFF in the atrophic regions than non-atrophic regions was observed only in the ataxia groups, not in the healthy group. In the healthy group, these regions were found to show low ALFF values. As described above, there was no difference in the ALFF values in these regions between the ataxia groups and the healthy group. This may raise the reasonable hypothesis that there is an overall ALFF reduction in the cerebellum in the ataxia groups, especially those regions without any structural atrophy. The assumption is that the functional cerebellum could be totally affected by the disease and hence show low ALFF at first, and then, those regions with structural loss, expending more energy and consuming more metabolism, show a higher ALFF than non-atrophy regions in the ataxia groups. Even though a different ALFF pattern was not reported in this study, further longitudinal studies are worth conducting to better understand the dynamic ALFF distribution of the overall cerebellum.

On the other hand, the high DC value of the structurally atrophic regions may suggest that these regions may have a wider responsibility for balancing the function of the cerebellum, especially these atrophic regions that are reported to be highly involved in motor and sensorimotor processing (Samson & Claassen, 2017). The fact that these regions were also observed to bear more responsibility in the cerebellum in the healthy group may indicate a shared general process across the three groups, and that they play a more

dominant role in monitoring the cerebellar functional system in the healthy group than being ataxia specific.

The main limitation of the present work was the number of subjects included in both ataxia groups. Further studies with larger sample sizes are necessary to explore the difference in ALFF/ DC values between the ataxia groups and the healthy group. Moreover, the present study did not aim to study any causality between the structural and functional measures. To advance the understanding of the disease, future studies should focus more closely on the longitudinal development of the structural atrophy and the functional connectivity in the ataxia groups.

3.3 Study 3: Global and regional organization of the cerebellar networks in MSA-C and SAOA

3.3.1 Introduction

Loss of cerebellar volume has been reported a conventional imaging marker for both MSA-C (Burk *et al.*, 2004; Carre *et al.*, 2020) and SAOA patient's (Abele *et al.*, 2007; Burk *et al.*, 2004; Klockgether, 2018). These degenerative changes are associated with a reduction in the efficiency of the brain networks at both local and global level (Nir *et al*, 2015; Sheng *et al*, 2017; Voets *et al*, 2012; Zeighami *et al*, 2015). In contrast, local functional connectivity (based on voxel-level ALFF and DC) in the cerebellum remains intact in both MSA-C and SAOA, despite the structural loss (**chapter 3.2**). Although an earlier study provided a better understanding of the local functional changes, it remains largely unclear whether these local changes could affect the efficiency of the functional networks in the cerebellum in both MSA-C and SAOA.

The topology of brain networks is usually defined in terms of integration and segregation of different parts of the brain with other regions, using global metrics such as clustering coefficient, characteristic path lengths and efficiency (Bullmore & Sporns, 2012). Graph theoretical approaches are widely used in investigating such topological measures of both structural and functional brain networks (Bullmore & Sporns, 2009; Bullmore & Bassett, 2011; Sporns, 2018). In MSA-C, it has been reported that the topology of white matter network is severely disrupted, resulting in reductions in the clustering coefficient and characteristic path lengths (Shah *et al*, 2019). The structural network is yet to be explored in SAOA. At the same time, it has been found that the structural network based on diffusion MRI cannot resolve the intrinsic connections easily and is also potential to weak the long-range connections when comparing with the functional networks (See a review: (Park & Friston, 2013)). However, no study has so far examined functional network architecture in both MSA-C and SAOA.

The cerebellum is considered one of the crucial subnetworks in the topological brain network architecture (Bullmore & Sporns, 2009; Smith *et al*, 2009). Previous fMRI studies have found that different cerebellar parts are connected to distinct cerebral regions (Buckner *et al.*, 2011; Stoodley *et al*, 2012). However, fMRI studies of cerebellum only, including of intracerebellar organization, are rare. The cerebellum as a distinct subnetwork,

the global and local topological networks needed to be explored to measure to what extent the cerebellum is integrated and segregated in both MSA-C and SAOA.

Therefore, in this study, we: 1) constructed the cerebellar networks and calculated the global and local network topological properties, 2) compared the network properties among three groups (the MSA-C group, the $SAOA_{>10y}$ group and the healthy group) and further assessed, by reviewing the correlations between clinical and network parameters, whether these topological network changes are associate with the ataxia symptoms.

3.3.2 Study specific methods

Graph theory

Graph theory is branch of mathematics that dates back to the 18th century. In 1736, Leonhard Euler solved a popular problem based on the bridges in the city of Königsberg. The Pregolya River, which passes through the city, was crossed by seven bridges that divided the city into separated parts (Figure 11a). The popular problem was whether it was possible to cross all seven bridges once and arrive back at starting point (Euler, 1741; Fornito *et al*, 2013).

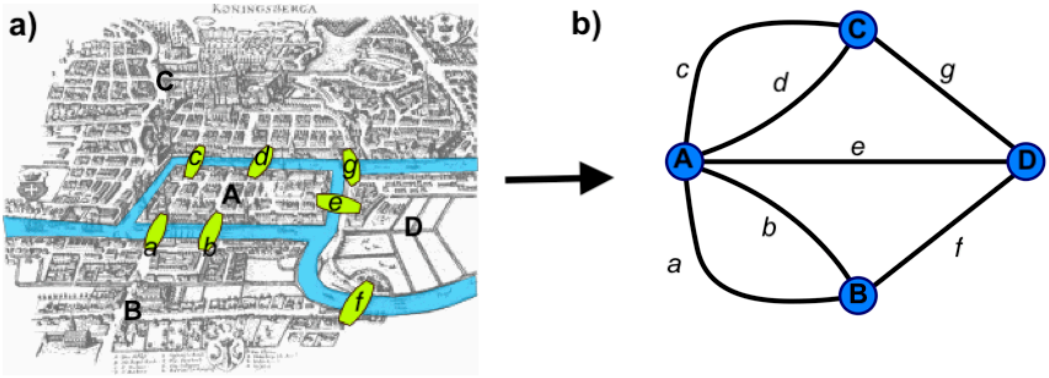

Figure 11. Königsberg bridges problem. a) an image shows seven bridges (a-f) separate the city into four parts (A-D). b) an graphical representation of seven edges (a-f) connected four nodes (A-D). Figure adopted from Wikipedia[5].

Euler embarked on solving this problem by taking the city parts as nodes and the bridges as edges (Figure 11b). The problem turned out to be a mathematical one, and Euler

[5] https://en.wikipedia.org/wiki/Seven_Bridges_of_Königsberg

proved that the proposition was impossible. Mathematically, it is only possible when every pair of nodes have odd number of connecting edges. This solution, as Euler's circle, is now part of graph theory.

In graph theory, a graph denotes a set of nodes and a set of edges (connecting nodes). In the present study, the cerebellum was mathematically considered as a graph (network).

Network construction

All the network analysis was applied using the GRETNA toolbox (Wang *et al.*, 2015). The nodes in the cerebellar network were defined from 28 lobules, selected using the SUIT hemispheric atlas (Diedrichsen, 2006). The names of these 28 regions are visualized in Figure 12 (10 lobules in the bilateral hemisphere and 8 lobules in the vermis).

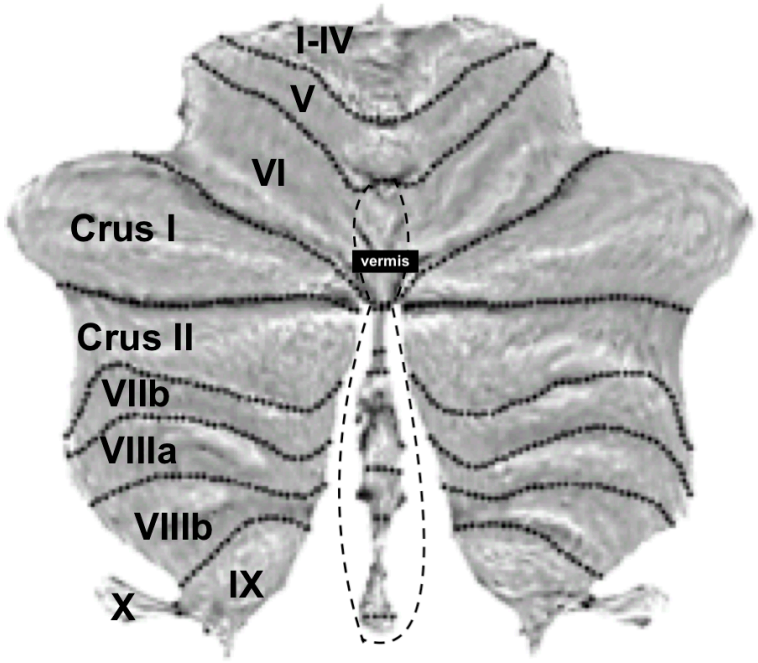

Figure 12. The flat-mapp visualization of cerebellar regions. The ten bilateral cerebellar lobules (labeled I-X) are labeled in the hemisphere and eight vermis regions (vermis VI-X) in the middle structure are circled by dot line.

Edges are defined as the connection between nodes. The connection between two nodes was assessed by correlating the mean time series obtained from the corresponding regions. This procedure was performed for all regions, leading to a 28×28 so-called adjacency matrix. An entry at the position ($\boldsymbol{i,j}$) displays the correlation coefficient of the

mean time series of region i with the time series of region j, or -in graph theory terminology- the connection between node i and node j. The value in the adjacency matrix is range from -1 to 1 with zeros on its diagonal (Figure 13A). The adjacency matrix was further thresholded by defining the connection whose statistical p value was < 0.05 as zero to exclude non-significant matrix elements (Zuo *et al.*, 2012).

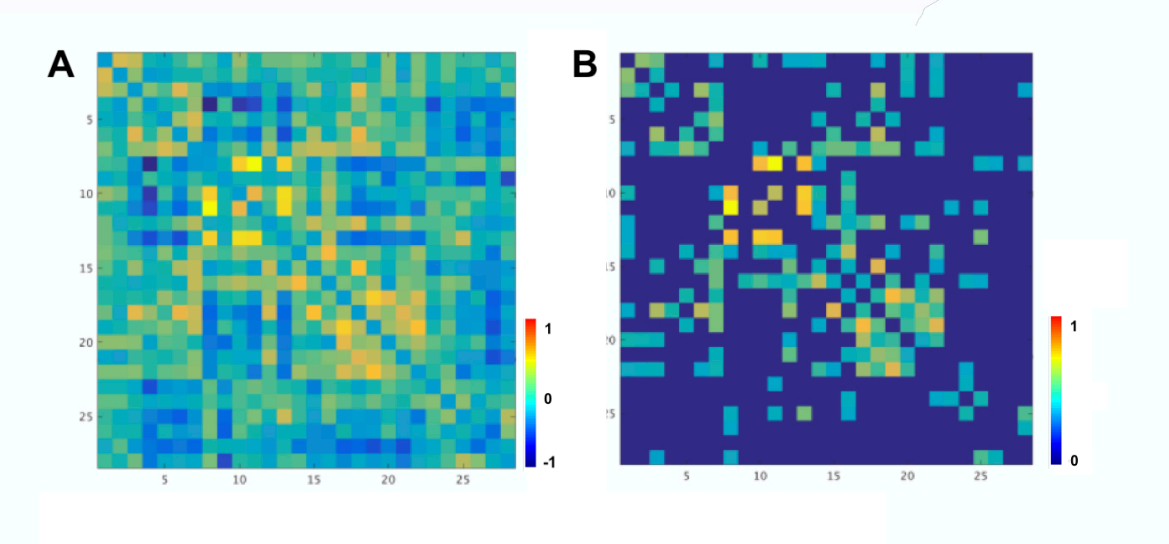

Figure 13. The adjacency matrix of a cerebellar network. A) shows the raw 28×28 adjacency and the value range between -1and 1, and zero on the diagonal; and B) shows the thresholded adjacency matrix.

Network properties analysis

The topologic characteristics of a network can be captured by graph theoretical measures at both global and local scales. Global measures includes network-wide attributes such as the clustering coefficient or efficiency, while nodal measures represents simple node relations such as nodal centralities. A detailed description of graph theoretical measures is provided in the following section (Figure 14).

Global network parameters

Clustering coefficient, C_p

For a node i, the C_p of this node is defined as the fraction of pairs of nodes who are connected with each other (Figure 14a) and expresses how close its neighbor nodes. For a graph G, the network C_p is the average of the clustering coefficient over all nodes (Watts & Strogatz, 1998):

$$C_p(G) = \frac{1}{N}\sum_{i \in G}\frac{E_i}{D_i}$$

$$D_i = \frac{k_i(k_i - 1)}{2},$$

where $\boldsymbol{k_i}$ is the number of edges connected to node $\boldsymbol{i}$, $\boldsymbol{D_i}$ is the total number of possible edges between node $\boldsymbol{i}$'s neighbors ($\boldsymbol{k}$), $\boldsymbol{E_i}$ is the number of edges connecting node $\boldsymbol{i}$'s neighbors, and $\boldsymbol{N}$ is the number of nodes in the graph $\boldsymbol{G}$.

Characteristic path length, $\boldsymbol{L_p}$

The path length between node ($\boldsymbol{i,j}$) is the number of edges connecting node $\boldsymbol{i}$ and node $\boldsymbol{j}$. Among all paths connecting $\boldsymbol{i}$ and $\boldsymbol{j}$, the $\boldsymbol{d_{ij}}$ is defined as the shortest path length (Figure 14b). For a graph $\boldsymbol{G}$, the $\boldsymbol{L_p}$ is the average of the $\boldsymbol{d_{ij}}$ over all nodes, giving a measure of how closely nodes are connected to one another (Watts & Strogatz, 1998):

$$L_p(G) = \frac{1}{N}\sum_{i \in G} L_i$$

$$L_i = \frac{1}{N-1}\sum_{i \neq j} d_{ij},$$

where $\boldsymbol{d_{ij}}$ is the shortest path length between nodes $\boldsymbol{i}$ and $\boldsymbol{j}$, $\boldsymbol{L_i}$ is the characteristic path length of node $\boldsymbol{i}$ and $\boldsymbol{N}$ is the number of nodes in the graph.

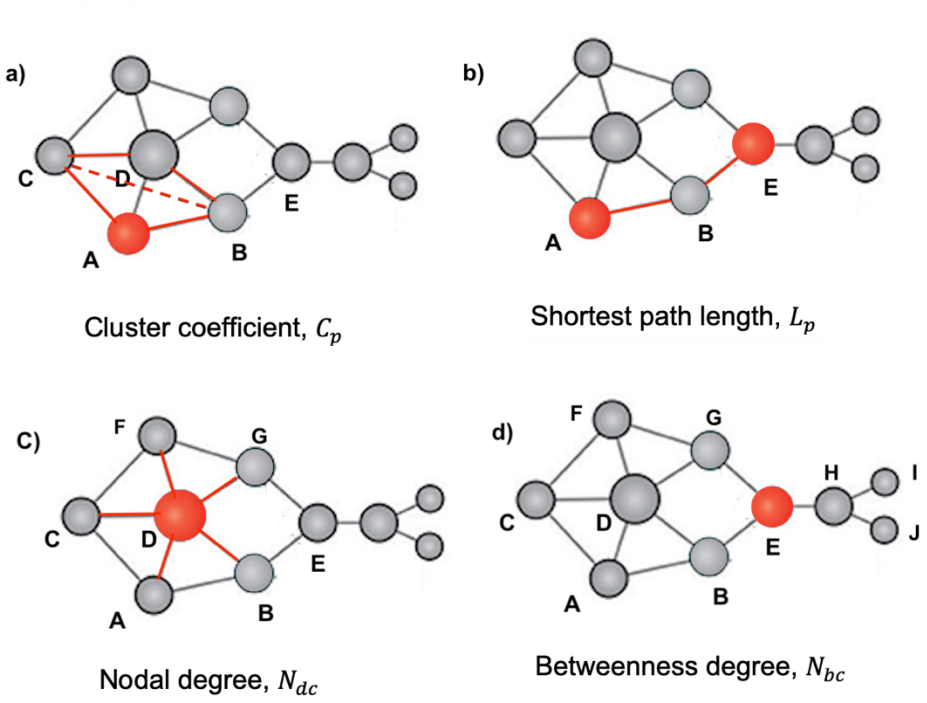

Figure 14. Overview of different graph measures. a) the clustering coefficient, C_p of a node is the fraction of its neighbors are connected to each other. For example, the C_p of node A is calculating as $C_p(A) = \frac{2}{3}$; b) the shorted path length, L_p reflects the shortest distance between pair of node. For example, the shortest path between node A and E is passing node B, the $L_p(A - E) = 2$; c) the nodal degree, $\mathrm{N_{dc}}$ of a node is measured as the sum of the edges connecting to this node. For example, five edges connected to node D, the $\mathrm{N_{dc}}(D) = 5$; d) the betweenness degree, $\mathrm{N_{bc}}$ of a node is computed as the fraction of how many number of shortest path between other node pairs are passing through this node. For example, the node E has the highest betweenness degree in this graph that $\mathrm{N_{bc}}(E) = 18$. Figure was drawn by Photoshop.

Global efficiency, E_{glob}

For a graph, the $\mathbf{E_{glob}}$ reflects how efficiently information can be exchanged over $\boldsymbol{G}$. The $\mathbf{E_{glob}}$ of $\boldsymbol{G}$ is defined as (Achard & Bullmore, 2007; Latora & Marchiori, 2001):

$$\mathrm{E_{glob}(G)} = \frac{1}{\mathrm{N(N-1)}} \sum_{\mathrm{i \neq j \in G}} \frac{1}{\mathrm{d_{ij}}}$$

Local efficiency, E_{loc}

For a graph, $\boldsymbol{E_{loc}}$ reveals how much a system is fault tolerant. It indicates how information exchange is altered for the neighbors of a node $\boldsymbol{i}$ when node $\boldsymbol{i}$ is removed (Latora &

Marchiori, 2001). This is done by defining a subnetwork that covers the neighbors of node $\boldsymbol{i}$, hence building a subgraph $\boldsymbol{G_i}$. By calculating its efficiency and averaging across all subgraphs $\boldsymbol{G_{i,}}$ a measure of the 'local' efficiency $\boldsymbol{E_{loc}}$ of $\boldsymbol{G}$ may be obtained: (Achard & Bullmore, 2007; Latora & Marchiori, 2001):

$$\mathrm{E_{loc}(G)} = \frac{1}{\mathrm{N}} \sum_{\mathrm{i \in G}} \mathrm{E_{glob}(G_i)},$$

where $\boldsymbol{E_{loc}(G_i)}$ is the global efficiency of the subgraph $\boldsymbol{G_i}$ and $\boldsymbol{N}$ is the number of nodes in the graph $\boldsymbol{G}$.

Regional network parameters

To examine the regional characteristics of functional brain networks, two nodal metrics were considered: the *nodal degree* ($\boldsymbol{D_{nod}}$) and the *betweeness degree* ($\boldsymbol{N_{bc}}$).

Nodal degree, $\mathbf{N_{dc}}$

$\mathbf{N_{dc}}(\boldsymbol{i})$ of a node $\boldsymbol{i}$ measures the importance of node $\boldsymbol{i}$ in the whole network. The $\mathbf{N_{dc}}(\boldsymbol{i})$ is calculated as the sum of edges connected to the node $\boldsymbol{i}$ (Figure 14c). In terms of the adjacency matrix, the $\mathbf{N_{dc}}$ of a node i is defined as:

$$\mathrm{N_{dc}(i)} = \sum_{\mathrm{j \neq i \in G}} \mathrm{a_{ij}},$$

where $\mathbf{a_{ij}}$ is the $(\boldsymbol{i}, \boldsymbol{j})$ th element in the adjacency matrix.

Betweenness degree, $\mathbf{N_{bc}}$

The $\mathbf{N_{bc}(i)}$ of a node $\boldsymbol{i}$ measures the influence of node $\boldsymbol{i}$ over information flow between other nodes in the whole network. The $\mathbf{N_{bc}(i)}$ of a node $\boldsymbol{i}$ is calculated as the fraction of pairs of nodes that are connected with each other (Figure 14d)

$$\mathrm{N_{bc}(i)} = \sum_{\mathrm{j \neq i \neq k \in G}} \frac{\delta_{\mathrm{jk}}(\mathrm{i})}{\delta_{\mathrm{jk}}},$$

where $\boldsymbol{\delta_{jk}}$ is the number of shortest paths from node $\boldsymbol{j}$ to node $\boldsymbol{k}$, and $\boldsymbol{\delta_{jk}(i)}$ is the number of those paths that pass through node $\boldsymbol{i}$.

Small-world topology

Network topology is the way in which a network is set up with nodes and edges. The topology is the key to understand the performance of a network, such as its efficiency, cost or optimality. The small-world topology here is an optimized organization that balances the advantages of both regular and random network topology.

Mathematically, the small-world topology of a network (Figure 15) is characterized by a higher clustering coefficient $\boldsymbol{C_p}$ and equal characteristic path length $\boldsymbol{L_p}$ when compared with a matched random network (Watts & Strogatz, 1998). Here, the matched random networks were generated using the random rewiring procedure described by Maslov and Sneppen. The matched random networks should have a random topology that shares the same size and degree (strength) distribution with the original network (Maslov & Sneppen, 2002). The small-world topology was calculated as:

$$\gamma = {\mathrm{C_p^{real}}}\Big/{\mathrm{C_p^{rand}}},$$

$$\lambda = {\mathrm{L_p^{real}}}\Big/{\mathrm{L_p^{rand}}},$$

where $\boldsymbol{C_p^{real}}$ and $\boldsymbol{L_p^{real}}$are clustering coefficient $\boldsymbol{C_p}$ and characteristic path length $\boldsymbol{L_p}$ of the real network (cerebellar networks in this study), and $\boldsymbol{C_p^{rand}}$ and $\boldsymbol{L_p^{rand}}$ of the matched random networks. Practically, a network could be categorized as small world if $\boldsymbol{\gamma > 1}$, $\boldsymbol{\lambda \approx 1}$ and also could be summarized into a simple quantitative measurement, small-worldness, $\boldsymbol{\sigma = {\gamma}/{\lambda} > 1}$.

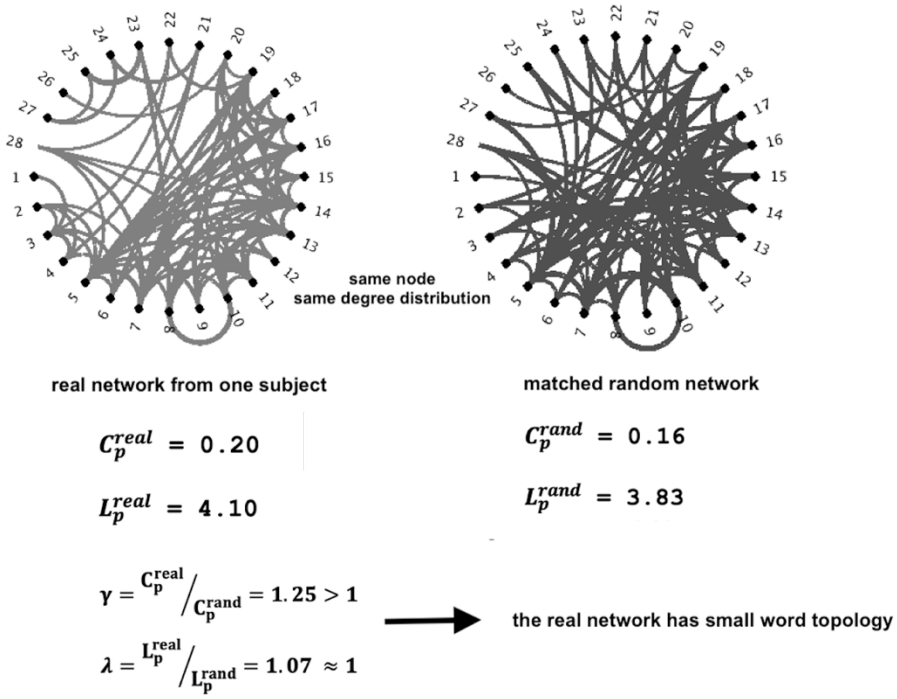

Figure 15. The illustration of a network with small-world topology and its matched random network. Two networks share the same nodes and degree distribution. A network was considered to show small world topology should have a higher clustering coefficient $\boldsymbol{C_p}$, but similar characteristic path length $\boldsymbol{L_p}$ when compared with the matched random network. Figure was drawn by Matlab2015.

Modularity analysis

Network modularity quantifies the degree to which a network can be optimally partitioned into distinct subnetworks. A network with a high modularity ensures the optimal balance of local segregation of function and global integration of information, see Figure 16. The algorithm of Newman (Newman & Girvan, 2004) was used here to determine the community structure of the network. The modularity ($\boldsymbol{Q}$) was calculated by:

$$Q = \frac{1}{2M}\sum_{i,j\in G}(a_{ij} - \frac{D_i D_j}{2M})\delta_{ij,}$$

where $\boldsymbol{M}$ is the total number of edges of the graph, $\boldsymbol{a_{ij}}$ is the $(\boldsymbol{i, j})$ th element in the adjacency matrix, the $\boldsymbol{D_i}$ and $\boldsymbol{D_j}$ are degree of nodes $\boldsymbol{i}$ and $\boldsymbol{j}$, respectively. The $\boldsymbol{\delta}$-function, $\boldsymbol{\delta_{ij}}$ is set to one if vertices $\boldsymbol{i}$ and $\boldsymbol{j}$ are in the same module, zero otherwise.

Here, Louvain method was used for module detection (Blondel *et al*, 2008). At first, each node was assigned to a different module and the beginning $\boldsymbol{Q}$ was equal to zero ($\boldsymbol{\delta_{ij} = 0}$).

Then, each node $\boldsymbol{i}$ was remove from its module and put it into another module $\boldsymbol{j}$. A new modularity $\boldsymbol{Q}$ was calculated and the node $\boldsymbol{i}$ could stay in the module $\boldsymbol{j}$ only when $\boldsymbol{Q}$ value increased, otherwise node $\boldsymbol{i}$ stays in its original module. This step was applied repeatedly and sequentially for all the nodes and in the end, when the maximum $\boldsymbol{Q}$ was obtained and its corresponding categorical variable containing all the nodes belong to which module was generated.

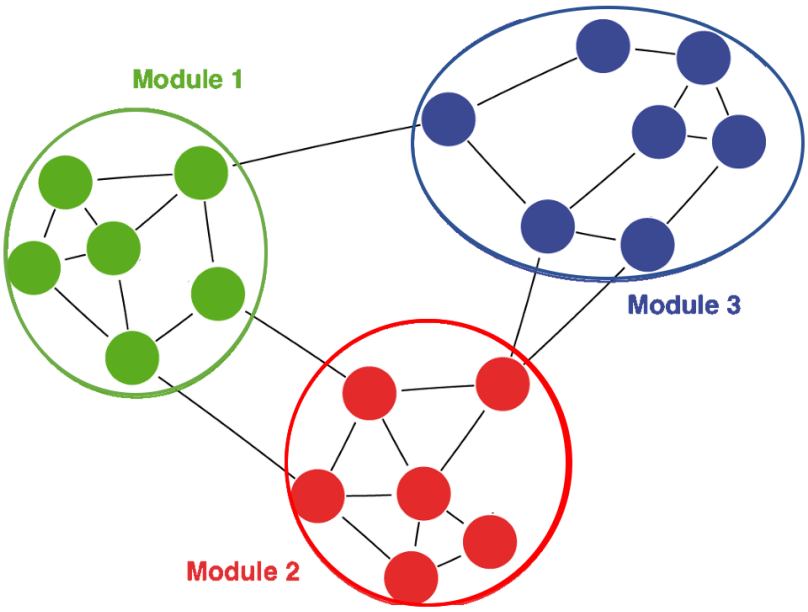

Figure 16. An example of a network with three different modules. A network with high modularity has more connection within the same module but less connection between the different modules. Figure was drawn by Photoshop.

Statistical analysis

Non-parametric analysis of covariance (ANCOVA) was used to compare the differences of the global network characterizations (C_p, L_p, $\mathrm{E_{glob}}$, $\mathrm{E_{loc}}$, γ, λ, σ, Q) among three groups.

Non-parametric ANCOVA models were applied to investigate the group difference in the regional nodal parameters ($\mathrm{D_{nod}}$, $\mathrm{N_{bc}}$) for the 28 cerebellar regions.

All the models were controlled for age, gender, site, and frame-wise displacement. As a statistical threshold, a Bonferroni-corrected p value less than 0.05 was considered as significant.

3.3.3 Results

Demographic and clinical data

The demographic and clinical data is previously presented in **chapter 3.1.3** (page 29). The three groups, 49 HC, 16 MSA-C, 13 $SAOA_{>10y}$ did not differ in age, gender but showed a marginal difference on site distribution. The average SARA scores and mean age of onset was statistically the same for both MSA-C and SAOA groups, but by definition the SAOA group has significant longer disease duration than MSA-C group.

Global network characterization in the cerebellar networks

ANOVA did not reveal a significant change in any of the global network metrics (C_p, L_p, $\mathrm{E_{glob}}$, $\mathrm{E_{loc}}$) (Table 3).

Small-world topology in the functional cerebellum

The cerebellar networks exhibit prominent features of small-world topology, not only in the healthy group but also in the two ataxia groups (Table 3, all σ > 1). The small-world topology was also expressed by a higher local efficiency (Table 3, all $\gamma > 1$) and a comparable lower global efficiency than random networks (Table 3, all $\lambda \approx 1$).

In addition, none of these small-work topology (γ, λ, σ) displayed significant difference among the three group (Table 3, all p > 0.05).

Modularity in the functional cerebellum

All the cerebellar functional networks were found to have a modular architecture. However, no significant differences were found in the cerebellar modularity among the three groups (Table 3, p > 0.05).

Network properties	Groups			Statistic
	HC	MSA-C	$SAOA_{>10y}$	F_{77} (p value)
C_p	0.37 ± 0.13	0.35 ± 0.08	0.36 ± 0.10	0.17 (0.84)
L_p	4.06 ± 1.61	4.47 ± 1.68	4.39 ± 2.00	0.45 (0.64)
E_{glob}	0.28 ± 0.12	0.25 ± 0.08	0.27 ± 0.11	0.62 (0.54)
E_{loc}	0.38 ± 0.13	0.35 ± 0.10	0.36 ± 0.10	0.41 (0.66)
γ	1.72 ± 0.92	2.10 ± 1.24	1.77 ± 0.82	0.93 (0.40)
λ	1.16 ± 0.15	1.17 ± 0.25	1.20 ± 0.28	0.22 (0.81)
σ	1.47 ± 0.70	1.79 ± 0.99	1.47 ± 0.64	1.13 (0.33)
Q	0.27 ± 0.14	0.34 ± 0.15	0.28 ± 0.14	1.28 (0.28)

Table 3. Global network characterization of functional cerebellar networks. Measures are presented as mean ± SD. The statistical values are given as F values together with original p value (uncorrected).

Considering this finding, the cerebellar networks of all the subjects were concatenated and averaged as a group-cerebellar network, and the final cerebellar modularity was calculated based on this group-level network.

The group-cerebellar network could be divided into three separate functional submodules (Q = 0.12). Module 1 consisted of bilateral I-IV-V-VI-Crus I-vermis VI, module 2 covered the midline structure including vermis Crus I-Crus II-VIIb-VIIIa-VIIIb-IX-X, and module 3 consisted of bilateral Crus II-VIIb-VIIIa-VIIIb-IX-X (Figure 17).

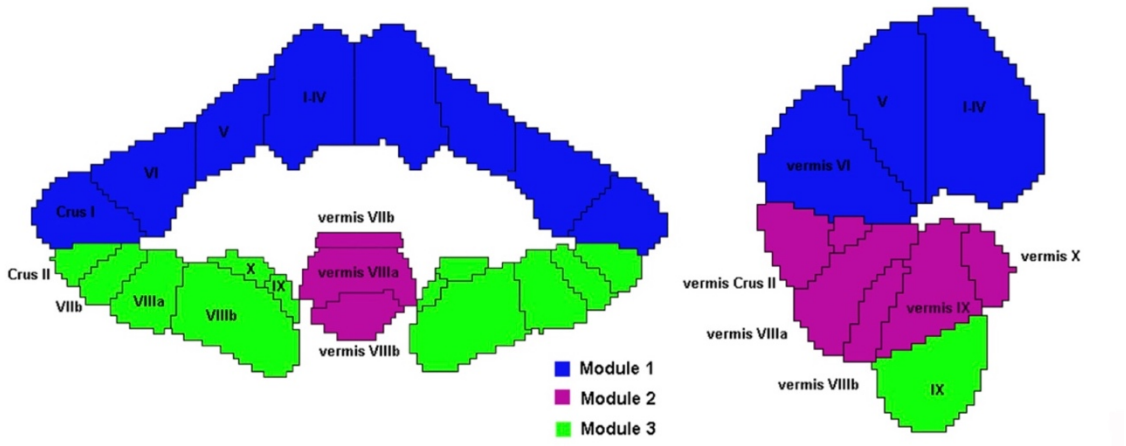

Figure 17. Modular architecture of the group-cerebellar networks. Within the cerebellar network, three distinct modules were found. The module 1 included bilateral I-IV-V-VI-Crus I-vermis VI, module 2 included the midline structure vermis Crus I-Crus II-VIIb-VIIIa-VIIIb-IX-X, and module 3 contained bilateral Crus II-VIIb-VIIIa-VIIIb-IX-X.

Regional network characterization in functional cerebellum

When corrected with Bonferroni correction ($p < 0.05$), none of the 28 cerebellar regions was significantly different from the HC group in the nodal degree and the betweenness degree in the two sporadic ataxia groups. Only the left X region of the cerebellum had a larger betweenness degree in the MSA-C group but it was uncorrected for multiple comparisons.

The original p values were presented in the Table 4a and 4b.

Node	***Left cerebellum***				***Right cerebellum***				***Vermis***			
	HC	**MSA-C**	**SAOA$_{>10y}$**	**F_{77} (p value)**	**HC**	**MSA-C**	**SAOA$_{>10y}$**	**F_{77} (p value)**	**HC**	**MSA-C**	**SAOA$_{>10y}$**	**F_{77} (p value)**
I-IV	3.86 ± 4.84	3.17 ± 2.48	3.65 ± 3.97	0.15 (0.86)	4.06 ± 4.81	3.16 ± 2.30	3.63 ± 4.15	0.27 (0.77)	/	/	/	/
V	4.52 ± 4.73	3.11 ± 2.00	5.38 ± 4.52	1.08 (0.35)	5.35 ± 5.15	3.98 ± 2.72	4.89 ± 3.85	0.55 (0.58)	/	/	/	/
VI	5.83 ± 4.76	5.08 ± 3.41	5.84 ± 4.32	0.18 (0.83)	6.70 ± 4.58	5.31 ± 3.12	5.56 ± 4.19	0.82 (0.44)	5.78 ± 5.17	4.39 ± 3.98	5.52 ± 4.55	0.51 (0.60)
crus I	7.17 ± 3.89	4.97 ± 3.40	7.05 ± 4.20	2.05 (0.14)	7.03 ± 4.06	5.18 ± 3.40	6.11 ± 4.54	1.35 (0.27)	1.53 ± 1.74	0.88 ± 1.00	1.56 ± 1.90	1.00 (0.37)
crus II	6.94 ± 3.58	5.71 ± 3.23	6.48 ± 4.00	0.71 (0.49)	6.99 ± 3.75	4.75 ± 3.10	6.31 ± 4.21	2.21 (0.12)	4.77 ± 4.84	2.87 ± 2.88	5.12 ± 4.40	1.28 (0.28)
VIIb	6.08 ± 4.12	5.23 ± 3.16	4.37 ± 4.08	1.07 (0.35)	6.18 ± 4.20	5.54 ± 3.28	4.71 ± 4.31	0.72 (0.49)	3.98 ± 3.95	2.29 ± 2.31	4.15 ± 3.01	1.53 (0.22)
VIIIa	5.13 ± 3.71	4.54 ± 3.01	4.67 ± 4.08	0.20 (0.82)	5.38 ± 4.02	4.78 ± 2.69	4.48 ± 3.86	0.37 (0.69)	5.11 ± 4.62	4.27 ± 3.45	5.18 ± 4.11	0.25 (0.78)
VIIIb	3.82 ± 3.97	3.65 ± 2.84	3.32 ± 3.11	0.10 (0.91)	4.05 ± 4.17	4.47 ± 2.87	3.76 ± 3.05	0.14 (0.87)	3.95 ± 3.97	3.19 ± 2.47	3.82 ± 4.89	0.23 (0.80)
IX	4.37 ± 4.69	4.01 ± 3.71	4.32 ± 4.34	0.02 (0.98)	4.94 ± 4.50	3.72 ± 3.03	4.49 ± 4.28	0.52 (0.60)	4.34 ± 4.23	3.61 ± 3.26	4.47 ± 3.82	0.23 (0.79)
X	3.33 ± 3.90	1.82 ± 1.85	1.84 ± 3.29	1.68 (0.19)	3.34 ± 3.70	1.15 ± 1.00	2.14 ± 2.26	3.21 (0.06)	2.25 ± 2.62	1.39 ± 1.41	1.58 ± 2.08	1.01 (0.37)

Table 4a. Summary of the nodal degree for the different cerebellar regions. Data are shown as mean ± SD. And the statistical values are given as F values and original p values.

Node	Left cerebellum				Right cerebellum				Vermis			
	HC	MSA-C	SAOA >10y	F 77(p value)	HC	MSA-C	SAOA >10y	F 77(p value)	HC	MSA-C	SAOA >10y	F 77(p value)
I-IV	11.78 ± 29.22	5.73 ± 8.02	3.38 ± 4.97	0.85 (0.43)	13.69 ± 28.89	10.71 ± 16.97	6.25 ± 10.84	0.49 (0.62)	/	/	/	/
V	10.65 ± 23.50	5.66 ± 8.62	14.71 ± 19.68	0.70 (0.50)	12.77 ± 16.53	10.72 ± 14.14	12.21 ± 12.97	0.11 (0.90)	/	/	/	/
VI	11.94 ± 17.91	15.24 ± 18.12	15.82 ± 14.64	0.38 (0.68)	20.61 ± 18.89	17.66 ± 21.62	12.67 ± 16.57	0.92 (0.40)	16.82 ± 26.01	19.69 ± 22.31	20.05 ± 34.23	0.12 (0.89)
crus I	16.81 ± 20.86	18.00 ± 20.90	24.32 ± 32.98	0.54 (0.59)	14.41 ± 16.74	13.74 ± 11.27	9.74 ± 10.74	0.51 (0.61)	2.92 ± 8.66	1.14 ± 2.84	2.67 ± 7.74	0.32 (0.72)
crus II	18.71 ± 25.46	24.28 ± 28.36	19.86 ± 21.61	0.29 (0.75)	15.41 ± 16.69	25.10 ± 27.78	13.27 ± 11.67	1.91 (0.16)	11.24 ± 15.99	18.56 ± 38.90	12.48 ± 17.21	0.63 (0.53)
VIIb	16.58 ± 18.45	12.02 ± 18.65	6.83 ± 12.12	1.70 (0.19)	18.26 ± 26.78	21.53 ± 27.95	10.57 ± 13.18	0.71 (0.50)	7.20 ± 12.51	7.46 ± 16.03	11.09 ± 16.01	0.41 (0.66)
VIIIa	14.86 ± 20.35	17.17 ± 19.10	9.81 ± 11.75	0.56 (0.57)	15.64 ± 20.15	21.40 ± 25.74	11.31 ± 13.97	0.90 (0.41)	15.86 ± 20.03	19.00 ± 15.62	9.62 ± 8.69	1.02 (0.36)
VIIIb	7.94 ± 15.44	6.98 ± 14.68	11.20 ± 15.16	0.31 (0.74)	8.85 ± 12.56	14.23 ± 17.69	14.53 ± 22.95	1.12 (0.33)	16.81 ± 27.18	17.12 ± 19.22	12.64 ± 23.96	0.15 (0.86)
IX	8.39 ± 14.29	15.39 ± 25.80	11.02 ± 15.24	1.00 (0.37)	12.83 ± 17.92	8.73 ± 12.59	25.31 ± 31.45	2.75 (0.07)	14.50 ± 17.57	15.71 ± 26.43	14.00 ± 13.62	0.03 (0.97)
X	4.57 ± 8.55	18.85 ± 38.20	1.71 ± 2.97	4.27 (0.02*)	7.70 ± 13.05	3.17 ± 5.89	3.79 ± 6.10	1.36 (0.26)	3.48 ± 9.40	7.20 ± 14.24	1.94 ± 4.50	1.16 (0.32)

Table 4b. Summary for the betweenness degree across all the cerebellar regions. Date are displayed by mean ± SD and the statistic values are displayed by F (original p values). Statistically, none of cerebellar regions showed significant difference among three groups but region X showed a higher betweenness degree in the MSA-C group in uncorrected level.

Correlation with clinical measures

No significant correlations were found between network measures and clinical variables (SARA scores, disease duration and age of onset) in either MSA-C or SAOA group.

3.3.4 Discussion

This study was the first describing the functional cerebellar network topology in the ataxia groups. Additionally, the modular architecture of the cerebellum was derived. The cerebellar networks in both ataxia groups showed no significant differences in global and local network organization from the healthy group. The cerebellar networks exhibited a small-world topology and consisted of three modules, which largely resemble the functional partition of the cerebellum.

This study was also the first to demonstrate that the cerebellum has optimal organization from a network science. Point of view It is largely accepted that the whole brain network has a well-organized configuration (Bassett & Bullmore, 2006; Sporns, 2018). However, the configure of the cerebellum, as a distinct subnetwork, has never previously been explored. Our network analysis revealed that the cerebellar functional networks had the small-world topology, reflecting a network that well-balanced the efficiency and the costs (Watts & Strogatz, 1998). Hence, the cerebellum in MSA-C and SAOA may act in cooperation with the brain network, suggesting a similar and optimized mechanism.

The modularity analysis revealed that the functional cerebellar network can be divided into three separate modules. Modules 1 comprises lobules I-IV, V, VI, and crus I, the vermis makes up module 2, and module 3 covers crus II and lobules VIIb, VIII, IX and X. This division showed high overlap with a previously reported structural parcellation of the cerebellum. In this structural parcellation, the cerebellum can be divided into the anterior cerebellum (lobules I-IV, V), the posterior cerebellum (lobules VI, crus I-II, VII, VIII, IX) and the flocculonodular (lobule X) lobe, each division regulating different functions. Generally speaking, the anterior cerebellum is mainly involved in motor processing, the posterior cerebellum in cognitive processing and the flocculonodular lobe in vestibule function and eye movement control (Samson & Claassen, 2017; Stoodley & Schmahmann, 2010). In the present study, the functional module 1 fitted the anterior cerebellum well, and the modules 2 and 3 were matched mainly to the posterior cerebellum. Thus, the high overlap between the functional modules and the structural parcellation may suggest a structural basis for the functional segregation in the cerebellum. At the same time, mismatches between the functional modules and structural parcellation were also found. First, lobules VI and crus I were clustered in a way more connected to anterior (motor) cerebellum than

to the posterior (cognition) cerebellum. This suggess that the functional boundary is vague; indeed, multiple processing involved in both motor activity and cognition has been reported in these two regions (Mottolese *et al*, 2013; Stoodley & Schmahmann, 2010; Stoodley *et al.*, 2012). Second, the lobule X was reported to bind closely with the posterior cerebellum – specifically, lobule IX – rather than being an isolated module (flocculonodular), suggesting its engagement with the posterior module (Guell & Schmahmann, 2020). In addition, the vermis was observed to be an independent functional module. The vermis is classically known as a middle part connecting the two hemispheres. Further, the role of the vermis in affective processing and limbic functions had been reported (Schmahmann, 2004; Stoodley & Schmahmann, 2010). Therefore, the finding in this study that the vermis is a functionally distinct module may lead to a better understanding of functional cerebellar representation.

In the ataxia groups, the functional cerebellar architecture as a whole exhibited a network topology that did not differ from that of the healthy group. For example, the small-world topology and modularity was observed in the ataxia groups as well. This finding may indicate the stability of the cerebellar system, giving the cerebellum the ability to combat the disease. This indication was more obvious when global and local efficiency was conserved in the ataxia groups. These two efficiency measurements were directly related to errors tolerance of a network (Latora & Marchiori, 2001). The unaltered efficiency of the cerebellar functional networks in the ataxia groups may indicate that the ataxia patients maintain the ability to deal with an attack of illness. The similarly unaffected voxel-level functional connectivity (ALFF and DC) in the Study 2 (**chapter 3.2**), further indicates that the cerebellum maintains its performance, including resilience to the disease at a global and local level.

This study has some methodological issues. First, the basic idea behind the study was to focus on the intracerebellar connectivity by isolating the cerebellum from the brain. This focus had the limitation of ignoring the connection between the cerebellum and the cerebrum, which may affect the cerebellar topology. Second, the small patient size may have failed to reveal all possible between-group differences. Finally, the topologic properties were dynamic rather than static; therefore, further studies with more datasets

are needed to examine whether the cerebellar networks dynamically works against the disease in MSA-C and SAOA in order to conserve the function.

3.4 Study 4: Cerebellar-cerebral functional connectivity in MSA-C and SAOA

3.4.1 Introduction

The cerebellum is closely connected with the cerebrum, and its connectivity pattern is intricately related to intrinsic cerebral networks (Buckner *et al.*, 2011; Habas *et al.*, 2009). However, it remains unclear how the functional modules of cerebellum, as described above, interact with the cerebral cortex. Investigation of the connectivity between the cerebellar functional modules, on the one hand, and the cerebellar cortex, on the other hand, could yield a better understanding of the way in which pathological changes within the cerebellum may affect cerebral function on a larger scale.

Recently, two studies examined the cerebellar-cerebral connectivity maps, by choosing cerebellar lobules as a region of interest (ROI) in MSA-C patients (Ren *et al.*, 2018; Zheng *et al.*, 2019). Ren and colleagues found that lobule VIII showed the most pronounced effect (i.e. largely decreased ALFF), leading to decreased connectivity to the inferior parietal lobule, lingual gyrus, parahippocampus and middle temporal gyrus in the MSA-C group (Ren *et al.*, 2018). Zheng and colleagues found a reduced regional cerebral blood flow in certain cerebellar regions including left crus I, left VI and vermis V, and a disconnection to the default mode network, sensorimotor network and visual associated cortices (Zheng *et al.*, 2019). However, taking only small parts of the cerebellum as a ROI may be too local a focus to provide a wider view in investigating the connections in cerebellar-cerebral circuits. Moreover, no study has examined such functional connectivity in SAOA patients so far. It also remains unknown whether the connections in the cerebellar-cerebral circuits show some differentiation between the two sporadic ataxia groups.

In the present study, this approach was extended by investigating connectivity changes on a functional module level. Whereas Ren et al., and Zheng et al., focused on small anatomical regions, here the ROIs were based on the modular structure of the cerebellum. The three cerebellar modules revealed in Study 3 (**chapter 3.3**) were considered as ROIs to analyse the their connectivity with the cerebrum. The analysis was extended to include the $SAOA_{>10y}$ group. The goals of the study were 1) to describe the cerebellar-cerebral connectivity, based on the functional modules of the cerebellum, and 2) to determine whether the cerebellar-cerebral connectivity patterns are altered in the ataxia groups.

3.4.2 Study specific methods

Cerebellar ROI-definition and connectivity

According to the results from Study 3 (Figure 17, page 57), the three cerebellar modules derived from the functional connectivity analysis were used as ROIs. For each ROI, the time series of every voxel within the ROI was extracted. The spatial average of each time series of a module was used for the subsequent connectivity analysis. This calculation was performed for each participant separately.

To generate an individual voxel-wise cerebellar-cerebral functional connectivity (ccFC) map, Pearson correlation coefficients were calculated between these module-specific time series and each voxel of the supratentorial cerebrum, finally generating three connectivity maps for each subject. These correlation coefficient maps were converted into z-maps by applying Fisher's r-to-z transformation to improve the normality of the distribution across coefficient maps (Fox *et al.*, 2005). As the final preprocessing step, the z-maps were spatially smoothed using an 8mm isotropic Gaussian smoothing kernel.

Statistical analysis

All image data were statistically analyzed using the SnPM toolbox (http://warwick.ac.uk/snpm).

Within-group cerebellar-cerebral functional connectivity pattern

A non-parametric one-sample t-test was used based on the z-maps to identify cerebral voxels that exhibited significant correlations with the given ROI. This step was performed for each group separately, leading to three maps per group representing the cerebellar-cerebral functional connectivity patterns with the corresponding cerebellar modules. The significance level was set at $p < 0.05$ FWE corrected.

For each cerebellar ROI in the following group difference analysis, a union mask was generated by the union set of all significant clusters from the within-group, one-sample t-tests. This step was to make sure that every voxel inside the mask was significantly connected to the cerebellar modules, at least in one group.

Group differences in the cerebellar-cerebral functional connectivity pattern

Within the union mask for each cerebellar ROI, a non-parametric, one-way ANCOVA was used to compare group differences of the ccFC maps among the three groups. The effects of age, gender, scanner site and motion parameters were modelled as covariates. The findings were further analyzed using post-hoc t-tests (HC and MSA-C, HC and $SAOA_{>10y}$, MSA-C and $SAOA_{>10y}$). The significance level here was set at FWE corrected $p < 0.01$.

Correlation analysis

To assess the relationship between altered ccFC maps and clinical assessments in the ataxia groups, linear regression models were used to analyze any relationship between connectivity and clinical variables like SARA total sum score, disease duration, and disease onset. The calculation were performed separately for each clinical variable. In order to control for unspecific effects, the influence of age, gender, scanning site and motion parameters were parceled out using the linear model. As statistical threshold, a Bonferroni-corrected $p < 0.05$ was chosen.

3.4.3 Results

Demographic and clinical data

As described in *3.1.3 Results- Demographic and clinical data* (page 29), the three groups, 49 HC, 16 MSA-C and 13 $SAOA_{>10y}$ did not differ in age and gender but a marginal difference on site distribution existed.

SARA scores and age of onset did not differ between MSA-C and $SAOA_{>10y}$ but SAOA group has a significant longer disease duration than MSA-C group.

Within-group cerebellar-cerebral functional connectivity pattern

In the HC group, the activity of all three cerebellar modules mainly showed a positive correlation with the signal fluctuations in the thalamus. Negative correlation patterns were exhibited in the postcentral gyrus and precentral gyrus. Beyond that, module 1 and 3 showed a positive correlation with the frontal gyrus and a negative correlation with gyrus rectus and the lingual gyrus (Figure 18A, Table 5, Table 6 and Table 7).

For the two sporadic ataxia groups, a negative correlation between all three modules and the postcentral and precentral gyrus was found, resembling the result obtained for HC, but the extend of the clusters was drastically reduced for both patient groups. In addition,

the activity of three cerebellar modules consistently showed a negative relation with the MR signal of the frontal/occipito-temporal cortex, even though the extend of the significant clusters was reduced, as already observed for the sensory-motor cortex. A positive correlation between the thalamus and the cerebellar modules was not found in the ataxia groups. Detailed listings of significant cerebellar-cerebral correlations as visualized in Figure 18 are given in Table 5, Table 6 and Table 7.

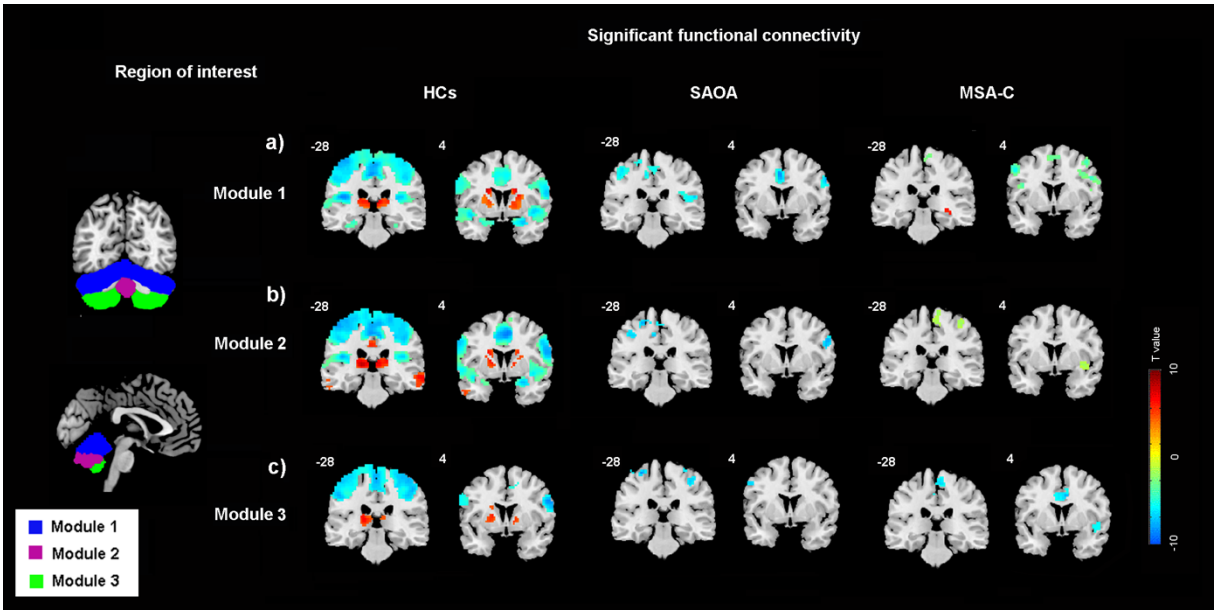

Figure 18. **Significant functional connectivity of cerebellar regions of interest with cortical and subcortical structure**. Patterns of significantly positive (red) and negative (blue) functional connectivity for the module 1 a), module 2 b) and module 3c) in the three groups. Multiple comparisons correction was performed using FWE corrected $p < 0.05$.

Group	Cluster size	MNI coordinates [mm] of the peak voxel			T-value	Side	Anatomical regions
		x	y	z			
HC	14585	-42	-30	18	-9.72	R	postcentral and precentral gyrus
	1061	-18	-12	21	9.97	R	caudate nucleus, thalamus
	567	30	51	-15	6.42	L	middle frontal gyrus
	435	-33	60	-6	5.80	R	middle/inferior frontal gyrus
	186	60	-51	36	4.46	L	angular gyrus, supramarginal gyrus
	144	42	27	51	5.12	L	middle frontal gyrus
	134	-42	-51	33	4.80	R	angular gyrus
	133	0	24	69	5.50	/	supplementary motor area, superior frontal gyrus
$SAOA_{>10y}$	529	0	0	36	-9.96	/	median and anterior cingulate
	265	51	-33	15	-10.04	L	superior temporal gyrus, precentral gyrus, rolandic operculum
	122	-42	-30	54	-6.71	R	postcentral and precentral gyrus
	118	15	48	51	-8.43	L	superior frontal gyrus
	115	-12	-105	0	11.26	R	middle/inferior occipital gyrus
MSA-C	1652	-6	42	45	-11.13	R	superior frontal gyrus, anterior cingulate
	687	39	36	-3	-7.39	L	inferior frontal gyrus
	223	-51	0	42	-7.50	R	precentral and postcentral gyrus
	158	-51	24	24	7.05	R	middle/inferior frontal gyrus
	120	-24	-42	66	5.50	R	precentral and postcentral gyrus
	98	12	-39	54	-7.32	L	precuneus, paracentral
	150	39	-39	-12	7.21	L	fusiform gyrus, hippocampus, inferior temporal gyrus
	100	27	-69	6	8.45	L	calcarine fissure, superior occipital gyrus

Table 5. Significant positive and negative functional connectivity between cerebellar module 1 and the cerebrum in three groups. Negative correlation between the activity of module 1 and postcentral and precentral gyrus was found in all three group, but the extent of the clusters are drastically reduced for both patient groups. In addition, positive correlation to the thalamus was only found in the HC group. Multiple comparisons correction was performed using FWE correction $p < 0.05$. *L, left; R, right*.

Group	Cluster size	MNI coordinates [mm] of peak voxel			T-value	Side	Anatomical regions
		x	y	z			
HC	5828	-54	-9	30	-6.80	R	postcentral and precentral gyrus
	695	-21	-21	15	7.42	R	thalamus
$SAOA_{>10y}$	252	-39	-6	42	-10.31	R	postcentral and precentral gyrus
	194	45	-21	60	-7.13	L	postcentral gyrus
MSA-C	368	15	45	54	-11.10	L	superior frontal gyrus, supplementary motor area
	175	54	30	12	-6.58	L	inferior frontal gyrus
	167	6	60	36	-7.68	L	superior/middle frontal gyrus
	139	3	-30	66	-7.43	L	paracentral lobule, precuneus, cingulate
	115	6	3	36	-7.56	L	cingulate, superior frontal gyrus
	85	42	9	-12	-7.13	L	insula, heschl gyrus

Table 6. Significant positive and negative functional connectivity between cerebellar module 2 and the cerebrum in three groups. Negative correlations between cerebellar module 2 and the precentral and postcentral gyrus was found in three groups. In the HC group, a positive correlation was found to be related to the thalamus. No positive correlations were found in the two ataxia group. Multiple comparisons correction was applied using FWE $p < 0.05$. *L, left; R, right*.

Group	Cluster size	MNI coordinates [mm] of peak voxel			T-value	Side	Anatomical regions
		x	y	z			
HC	9923	0	-15	51	-9.32	/	postcentral and precentral gyrus, supplementary motor area
	4624	18	-48	0	-7.44	L	lingual gyrus
	87	9	21	-12	-5.31	L	rectus gyrus
	3553	36	15	42	7.25	L	middle/inferior frontal gyrus
	818	45	-75	42	8.49	L	angular gyrus
	780	-21	-18	12	7.66	R	thalamus
	746	-45	-66	48	7.57	R	angular gyrus
	626	0	-39	36	7.05	/	cingulate, precuneus
	432	-60	-57	-12	7.54	R	inferior/middle temporal gyrus
$SAOA_{>10y}$	352	-24	-33	60	-10.28	R	postcentral and precentral gyrus
	225	30	-6	60	-8.49	L	postcentral and precentral gyrus
MSA-C	372	51	-12	42	-22.66	L	postcentral and precentral gyrus
	244	12	60	15	-7.40	L	superior frontal gyrus
	126	6	-33	63	-8.76	L	paracentral lobule, supplementary motor area
	98	39	-3	-3	-6.64	L	insula
	74	-21	-48	69	-6.02	R	superior parietal gyrus, paracentral lobule
	68	18	18	51	-5.58	L	superior frontal gyrus

Table 7. Significant positive and negative functional connectivity between cerebellar module 3 and the cerebrum in three groups. Negative correlations were found between the activity of module 3 and the precentral and postcentral gyrus in the HC group as well as in the two ataxia groups. However, positive correlations were only observed in the HC group, between module 3 and thalamus and angular gyrus. Results were thresholded by FWE $p<0.05$. *L, left; R, right*.

Group differences in the cerebellar-cerebral functional connectivity pattern

The MSA-C group showed a reduced positive connectivity between module 1 and the inferior/middle frontal gyrus and a reduced negative connectivity between module 1 and the postcentral gyrus when compared with the HC group. The negative connectivity between module 1 and the parahippocampal, fusiform and lingual gyrus is increased. (Figure 19, Table 8). For the $SAOA_{>10y}$ group, no difference in connectivity was observed for module 1 compared with the HC group or with the MSA-C group.

For module 2, no statistically significant difference was found among the three groups.

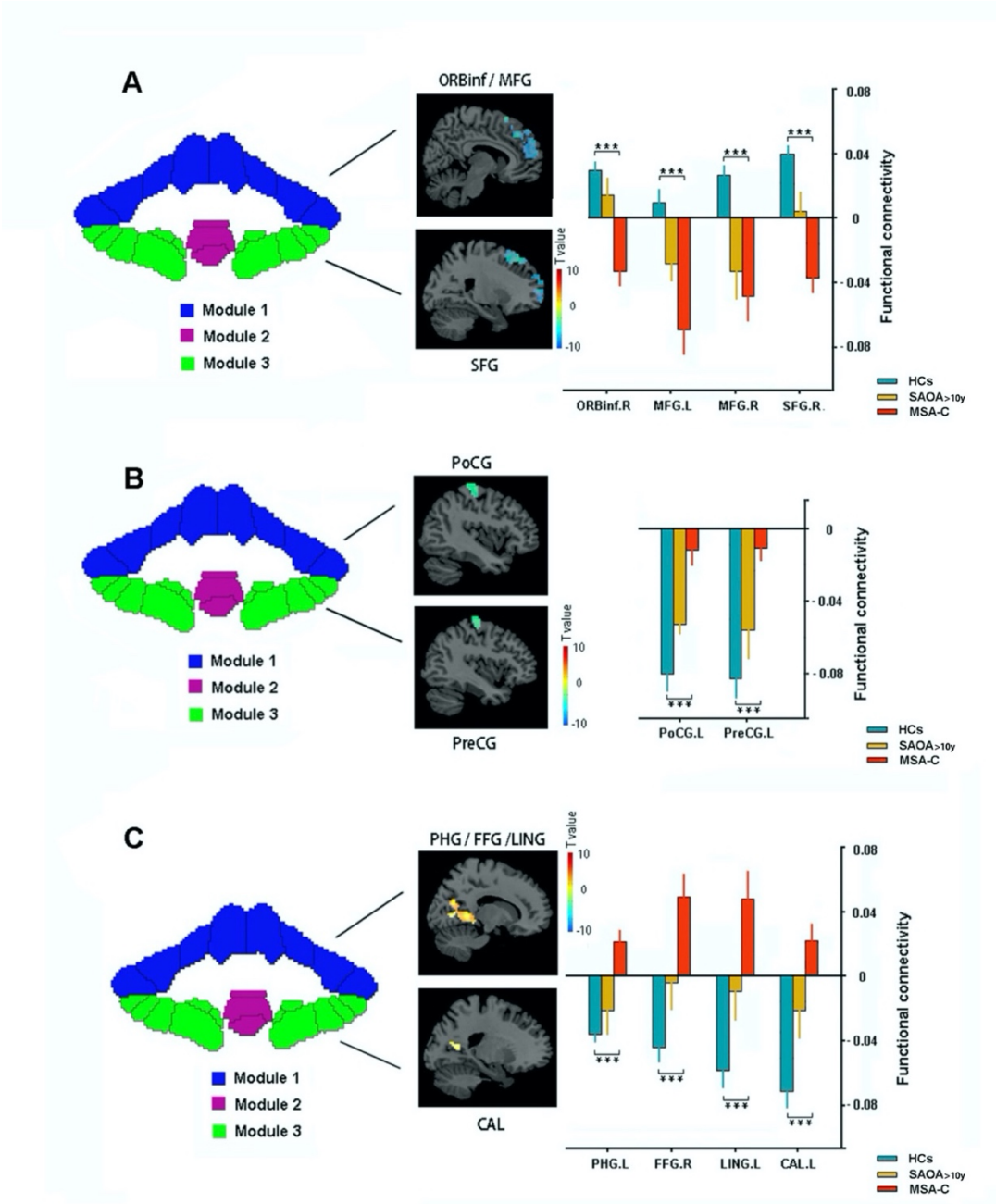

Figure 19. Three group differences in the functional connectivity between cerebellar modules and the cerebrum. The MSA-C group showed A) a reduced positive connectivity between the cerebellum and the ORBinf/MFG/SFG; B) a reduced negative connectivity between the cerebellum and the PoCG/PreCG; and in addition, C) an increased negative connectivity between the cerebellum and the PHG/FFG/LING/CAL when compared with the healthy control group. In $SAOA_{>10y}$ group, no difference was observed when compared with MSA-C and HC. The significance level was set at FWE corrected $p < 0.01$. *ORBinf, orbital part of inferior frontal gyrus; MFG, middle frontal gyrus; SFG, superior frontal gyrus; PoCG, postcentral gyrus; PreCG, precentral gyrus; PHG, parahippocampal gyrus; FFG, fusiform gyrus; LING, lingual gyrus; CAL, calcarine gyrus.*

For module 3, reduced positive connectivity with the superior frontal gyrus was found in the MSA-C group compared to the HC group. The negative correlation was also reduced for the precentral gyrus, while the negative connectivity of module 3 with the calcarine gyrus was increased in the MSA-C group (Figure 19 and Table 8). For the $SAOA_{>10y}$ group, no group difference was observed with neither the MSA-C nor the HC group.

Post hoc results in MSA-C		Cluster size	MNI coordinates [mm] of peak voxel			T-value	Side	Anatomical regions
			x	y	z			
Module 1	**reduced positivity**	243	39	42	-9	5.42	L	ORBinf
		923	-18	45	27	5.15	R	MFG
		208	33	15	39	6.23	L	MFG
	reduced negativity	109	-48	-21	63	4.16	R	PoCG
	increased negativity	460	30	-48	-15	5.35	L	FFA
		296	-27	-48	-6	4.89	R	LING
		71	-30	-21	-21	4.71	R	pPHG
Module3	**reduced postivity**	1620	9	24	69	6.30	L	SFG
	reduced negativity	108	-45	-18	66	4.33	R	PreCG
	increased negativity	66	-15	-75	15	4.55	R	CAL

Table 8. Post hoc analysis showing altered cerebra-cerebellar functional connectivity in the MSA-C group. For the activity in the cerebellar module 1 and module 3, reduced positive connectivity to frontal gyrus and reduce negative connectivity to the precentral and postcentral gyrus, together with increased negative connectivity to occipto-temporal gyrus was found in the MSA-C group when compared with HC. Results were reported applied FWE corrected $p < 0.01$. *ORBinf, orbital part of inferior frontal gyrus; MFG, middle frontal gyrus; SFG, superior frontal gyrus; PoCG, postcentral gyrus; PreCG, precentral gyrus; PHG, parahippocampal gyrus; FFG, fusiform gyrus; LING, lingual gyrus; CAL, calcarine gyrus; L, left; R, right.*

Relationships between ccFC and clinical variables

The correlations between altered cerebellar-cerebral functional connectivity and clinical variables were estimated in the MSA-C group and the SAOA>10y group. However, no significant correlation was observed (Table 11).

		$SAOA_{>10y}$ group			MSA-C group		
		SARA	Duration	Age of onset	SARA	Duration	Age of onset
Module 1	ORBinf	-0.14 (0.72)	-0.15 (0.69)	0.15 (0.70)	-0.08 (0.80)	-0.17 (0.58)	0.03 (0.92)
	MFG	-0.28 (0.47)	-0.38 (0.31)	0.40 (0.28)	0.18 (0.57)	-0.02 (0.94)	0.19 (0.54)
	MFG	-0.51 (0.16)	0.03 (0.95)	-0.09 (0.82)	-0.11 (0.72)	-0.27 (0.39)	0.37 (0.21)
	PoCG	0.66 (0.06)	-0.01 (0.98)	0.04 (0.92)	0.08 (0.81)	0.17 (0.60)	-0.09 (0.76)
	FFG	0.48 (0.19)	-0.42 (0.27)	0.40 (0.28)	0.10 (0.75)	-0.02 (0.94)	-0.15 (0.62)
	LING	0.66 (0.06)	-0.06 (0.87)	0.06 (0.87)	0.25 (0.44)	0.17 (0.58)	-0.26 (0.38)
	PHG	0.24 (0.53)	0.17 (0.66)	-0.16 (0.68)	0.26 (0.41)	0.23 (0.46)	-0.20 (0.50)
Module 3	SFG	-0.37 (0.33)	-0.66 (0.06)	0.66 (0.06)	0.06 (0.85)	0.10 (0.76)	-0.20 (0.50)
	PreCG	0.46 (0.22)	0.05 (0.89)	-0.03 (0.92)	0.22 (0.50)	0.26 (0.42)	-0.28 (0.35)
	CAL	0.49 (0.17)	0.37 (0.33)	-0.32 (0.40)	-0.35 (0.26)	-0.38 (0.22)	-0.28 (0.35)

Table 9. Summary for the relationship between ccFC and clinical variables in ataxia groups. Data are displayed as correlation coefficients (original p value). Statistically, none of ccFC showed significantly correlated with clinical variables in the SAOA>10y group, and in MSA-C group. *ORBinf, orbital part of inferior frontal gyrus; MFG, middle frontal gyrus; SFG, superior frontal gyrus; PoCG, postcentral gyrus; PreCG, precentral gyrus; PHG, parahippocampal gyrus; FFG, fusiform gyrus; LING, lingual gyrus; CAL, calcarine gyrus.*

3.4.4 Discussion

In this study, the functional connectivity between the cerebellar network modules and the supratentorial cerebrum was analyzed and compared between the HC and the two ataxia patient groups. The main findings were as follows: 1) the activity of cerebellar modules was negatively correlated to the postcentral and precentral gyrus in all three groups; 2) compared with the HC group, a significantly altered cerebellar-cerebral functional connectivity pattern was found in the MSA-C but not in the $SAOA_{>10y}$ groups; 3) the observed connectivity changes were not related to clinical measures in the MSA-C group.

The functional cerebellum can be clustered into three different network modules (see Study 3, page 57). This partition largely represents the functional division of the cerebellum into the motor, cognitive and limbic cerebellum, as suggested by previous

reviews (Samson & Claassen, 2017; Stoodley & Schmahmann, 2010). The present analysis of cerebellar-cerebral connectivity revealed that, even though the modules represent distinct brain functions, they project on highly overlapping brain regions. All three cerebellar modules presented consistent positive correlation to the thalamus in the HC group. This point towards a common communication path for information from and to the cerebellum, a central hub in the brain through which all information has to be passed in order to be processed. It is not surprising that the structure identified as the central hub is the thalamus. Of course, this information is not new. The central role of the thalamus is to serve as gateway to consciousness. All incoming information is preprocessed in the thalamus before it is transferred to the cortex. So, our finding fits well with current knowledge about the overall organization of the cortex; however, it should be noted that these results, even if already known, are derived using complex mathematical procedures (like the module construction), without any anatomical or functional assumptions. The results also agree well with the findings of Sang and colleagues (Sang *et al*, 2012), who reported that most cerebellar subregions are positively correlated with the thalamus. The authors argued that this finding may indicate a free and accessible information exchange between the cerebellum and thalamus. Further evidences of the tight anatomical connection between the thalamus and the cerebellum has also been reported in previous DTI studies (Granziera *et al*, 2009; Habas & Cabanis, 2007; Wakana *et al*, 2004), suggesting that our results have a direct structural basis. In the present study, the activity of the thalamus has lost convergence with the activity of the cerebellum in the ataxia groups. To date, the functional cerebellar-thalamus-cerebral circuit has rarely been a ROI in the study of ataxia patients. Further research is needed to explore how ataxia disease interrupts interconnectivity in the cerebellar-thalamus circuit.

So far, only the positive correlations have been discussed. However, negative correlations also were observed in the analysis of cerebellar-cerebral connectivity. In general, negative correlations are more complex than positive correlations. Most previous studies paid no attention to negative functional connectivity in describing the cerebellar-cerebral connectivity pattern. Some authors argue that the nature of negativity is too complex and remains uninterpretable (Buckner *et al.*, 2011; Ren *et al*, 2019). This point of view goes back to the debate about whether the anti-correlation observed in the resting fMRI is artificial or meaningful. It has been argued that the negativity is likely introduced by global

signal regression (Murphy *et al*, 2009). However, Chai and colleagues found that anti-correlations are still present when the resting-state fMRI data are processed without global signal regression (Chai *et al*, 2012). This being so, the negative functional connectivity is not artificially caused by any scaling or regression effect, being frequently observed in long-range connections (Fox *et al*, 2009). This agrees well with the observations presented here. A negative correlation was found between the sensory-motor cortex and all three cerebellar modules. Moreover, the precentral and postcentral gyri appear to be the convergence regions negatively connected to all three cerebellar modules. Some studies have tried to point out the biological basis underlying the anti-correlation (Fox *et al.*, 2009; Liu *et al*, 2015). Fox reported anti-correlations between task-negative regions (e.g. default mode network) and task-positive regions (e.g. dorsolateral prefrontal cortex) and interpreted the finding as evidence that these anti-correlated regions may serve opposite goals or computing representations (Fox *et al.*, 2005). However, the anti-correlations may also indicate that integrative regions are orchestrating different regions to process together. There seems to be a relation between the correlation strength and functional output, at least in the cognitive domain. Murphy and colleagues showed that the strength of anti-correlations between task-negative and task-positive regions related to cognitive task performance. Better task performance was associated with stronger anti-correlations (Kelly *et al*, 2008). Similar results were reported by Hampson et al. (2010), the strength of the anticorrelations being correlated positively with working memory performance. The authors' interpretation was that the anti-correlation may serve as an integrative hub for combined processing (Hampson *et al*, 2010; Hampson *et al*, 2006). Following their line of argumentation, the negative connectivity between the cerebellum and the motor cortex could be interpreted as evidence of the interaction between the cerebellum and the sensorimotor cortex to ensure appropriate motor functions.

Although the cerebellar modules keep their modularity within the cerebellum, the long-distance connections with the supratentorial regions are altered in the ataxia groups. In this study, significant reduced negativity in MSA-C compared to the HC group was demonstrated. The connections (strength) between the anterior cerebellum (module 1) and primary somatosensory cortex (S1), as well as the correlation between the posterior cerebellum (module 3) and the primary motor cortex (M1), were significantly reduced in the MSA-C group. Because the cerebellum receives convergent inputs from the

somatosensory cortex (S1) and issues the output mainly to the motor cortex (M1) (Leergaard *et al*, 2006; Luft *et al*, 2005; Petrof *et al*, 2015), a disruption in the circuit could contribute to the motor dysfunction observed in the MSA-C group. However, it should be noted that no quantitative relations with any clinical measures were observed to further confirm this assumption. On the other hand, the observed disconnection was in line with previous MSA-C studies. Zheng and colleague extracted cerebellar regions with decreased regional cerebral blood flow. Although a different MRI modality was used, the data show decreased connectivity of the cerebellum with the postcentral gyrus in the MSA-C group (Zheng *et al.*, 2019). It is assumed that the reduced anti-correlation may reflect a dysfunctional motor system.

Another altered anti-correlation pattern between the anterior cerebellum (module 1) and occipito-temporal cortex (OTC), and between the posterior cerebellum (module 3) and calcarine sulcus, was found in the MSA-C group compared with HC group. As is commonly known, the visual cortex and the cerebellum act jointly as a visual-motor system guiding whole-body movements (Calvo-Merino *et al*, 2006; Clarke & Tyler, 2015; Glickstein, 2000). The increased connectivity found here may be interpreted as a compensatory mechanism, that is, that MSA-C patients may need more visual control to compensate for deficits in proprioceptive sensory-motor loops, in order to maintain their impaired motor abilities. Moreover, functional changes in the cerebellar-visual cortex circuit have been frequently reported in other types of ataxia. For example, Hernandez-Castillo and colleagues peformed a whol-brain functional connectivity analysis and reported increased connectivity between the cerebellun and visual areas (including lingual gyrus, inferior/middle occipital gyrus) in spinocerebellar ataxia type 7 (SCA7) patients (Hernandez-Castillo *et al*, 2013). They interpreted this disruption as a compensatory mechanism, suggesting it may related to cognitive deficits in SCA7 patients. Nevertheless, the disruption did not show any significant correlation with clinical variables, a matter that deserves further investigation.

In addition, we found the hint of a functional disconnection between the cerebellum and the frontal gyrus in the MSA-C group. This may accord well with the cognitive deficits involving executive functions and verbal learning reported in MSA-C patients (Burk *et al.*, 2006; Chang *et al.*, 2009). Previous studies have pointed out that a processing loop exists.

The cerebellar cortex receives cognitive information processed from the frontal cortex and projects back responses to corresponding frontal cortex (Leiner *et al*, 1989; Schmahmann, 1996). Recent fMRI studies have provided further evidence for the existence of this loop. It has been demonstrated that lobules IV, VI, VIII and crus I-II are functionally connected to the prefrontal cortex (Buckner *et al.*, 2011; Krienen & Buckner, 2009). It is also worth noting that local atrophy in both regions, i.e. the cerebellum and the frontal cortex, has already been described in regard to MSA-C in previous studies (Chang *et al.*, 2009; Ciolli *et al.*, 2014; Gilman *et al.*, 2008). In addition, abnormal functional connectivity within frontal subregions and reduced connectivity between the cerebellum and the frontal regions in MSA-C have been reported frequently (Franciotti *et al*, 2015; Rosskopf *et al.*, 2018; You *et al.*, 2011; Zheng *et al.*, 2019). Although the findings in the present study fits well with other studies, and it appears to be indisputable that a distorted cerebellar–frontal circuit contributes to the cognitive impairment in MSA-C, no significant association between altered connectivity and clinical variables has been proven.

It should be noted that an altered cerebellar-cerebral functional connectivity pattern was not observed in the $SAOA_{>10y}$ group. This finding might be in line with the stable functional connectivity pattern within the cerebellum and in cerebellar-cerebral circuits reported earlier (**chapter 3.2 and chapter 3.3**), however, comparing $SAOA_{>10y}$ and MSA-C directly did not yield a significant group difference, suggesting a power problem due to the small sample size of the SAOA group.

An additional limitation of the present study is the relatively small sample size of patients, as we discussed in previous chapters. Furthermore, a lack of detailed cognitive characterization of ataxia patients limits the interpretation of the functional disruption. Finally, integration between the functional connectivity with cerebellar and extra-cerebellar volume should be further considered, since the absence of structure may depend largely on the construction of functional connectivity, especially in the ataxia groups.

4. General discussion

4.1 Aims and main findings

This study systematically investigated the structural and functional characterization of the cerebellum in two sporadic ataxia groups, the MSA-C group and the $SAOA_{>10y}$ group. The aim of this thesis was to characterize a meaningful picture of the cerebellum and try to discover whether neuroimaging measurements are capable of distinguishing between MSA-C group and $SAOA_{>10y}$ group.

The first study was to examine the structural changes of the cerebellum in two ataxia groups in more detail (**chapter 3.1**). In this study, abnormal gray matter volume was found mainly in bilateral I-IV, V, VI, right crus I-II-VIIb-VIIIa-IX in both ataxia groups, with additional atrophy in vermis VIIIa-VIIIb-IX in $SAOA_{>10y}$ group only. The atrophy was observed in regions that are known to be involved in motor and somatosensory processing (Samson & Claassen, 2017; Stoodley & Schmahmann, 2009; Stoodley *et al.*, 2012). The spatial distribution of the atrophy was in line with previous studies (Abele *et al.*, 2007; Burk *et al.*, 2004; Faber *et al.*, 2020) and corresponded well with the clinical presentation of both ataxia types (Gilman *et al.*, 2008; Klockgether, 2018). However, it was found the structural changes did not correlate with clinical variables. One possible reason may be the small sample size, which seriously limited the power.

The follow-up region of interest study, based on **study 1** (**chapter 3.1**), was designed to analyze the way in which local atrophy impacts intracerebellar functional connectivity (**chapter 3.2**). ALFF and DC were analyzed to investigate if functional connectivity is altered in the atrophic cerebellum in the two sporadic ataxia phenotypes. An intact functional cerebellum pattern in the MSA-C group and SAOA group was revealed in the study, indicating relatively normal neural activity and network integration, despite the structural damage. A further avenue to explore was whether the cerebellar architecture has the ability to functionally compensate for structural changes, using bootstrapping to compare the functional connectivity between structurally atrophic and non-atrophic parts. It was clear that the structurally atrophic regions had higher functional connectivity than the rest of the cerebellum. It could be assumed that the structurally atrophic regions with higher DC values have more responsibility for balancing the function (Liang *et al.*, 2013;

Zuo *et al.*, 2012), and higher ALFF values with more energy, enabling more flexibility (Biswal *et al.*, 1995). This analysis holds true for the MSA-C group and the $SAOA_{>10y}$ group, indicating these two subtype ataxias may have a shared mechanism for regulating function to operate the atrophic cerebellum. Further longitudinal studies are worth conducting to investigate the dynamic functional connectivity of overall cerebellum to better understand the compensatory mechanisms.

In the third study, a further step was taken to look at global and regional functional features of the overall cerebellum in the three groups under investigation (**chapter 3.3**). To the knowledge, this is the first study to investigate the global and regional properties of the cerebellar network in two ataxia groups, using the graph theory. In the study, small-world topology was first found in the cerebellar functional networks, indicating a well-organized system in the cerebellum to maximize the efficiency and minimize the costs, which has been reported in the human brain before (Bassett & Bullmore, 2006; Liao *et al*, 2017; Sporns, 2018). It is noteworthy that the cerebellar small-world features was also observed in the two ataxia group. In the data, there were no significant differences among groups in all global and nodal parameters, suggesting that the cerebellum supports an optimal balance between global integration and local specialization, creating a condition that confers resilience against pathological attacks (Achard *et al*, 2006; Sporns, 2013). We also found a consistent modularity in the two sporadic ataxia groups as well as in the control group, which resembles the partition of the cerebellum into three different modules.

As mentioned before, three cerebellar modules were defined and **study 4** explored how these modules contribute to the cerebellar-cerebral functional connectivity (ccFC) maps (**chapter 3.4**). The intrinsic connectivity in the cerebellar-cerebral circuit was assessed by taking every cerebellar modular as a ROI to corelate with cerebral regions in a voxel-wise manner. It was interesting that the three cerebellar modules displayed highly overlapping ccFC maps in the healthy group. For example, all three cerebellar modules presented consistent positive connectivity to the thalamus, which agrees well with the findings of Sang and colleagues that most of the cerebellar subregions are positively correlated with the thalamus (Sang *et al.*, 2012). In this condition, the connectivity patterns between the cerebellum and the cerebrum were altered in the MSA-C group but not in the $SAOA_{>10y}$ group. The disconnection of the cerebellum from the motor cortex and the frontal cortex

were consistent with a previous study of MSA-C patients (Zheng *et al.*, 2019), however, the increased connectivity between the cerebellum and the visual cortex in the study was contrary to the findings of previous studies (Ren *et al.*, 2018; Zheng *et al.*, 2019). Further studies with more sample size are required. Interestingly, altered cerebellar-cerebral functional connectivity pattern was not observed in the $SAOA_{>10y}$ group in comparison with the HC group, although $SAOA_{>10y}$ patients typically present with ataxia deficit (Giordano *et al.*, 2017; Klockgether, 2018). This finding is in line with the our previous chapters (**Chapter 3.2** and **Chapter 3.3**) depicting a stable functional connectivity pattern, not only within the cerebellum but also in cerebellar-cerebral circuits in $SAOA_{>10y}$ patients. Comparing $SAOA_{>10y}$ group and MSA-C group also did not yield a significant group difference in the cerebellar-cerebral functional connectivity pattern. The reason could be the small sample size of the SAOA group and the fact that there was no clear disease severity assessment between the two ataxia groups.

4.2 Limitations and future perspectives

A relevant limitation of this study is the small sample size, which limits the statistical power and reproducibility of the results. Although the date of the SPORTAX cohort did provide a detailed quantitative account of the clinical phenotype and natural history of sporadic ataxias with adult onset. However, considering the early stage of the project, the sample number collected in the study is largely limited. Perhaps partly for this reason, the study failed to find any significant brain-clinical correlation. Another limitation was the lack of follow-up verification; it is suggested that the decline of gray matter and the structural-functional interaction in this study could be confirmed by more longitudinal assessments.

In this thesis, neuroimaging analyses were applied to study the structural and functional cerebellar characterizations. The technological and methodological details should also be critically considered. From the technological point of view, higher spatial resolution images might allow a more detailed view of cerebellar structure and the responses of cerebellar function (Goense *et al*, 2016), which may increase sensitivity in investigating the SAOA group. From the methodological view, a common consideration related to the functional MRI studies is the motion correction (Friston *et al.*, 1996). In this thesis, the frame displacement did not differed among three groups and the motion parameters had already been added to regress out motion-related signal. Moreover, the studies described in this

thesis are based on multicenter data and there was a marginal site difference among the three group. Although the site information was added as covariate to be regressed out from the statistical models, the homogeneity between the centers and the relationship between the quality of the images and the site distribution constitute a further limitation of the study.

4.3 Conclusion

The objective of this thesis was to assess the involvement of the structural and functional cerebellum in sporadic ataxia groups. A structurally atrophic cerebellum and a functionally conserved cerebellum was found in the MSA-C and $SAOA_{>10y}$ groups. The atrophic cerebellar regions that have been reported in motor and sensorimotor processing, together with findings from previous studies, suggesting that this is a prominent lesion in the two ataxia groups. Moreover, an additional altered cerebellar-cerebral circuit, which mainly affected the frontal cortex, visual cortex and motor cortex, was observed in the MSA-C group, but not in the $SAOA_{>10y}$ group. These may lead to the assumption that the severe ataxia symptom in MSA-C could be the consequence of influenced from multiple regions. Further studies are needed to show if these findings are robust and to verify how well they were used to predict the development of patients in SAOA with a disease duration less than 10 years.

5. Abstract

Sporadic ataxia is a group of progressive neurodegenerative diseases that can be subdivided into two groups, sporadic adult onset ataxia (SAOA), and the cerebellar type of multiple system atrophy (MSA-C). In the first years after ataxia onset, a reliable distinction between MSA-C and SAOA is often not possible. In particular, some SAOA conditions may turn to MSA-C, and it is known that the conversion becomes very unlikely when a patient with SAOA has a duration of illness longer than 10 years. In this thesis, MSA-C vs. $SAOA_{>10y}$ (defined as SAOA patients with a disease duration longer than 10 years) were compared in an attempt to identify the essential difference between the two conditions. To this end, 16 patients with MSA-C, 13 patients with $SAOA_{>10y}$ and 49 healthy controls were included in this thesis. **Chapter 1** first introduces the reader to the concept of sporadic ataxias and gives an overview of MSA-C and SAOA. This is followed by a review of the current state of knowledge of how neuroimaging technology aids understanding of sporadic ataxias. **Chapter 2** outlines the gen**e**ral methodologies used for the presented studies. **Chapter 3** contains four study results. In **study 1**, the structural changes of the cerebellum in two ataxia groups were examined to show abnormal gray matter volume in the bilateral anterior part and right posterior part of the cerebellum in both groups and an additional atrophy in vermis cerebellum in the $SAOA_{>10y}$ group. In **study 2**, the intracerebellar functional connectivity affected by local atrophy was investigated in the two sporadic ataxias by the amplitude of low-frequency fluctuation and degree centrality. An intact functional connectivity pattern was observed in the atrophic cerebellum in the MSA-C and SAOA groups, the atrophic cerebellum being characterized by high ALFF and high DC compared with non-atrophic cerebellum. In **study 3**, the topological features of the functional cerebellar network were assessed by graph theory analysis. It was found that a well-organized small-world network organization and intact global and regional properties existed in the functional cerebellar system in the ataxia groups. In **study 4**, the connectivity between different cerebellar parts and cerebral regions was explored, taking every functional cerebellar module as a region of interest. It was observed that the activities of cerebellar modules were positively correlated with the thalamus and negatively connected to the postcentral and precentral gyrus in the healthy group. When compared with the HC group, altered connections between the cerebellum

and the visual cortex, the motor cortex and the frontal cortex were found in the MSA-C but not in the $SAOA_{>10y}$ groups. **Chapter 4** contains a summary discussion of all four studies, as well as discussing the limitations of the current researches and offering an outlook on future research perspectives.

6. List of figures

7. List of tables

8. References

Abele M, Burk K, Schols L, Schwartz S, Besenthal I, Dichgans J, Zuhlke C, Riess O, Klockgether T (2002) The aetiology of sporadic adult-onset ataxia. *Brain* 125: 961-968

Abele M, Minnerop M, Urbach H, Specht K, Klockgether T (2007) Sporadic adult onset ataxia of unknown etiology : a clinical, electrophysiological and imaging study. *J Neurol* 254: 1384-1389

Achard S, Bullmore E (2007) Efficiency and cost of economical brain functional networks. *PLoS Comput Biol* 3: e17

Achard S, Salvador R, Whitcher B, Suckling J, Bullmore E (2006) A resilient, low-frequency, small-world human brain functional network with highly connected association cortical hubs. *J Neurosci* 26: 63-72

Amaro E, Jr., Barker GJ (2006) Study design in fMRI: basic principles. *Brain Cogn* 60: 220-232

Ashburner J (2007) A fast diffeomorphic image registration algorithm. *Neuroimage* 38: 95-113

Ashburner J, Friston KJ (2000) Voxel-based morphometry--the methods. *Neuroimage* 11: 805-821

Ashizawa T, Xia G (2016) Ataxia. *Continuum (Minneap Minn)* 22: 1208-1226

Balas M, Balash Y, Giladi N, Gurevich T (2010) Cognition in multiple system atrophy: neuropsychological profile and interaction with mood. *J Neural Transm (Vienna)* 117: 369-375

Baloh RW, Yee RD, Honrubia V (1986) Late cortical cerebellar atrophy. Clinical and oculographic features. *Brain* 109 (Pt 1): 159-180

Barmack NH (2003) Central vestibular system: vestibular nuclei and posterior cerebellum. *Brain Res Bull* 60: 511-541

Bassett DS, Bullmore E (2006) Small-world brain networks. *Neuroscientist* 12: 512-523

Beh SC, Frohman TC, Frohman EM (2017) Cerebellar Control of Eye Movements. *J Neuroophthalmol* 37: 87-98

Biswal B, Hudetz AG, Yetkin FZ, Haughton VM, Hyde JS (1997) Hypercapnia reversibly suppresses low-frequency fluctuations in the human motor cortex during rest using echo-planar MRI. *J Cereb Blood Flow Metab* 17: 301-308

Biswal B, Yetkin FZ, Haughton VM, Hyde JS (1995) Functional connectivity in the motor cortex of resting human brain using echo-planar MRI. *Magn Reson Med* 34: 537-541

Blain CR, Barker GJ, Jarosz JM, Coyle NA, Landau S, Brown RG, Chaudhuri KR, Simmons A, Jones DK, Williams SC *et al* (2006) Measuring brain stem and cerebellar damage in parkinsonian syndromes using diffusion tensor MRI. *Neurology* 67: 2199-2205

Blondel VD, Guillaume J-L, Lambiotte R, Lefebvre E (2008) Fast unfolding of communities in large networks. *Journal of Statistical Mechanics: Theory and Experiment* 2008

Brusse E, Maat-Kievit JA, van Swieten JC (2007) Diagnosis and management of early- and late-onset cerebellar ataxia. *Clin Genet* 71: 12-24

Buckner RL, Andrews-Hanna JR, Schacter DL (2008) The brain's default network: anatomy, function, and relevance to disease. *Ann N Y Acad Sci* 1124: 1-38

Buckner RL, Krienen FM, Castellanos A, Diaz JC, Yeo BT (2011) The organization of the human cerebellum estimated by intrinsic functional connectivity. *J Neurophysiol* 106: 2322-2345

Buckner RL, Sepulcre J, Talukdar T, Krienen FM, Liu H, Hedden T, Andrews-Hanna JR, Sperling RA, Johnson KA (2009) Cortical hubs revealed by intrinsic functional connectivity: mapping, assessment of stability, and relation to Alzheimer's disease. *J Neurosci* 29: 1860-1873

Bullmore E, Sporns O (2009) Complex brain networks: graph theoretical analysis of structural and functional systems. *Nat Rev Neurosci* 10: 186-198

Bullmore E, Sporns O (2012) The economy of brain network organization. *Nat Rev Neurosci* 13: 336-349

Bullmore ET, Bassett DS (2011) Brain graphs: graphical models of the human brain connectome. *Annu Rev Clin Psychol* 7: 113-140

Burk K, Buhring U, Schulz JB, Zuhlke C, Hellenbroich Y, Dichgans J (2005) Clinical and magnetic resonance imaging characteristics of sporadic cerebellar ataxia. *Arch Neurol* 62: 981-985

Burk K, Daum I, Rub U (2006) Cognitive function in multiple system atrophy of the cerebellar type. *Mov Disord* 21: 772-776

Burk K, Globas C, Wahl T, Buhring U, Dietz K, Zuhlke C, Luft A, Schulz JB, Voigt K, Dichgans J (2004) MRI-based volumetric differentiation of sporadic cerebellar ataxia. *Brain* 127: 175-181

Calvo-Merino B, Grezes J, Glaser DE, Passingham RE, Haggard P (2006) Seeing or doing? Influence of visual and motor familiarity in action observation. *Curr Biol* 16: 1905-1910

Carre G, Dietemann JL, Gebus O, Montaut S, Lagha-Boukbiza O, Wirth T, Kremer S, Namer IJ, Anheim M, Tranchant C (2020) Brain MRI of multiple system atrophy of cerebellar type: a prospective study with implications for diagnosis criteria. *J Neurol*

Chai XJ, Castanon AN, Ongur D, Whitfield-Gabrieli S (2012) Anticorrelations in resting state networks without global signal regression. *Neuroimage* 59: 1420-1428

Chang CC, Chang YY, Chang WN, Lee YC, Wang YL, Lui CC, Huang CW, Liu WL (2009) Cognitive deficits in multiple system atrophy correlate with frontal atrophy and disease duration. *Eur J Neurol* 16: 1144-1150

Chelban V, Bocchetta M, Hassanein S, Haridy NA, Houlden H, Rohrer JD (2019) An update on advances in magnetic resonance imaging of multiple system atrophy. *J Neurol* 266: 1036-1045

Ciolli L, Krismer F, Nicoletti F, Wenning GK (2014) An update on the cerebellar subtype of multiple system atrophy. *Cerebellum Ataxias* 1: 14

Clarke A, Tyler LK (2015) Understanding What We See: How We Derive Meaning From Vision. *Trends Cogn Sci* 19: 677-687

Conturo TE, Lori NF, Cull TS, Akbudak E, Snyder AZ, Shimony JS, McKinstry RC, Burton H, Raichle ME (1999) Tracking neuronal fiber pathways in the living human brain. *Proc Natl Acad Sci U S A* 96: 10422-10427

Dash SK, Stezin A, Takalkar T, George L, Kamble NL, Netravathi M, Yadav R, Kumar KJ, Ingalhalikar M, Saini J *et al* (2019) Abnormalities of white and grey matter in early multiple system atrophy: comparison of parkinsonian and cerebellar variants. *Eur Radiol* 29: 716-724

Della Nave R, Foresti S, Tessa C, Moretti M, Ginestroni A, Gavazzi C, Guerrini L, Salvi F, Piacentini S, Mascalchi M (2004) ADC mapping of neurodegeneration in the brainstem and cerebellum of patients with progressive ataxias. *Neuroimage* 22: 698-705

Diedrichsen J (2006) A spatially unbiased atlas template of the human cerebellum. *Neuroimage* 33: 127-138

Diedrichsen J, Zotow E (2015) Surface-Based Display of Volume-Averaged Cerebellar Imaging Data. *PLoS One* 10: e0133402

Euler L (1741) Solutio problematis ad geometriam situs pertinentis. *Commentarii academiae scientiarum Petropolitanae*: 128-140

Faber J, Giordano I, Jiang X, Kindler C, Spottke A, Acosta-Cabronero J, Nestor PJ, Machts J, Duzel E, Vielhaber S *et al* (2020) Prominent White Matter Involvement in Multiple System Atrophy of Cerebellar Type. *Mov Disord*

Fanciulli A, Wenning GK (2015) Multiple-system atrophy. *N Engl J Med* 372: 249-263

Fogel BL, Perlman S (2006) An approach to the patient with late-onset cerebellar ataxia. *Nat Clin Pract Neurol* 2: 629-635; quiz 621 p following 635

Fornito A, Zalesky A, Breakspear M (2013) Graph analysis of the human connectome: promise, progress, and pitfalls. *Neuroimage* 80: 426-444

Fox MD, Raichle ME (2007) Spontaneous fluctuations in brain activity observed with functional magnetic resonance imaging. *Nat Rev Neurosci* 8: 700-711

Fox MD, Snyder AZ, Vincent JL, Corbetta M, Van Essen DC, Raichle ME (2005) The human brain is intrinsically organized into dynamic, anticorrelated functional networks. *Proc Natl Acad Sci U S A* 102: 9673-9678

Fox MD, Zhang D, Snyder AZ, Raichle ME (2009) The global signal and observed anticorrelated resting state brain networks. *J Neurophysiol* 101: 3270-3283

Franciotti R, Delli Pizzi S, Perfetti B, Tartaro A, Bonanni L, Thomas A, Weis L, Biundo R, Antonini A, Onofrj M (2015) Default mode network links to visual hallucinations: A comparison between Parkinson's disease and multiple system atrophy. *Mov Disord* 30: 1237-1247

Friston KJ (2011) Functional and effective connectivity: a review. *Brain Connect* 1: 13-36

Friston KJ, Williams S, Howard R, Frackowiak RS, Turner R (1996) Movement-related effects in fMRI time-series. *Magn Reson Med* 35: 346-355

Fukui Y, Hishikawa N, Sato K, Nakano Y, Morihara R, Ohta Y, Yamashita T, Abe K (2016) Characteristic diffusion tensor tractography in multiple system atrophy with predominant cerebellar ataxia and cortical cerebellar atrophy. *J Neurol* 263: 61-67

Gebus O, Montaut S, Monga B, Wirth T, Cheraud C, Alves Do Rego C, Zinchenko I, Carre G, Hamdaoui M, Hautecloque G *et al* (2017) Deciphering the causes of sporadic late-onset cerebellar ataxias: a prospective study with implications for diagnostic work. *J Neurol* 264: 1118-1126

Gellersen HM, Guo CC, O'Callaghan C, Tan RH, Sami S, Hornberger M (2017) Cerebellar atrophy in neurodegeneration-a meta-analysis. *J Neurol Neurosurg Psychiatry* 88: 780-788

Gilman S, Wenning GK, Low PA, Brooks DJ, Mathias CJ, Trojanowski JQ, Wood NW, Colosimo C, Durr A, Fowler CJ *et al* (2008) Second consensus statement on the diagnosis of multiple system atrophy. *Neurology* 71: 670-676

Giordano I, Harmuth F, Jacobi H, Paap B, Vielhaber S, Machts J, Schols L, Synofzik M, Sturm M, Tallaksen C *et al* (2017) Clinical and genetic characteristics of sporadic adult-onset degenerative ataxia. *Neurology* 89: 1043-1049

Glickstein M (2000) How are visual areas of the brain connected to motor areas for the sensory guidance of movement? *Trends Neurosci* 23: 613-617

Goense J, Bohraus Y, Logothetis NK (2016) fMRI at High Spatial Resolution: Implications for BOLD-Models. *Front Comput Neurosci* 10: 66

Granziera C, Schmahmann JD, Hadjikhani N, Meyer H, Meuli R, Wedeen V, Krueger G (2009) Diffusion spectrum imaging shows the structural basis of functional cerebellar circuits in the human cerebellum in vivo. *PLoS One* 4: e5101

Grodd W, Hulsmann E, Lotze M, Wildgruber D, Erb M (2001) Sensorimotor mapping of the human cerebellum: fMRI evidence of somatotopic organization. *Hum Brain Mapp* 13: 55-73

Guell X, Schmahmann J (2020) Cerebellar Functional Anatomy: a Didactic Summary Based on Human fMRI Evidence. *Cerebellum* 19: 1-5

Habas C, Cabanis EA (2007) Cortical projection to the human red nucleus: complementary results with probabilistic tractography at 3 T. *Neuroradiology* 49: 777-784

Habas C, Kamdar N, Nguyen D, Prater K, Beckmann CF, Menon V, Greicius MD (2009) Distinct cerebellar contributions to intrinsic connectivity networks. *J Neurosci* 29: 8586-8594

Hampson M, Driesen N, Roth JK, Gore JC, Constable RT (2010) Functional connectivity between task-positive and task-negative brain areas and its relation to working memory performance. *Magn Reson Imaging* 28: 1051-1057

Hampson M, Driesen NR, Skudlarski P, Gore JC, Constable RT (2006) Brain connectivity related to working memory performance. *J Neurosci* 26: 13338-13343

Harding AE (1981) "Idiopathic" late onset cerebellar ataxia. A clinical and genetic study of 36 cases. *J Neurol Sci* 51: 259-271

Harding AE (1983) Classification of the hereditary ataxias and paraplegias. *Lancet* 1: 1151-1155

Hernandez-Castillo CR, Alcauter S, Galvez V, Barrios FA, Yescas P, Ochoa A, Garcia L, Diaz R, Gao W, Fernandez-Ruiz J (2013) Disruption of visual and motor connectivity in spinocerebellar ataxia type 7. *Mov Disord* 28: 1708-1716

Hohenfeld C, Werner CJ, Reetz K (2018) Resting-state connectivity in neurodegenerative disorders: Is there potential for an imaging biomarker? *Neuroimage Clin* 18: 849-870

Iranzo A, Santamaria J, Rye DB, Valldeoriola F, Marti MJ, Munoz E, Vilaseca I, Tolosa E (2005) Characteristics of idiopathic REM sleep behavior disorder and that associated with MSA and PD. *Neurology* 65: 247-252

Ito T, Sakakibara R, Yasuda K, Yamamoto T, Uchiyama T, Liu Z, Yamanishi T, Awa Y, Yamamoto K, Hattori T (2006) Incomplete emptying and urinary retention in multiple-system atrophy: when does it occur and how do we manage it? *Mov Disord* 21: 816-823

Jacobi H, Rakowicz M, Rola R, Fancellu R, Mariotti C, Charles P, Durr A, Kuper M, Timmann D, Linnemann C *et al* (2013) Inventory of Non-Ataxia Signs (INAS): validation of a new clinical assessment instrument. *Cerebellum* 12: 418-428

Jao CW, Soong BW, Huang CW, Duan CA, Wu CC, Wu YT, Wang PS (2019) Diffusion Tensor Magnetic Resonance Imaging for Differentiating Multiple System Atrophy Cerebellar Type and Spinocerebellar Ataxia Type 3. *Brain Sci* 9

Jecmenica-Lukic M, Poewe W, Tolosa E, Wenning GK (2012) Premotor signs and symptoms of multiple system atrophy. *Lancet Neurol* 11: 361-368

Jessen F, Spottke A, Boecker H, Brosseron F, Buerger K, Catak C, Fliessbach K, Franke C, Fuentes M, Heneka MT *et al* (2018) Design and first baseline data of the DZNE multicenter observational study on predementia Alzheimer's disease (DELCODE). *Alzheimers Res Ther* 10: 15

Jiang X, Faber J, Giordano I, Machts J, Kindler C, Dudesek A, Speck O, Kamm C, Duzel E, Jessen F *et al* (2019) Characterization of Cerebellar Atrophy and Resting State Functional Connectivity Patterns in Sporadic Adult-Onset Ataxia of Unknown Etiology (SAOA). *Cerebellum* 18: 873-881

Johnson RW (2001) An Introduction to the Bootstrap.

Kawai Y, Suenaga M, Takeda A, Ito M, Watanabe H, Tanaka F, Kato K, Fukatsu H, Naganawa S, Kato T *et al* (2008) Cognitive impairments in multiple system atrophy: MSA-C vs MSA-P. *Neurology* 70: 1390-1396

Kelly AM, Uddin LQ, Biswal BB, Castellanos FX, Milham MP (2008) Competition between functional brain networks mediates behavioral variability. *Neuroimage* 39: 527-537

Kheradmand A, Zee DS (2011) Cerebellum and ocular motor control. *Front Neurol* 2: 53

Kirchhof K, Apostolidis AN, Mathias CJ, Fowler CJ (2003) Erectile and urinary dysfunction may be the presenting features in patients with multiple system atrophy: a retrospective study. *Int J Impot Res* 15: 293-298

Kitayama M, Wada-Isoe K, Irizawa Y, Nakashima K (2009) Assessment of dementia in patients with multiple system atrophy. *Eur J Neurol* 16: 589-594

Klein AP, Ulmer JL, Quinet SA, Mathews V, Mark LP (2016) Nonmotor Functions of the Cerebellum: An Introduction. *AJNR Am J Neuroradiol* 37: 1005-1009

Klockgether T (2008) The clinical diagnosis of autosomal dominant spinocerebellar ataxias. *Cerebellum* 7: 101-105

Klockgether T (2010) Sporadic ataxia with adult onset: classification and diagnostic criteria. *Lancet Neurol* 9: 94-104

Klockgether T (2012) Sporadic adult-onset ataxia of unknown etiology. *Handb Clin Neurol* 103: 253-262

Klockgether T (2018) Sporadic adult-onset ataxia. *Handb Clin Neurol* 155: 217-225

Klockgether T, Schroth G, Diener HC, Dichgans J (1990) Idiopathic cerebellar ataxia of late onset: natural history and MRI morphology. *J Neurol Neurosurg Psychiatry* 53: 297-305

Koga S, Parks A, Uitti RJ, van Gerpen JA, Cheshire WP, Wszolek ZK, Dickson DW (2017) Profile of cognitive impairment and underlying pathology in multiple system atrophy. *Mov Disord* 32: 405-413

Kollensperger M, Geser F, Ndayisaba JP, Boesch S, Seppi K, Ostergaard K, Dupont E, Cardozo A, Tolosa E, Abele M *et al* (2010) Presentation, diagnosis, and management of multiple system atrophy in Europe: final analysis of the European multiple system atrophy registry. *Mov Disord* 25: 2604-2612

Krienen FM, Buckner RL (2009) Segregated fronto-cerebellar circuits revealed by intrinsic functional connectivity. *Cereb Cortex* 19: 2485-2497

Krismer F, Wenning GK (2017) Multiple system atrophy: insights into a rare and debilitating movement disorder. *Nat Rev Neurol* 13: 232-243

Latora V, Marchiori M (2001) Efficient behavior of small-world networks. *Phys Rev Lett* 87: 198701

Le Bihan D, Mangin JF, Poupon C, Clark CA, Pappata S, Molko N, Chabriat H (2001) Diffusion tensor imaging: concepts and applications. *J Magn Reson Imaging* 13: 534-546

Leergaard TB, Lillehaug S, De Schutter E, Bower JM, Bjaalie JG (2006) Topographical organization of pathways from somatosensory cortex through the pontine nuclei to tactile regions of the rat cerebellar hemispheres. *Eur J Neurosci* 24: 2801-2812

Leiner HC, Leiner AL, Dow RS (1989) Reappraising the cerebellum: what does the hindbrain contribute to the forebrain? *Behav Neurosci* 103: 998-1008

Leone M, Bottacchi E, D'Alessandro G, Kustermann S (1995) Hereditary ataxias and paraplegias in Valle d'Aosta, Italy: a study of prevalence and disability. *Acta Neurol Scand* 91: 183-187

Liang X, Zou Q, He Y, Yang Y (2013) Coupling of functional connectivity and regional cerebral blood flow reveals a physiological basis for network hubs of the human brain. *Proc Natl Acad Sci U S A* 110: 1929-1934

Liao X, Vasilakos AV, He Y (2017) Small-world human brain networks: Perspectives and challenges. *Neurosci Biobehav Rev* 77: 286-300

Lin DJ, Hermann KL, Schmahmann JD (2016) The Diagnosis and Natural History of Multiple System Atrophy, Cerebellar Type. *Cerebellum* 15: 663-679

Liu TT, Brown GG (2007) Measurement of cerebral perfusion with arterial spin labeling: Part 1. Methods. *J Int Neuropsychol Soc* 13: 517-525

Liu Y, Huang L, Li M, Zhou Z, Hu D (2015) Anticorrelated networks in resting-state fMRI-BOLD data. *Biomed Mater Eng* 26 Suppl 1: S1201-1211

Luft AR, Manto MU, Ben Taib NO (2005) Modulation of motor cortex excitability by sustained peripheral stimulation: the interaction between the motor cortex and the cerebellum. *Cerebellum* 4: 90-96

Maslov S, Sneppen K (2002) Specificity and stability in topology of protein networks. *Science* 296: 910-913

McEwen BS (1997) Possible mechanisms for atrophy of the human hippocampus. *Mol Psychiatry* 2: 255-262

Minnerop M, Specht K, Ruhlmann J, Schimke N, Abele M, Weyer A, Wullner U, Klockgether T (2007) Voxel-based morphometry and voxel-based relaxometry in multiple system atrophy-a comparison between clinical subtypes and correlations with clinical parameters. *Neuroimage* 36: 1086-1095

Morton SM, Bastian AJ (2004) Cerebellar control of balance and locomotion. *Neuroscientist* 10: 247-259

Mottolese C, Richard N, Harquel S, Szathmari A, Sirigu A, Desmurget M (2013) Mapping motor representations in the human cerebellum. *Brain* 136: 330-342

Murphy K, Birn RM, Handwerker DA, Jones TB, Bandettini PA (2009) The impact of global signal regression on resting state correlations: are anti-correlated networks introduced? *Neuroimage* 44: 893-905

Muzaimi MB, Thomas J, Palmer-Smith S, Rosser L, Harper PS, Wiles CM, Ravine D, Robertson NP (2004) Population based study of late onset cerebellar ataxia in south east Wales. *J Neurol Neurosurg Psychiatry* 75: 1129-1134

Newman ME, Girvan M (2004) Finding and evaluating community structure in networks. *Phys Rev E Stat Nonlin Soft Matter Phys* 69: 026113

Nicoletti G, Rizzo G, Barbagallo G, Tonon C, Condino F, Manners D, Messina D, Testa C, Arabia G, Gambardella A *et al* (2013) Diffusivity of cerebellar hemispheres enables discrimination of cerebellar or parkinsonian multiple system atrophy from progressive supranuclear palsy-Richardson syndrome and Parkinson disease. *Radiology* 267: 843-850

Nir TM, Jahanshad N, Toga AW, Bernstein MA, Jack CR, Jr., Weiner MW, Thompson PM, Alzheimer's Disease Neuroimaging I (2015) Connectivity network measures predict volumetric atrophy in mild cognitive impairment. *Neurobiol Aging* 36 Suppl 1: S113-120

Ogawa S, Lee TM, Kay AR, Tank DW (1990) Brain magnetic resonance imaging with contrast dependent on blood oxygenation. *Proc Natl Acad Sci U S A* 87: 9868-9872

Park HJ, Friston K (2013) Structural and functional brain networks: from connections to cognition. *Science* 342: 1238411

Petrof I, Viaene AN, Sherman SM (2015) Properties of the primary somatosensory cortex projection to the primary motor cortex in the mouse. *J Neurophysiol* 113: 2400-2407

Polo JM, Calleja J, Combarros O, Berciano J (1991) Hereditary ataxias and paraplegias in Cantabria, Spain. An epidemiological and clinical study. *Brain* 114 (Pt 2): 855-866

Power JD, Barnes KA, Snyder AZ, Schlaggar BL, Petersen SE (2012) Spurious but systematic correlations in functional connectivity MRI networks arise from subject motion. *Neuroimage* 59: 2142-2154

Quinn N (1989) Multiple system atrophy--the nature of the beast. *J Neurol Neurosurg Psychiatry* Suppl: 78-89

Raichle ME, MacLeod AM, Snyder AZ, Powers WJ, Gusnard DA, Shulman GL (2001) A default mode of brain function. *Proc Natl Acad Sci U S A* 98: 676-682

Reetz K, Dogan I, Rolfs A, Binkofski F, Schulz JB, Laird AR, Fox PT, Eickhoff SB (2012) Investigating function and connectivity of morphometric findings--exemplified on cerebellar atrophy in spinocerebellar ataxia 17 (SCA17). *Neuroimage* 62: 1354-1366

Ren S, Zhang H, Zheng W, Liu M, Gao F, Wang Z, Chen Z (2018) Altered Functional Connectivity of Cerebello-Cortical Circuit in Multiple System Atrophy (Cerebellar-Type). *Front Neurosci* 12: 996

Ren Y, Guo L, Guo CC (2019) A connectivity-based parcellation improved functional representation of the human cerebellum. *Sci Rep* 9: 9115

Roncevic D, Palma JA, Martinez J, Goulding N, Norcliffe-Kaufmann L, Kaufmann H (2014) Cerebellar and parkinsonian phenotypes in multiple system atrophy: similarities, differences and survival. *J Neural Transm (Vienna)* 121: 507-512

Rosskopf J, Gorges M, Muller HP, Pinkhardt EH, Ludolph AC, Kassubek J (2018) Hyperconnective and hypoconnective cortical and subcortical functional networks in multiple system atrophy. *Parkinsonism Relat Disord* 49: 75-80

Samson M, Claassen DO (2017) Neurodegeneration and the Cerebellum. *Neurodegener Dis* 17: 155-165

Sang L, Qin W, Liu Y, Han W, Zhang Y, Jiang T, Yu C (2012) Resting-state functional connectivity of the vermal and hemispheric subregions of the cerebellum with both the cerebral cortical networks and subcortical structures. *Neuroimage* 61: 1213-1225

Scharmuller W, Ille R, Schienle A (2013) Cerebellar contribution to anger recognition deficits in Huntington's disease. *Cerebellum* 12: 819-825

Schmahmann JD (1996) From movement to thought: anatomic substrates of the cerebellar contribution to cognitive processing. *Hum Brain Mapp* 4: 174-198

Schmahmann JD (2004) Disorders of the cerebellum: ataxia, dysmetria of thought, and the cerebellar cognitive affective syndrome. *J Neuropsychiatry Clin Neurosci* 16: 367-378

Schmitz-Hubsch T, du Montcel ST, Baliko L, Berciano J, Boesch S, Depondt C, Giunti P, Globas C, Infante J, Kang JS *et al* (2006) Scale for the assessment and rating of ataxia: development of a new clinical scale. *Neurology* 66: 1717-1720

Schols L, Bauer P, Schmidt T, Schulte T, Riess O (2004) Autosomal dominant cerebellar ataxias: clinical features, genetics, and pathogenesis. *Lancet Neurol* 3: 291-304

Shah A, Prasad S, Rastogi B, Dash S, Saini J, Pal PK, Ingalhalikar M (2019) Altered structural connectivity of the motor subnetwork in multiple system atrophy with cerebellar features. *Eur Radiol* 29: 2783-2791

Sheng C, Xia M, Yu H, Huang Y, Lu Y, Liu F, He Y, Han Y (2017) Abnormal global functional network connectivity and its relationship to medial temporal atrophy in patients with amnestic mild cognitive impairment. *PLoS One* 12: e0179823

Shiga K, Yamada K, Yoshikawa K, Mizuno T, Nishimura T, Nakagawa M (2005) Local tissue anisotropy decreases in cerebellopetal fibers and pyramidal tract in multiple system atrophy. *J Neurol* 252: 589-596

Shin H, Lee DK, Lee JM, Huh YE, Youn J, Louis ED, Cho JW (2016) Atrophy of the Cerebellar Vermis in Essential Tremor: Segmental Volumetric MRI Analysis. *Cerebellum* 15: 174-181

Siri C, Duerr S, Canesi M, Delazer M, Esselink R, Bloem BR, Gurevich T, Balas M, Giladi N, Santacruz P *et al* (2013) A cross-sectional multicenter study of cognitive and behavioural features in multiple system atrophy patients of the parkinsonian and cerebellar type. *J Neural Transm (Vienna)* 120: 613-618

Smith SM, Fox PT, Miller KL, Glahn DC, Fox PM, Mackay CE, Filippini N, Watkins KE, Toro R, Laird AR *et al* (2009) Correspondence of the brain's functional architecture during activation and rest. *Proc Natl Acad Sci U S A* 106: 13040-13045

Smith SM, Jenkinson M, Woolrich MW, Beckmann CF, Behrens TE, Johansen-Berg H, Bannister PR, De Luca M, Drobnjak I, Flitney DE *et al* (2004) Advances in functional and structural MR image analysis and implementation as FSL. *Neuroimage* 23 Suppl 1: S208-219

Sporns O (2013) Structure and function of complex brain networks. *Dialogues Clin Neurosci* 15: 247-262

Sporns O (2018) Graph theory methods: applications in brain networks. *Dialogues Clin Neurosci* 20: 111-121

Stoodley CJ, Schmahmann JD (2009) Functional topography in the human cerebellum: a meta-analysis of neuroimaging studies. *Neuroimage* 44: 489-501

Stoodley CJ, Schmahmann JD (2010) Evidence for topographic organization in the cerebellum of motor control versus cognitive and affective processing. *Cortex* 46: 831-844

Stoodley CJ, Valera EM, Schmahmann JD (2012) Functional topography of the cerebellum for motor and cognitive tasks: an fMRI study. *Neuroimage* 59: 1560-1570

Tanabe J, Miller D, Tregellas J, Freedman R, Meyer FG (2002) Comparison of detrending methods for optimal fMRI preprocessing. *Neuroimage* 15: 902-907

Thompson PM, Hayashi KM, de Zubicaray G, Janke AL, Rose SE, Semple J, Herman D, Hong MS, Dittmer SS, Doddrell DM *et al* (2003) Dynamics of gray matter loss in Alzheimer's disease. *J Neurosci* 23: 994-1005

Timmann D, Brandauer B, Hermsdorfer J, Ilg W, Konczak J, Gerwig M, Gizewski ER, Schoch B (2008) Lesion-symptom mapping of the human cerebellum. *Cerebellum* 7: 602-606

Tison F, Wenning GK, Volonte MA, Poewe WR, Henry P, Quinn NP (1996) Pain in multiple system atrophy. *J Neurol* 243: 153-156

Tsuji S, Onodera O, Goto J, Nishizawa M, Study Group on Ataxic D (2008) Sporadic ataxias in Japan--a population-based epidemiological study. *Cerebellum* 7: 189-197

Voets NL, Beckmann CF, Cole DM, Hong S, Bernasconi A, Bernasconi N (2012) Structural substrates for resting network disruption in temporal lobe epilepsy. *Brain* 135: 2350-2357

Wakana S, Jiang H, Nagae-Poetscher LM, van Zijl PC, Mori S (2004) Fiber tract-based atlas of human white matter anatomy. *Radiology* 230: 77-87

Wang J, Wang X, Xia M, Liao X, Evans A, He Y (2015) GRETNA: a graph theoretical network analysis toolbox for imaging connectomics. *Front Hum Neurosci* 9: 386

Wang PS, Wu HM, Lin CP, Soong BW (2011) Use of diffusion tensor imaging to identify similarities and differences between cerebellar and Parkinsonism forms of multiple system atrophy. *Neuroradiology* 53: 471-481

Watanabe H, Saito Y, Terao S, Ando T, Kachi T, Mukai E, Aiba I, Abe Y, Tamakoshi A, Doyu M *et al* (2002) Progression and prognosis in multiple system atrophy: an analysis of 230 Japanese patients. *Brain* 125: 1070-1083

Watts DJ, Strogatz SH (1998) Collective dynamics of 'small-world' networks. *Nature* 393: 440-442

Wenning GK, Ben Shlomo Y, Magalhaes M, Daniel SE, Quinn NP (1994) Clinical features and natural history of multiple system atrophy. An analysis of 100 cases. *Brain* 117 (Pt 4): 835-845

Wenning GK, Colosimo C, Geser F, Poewe W (2004a) Multiple system atrophy. *Lancet Neurol* 3: 93-103

Wenning GK, Tison F, Seppi K, Sampaio C, Diem A, Yekhlef F, Ghorayeb I, Ory F, Galitzky M, Scaravilli T *et al* (2004b) Development and validation of the Unified Multiple System Atrophy Rating Scale (UMSARS). *Mov Disord* 19: 1391-1402

Yang H, Wang N, Luo X, Lv H, Liu H, Li Y, Fan G (2019) Cerebellar atrophy and its contribution to motor and cognitive performance in multiple system atrophy. *Neuroimage Clin* 23: 101891

You H, Wang J, Wang H, Zang YF, Zheng FL, Meng CL, Feng F (2011) Altered regional homogeneity in motor cortices in patients with multiple system atrophy. *Neurosci Lett* 502: 18-23

Zang YF, He Y, Zhu CZ, Cao QJ, Sui MQ, Liang M, Tian LX, Jiang TZ, Wang YF (2007) Altered baseline brain activity in children with ADHD revealed by resting-state functional MRI. *Brain Dev* 29: 83-91

Zanigni S, Evangelisti S, Testa C, Manners DN, Calandra-Buonaura G, Guarino M, Gabellini A, Gramegna LL, Giannini G, Sambati L *et al* (2017) White matter and cortical changes in atypical parkinsonisms: A multimodal quantitative MR study. *Parkinsonism Relat Disord* 39: 44-51

Zeighami Y, Ulla M, Iturria-Medina Y, Dadar M, Zhang Y, Larcher KM, Fonov V, Evans AC, Collins DL, Dagher A (2015) Network structure of brain atrophy in de novo Parkinson's disease. *Elife* 4

Zheng W, Ren S, Zhang H, Liu M, Zhang Q, Chen Z, Wang Z (2019) Spatial Patterns of Decreased Cerebral Blood Flow and Functional Connectivity in Multiple System Atrophy (Cerebellar-Type): A Combined Arterial Spin Labeling Perfusion and Resting State Functional Magnetic Resonance Imaging Study. *Front Neurosci* 13: 777

Zuo XN, Ehmke R, Mennes M, Imperati D, Castellanos FX, Sporns O, Milham MP (2012) Network centrality in the human functional connectome. *Cereb Cortex* 22: 1862-1875

9. Acknowledgements

Four years ago, I was a master student in clinical neuroscience, mainly doing research on psychiatry disease. However, this raised questions in my mind, because structural changes in psychiatric illness are not observable, although various functional changes can be detected by MRI in diseases such as depression or schizophrenia. One day, I noticed that there was a Ph.D. opening in the study of ataxia with sever structural atrophy, which interested me greatly. I contacted Prof. Dr. Lukas Scheef immediately and that's how the story began.

First, I am happy to express my appreciation for my supervisor, Prof. Dr. Lukas Scheef for his continuous support during my whole Ph.D. studies. He made a good impression on me the first time we met, giving me high expectations of our collaboration. During the four years of my studies, his expertise has provided valuable guidance in my research, for example how better to structure a paper and how to organize my work. Sharing his experience with me has encouraged me to work through the difficulties in academic exploration.

I have also been fortunate to have received the help from the members of my thesis committee: Prof. Dr. Thomas Klockgether, Prof. Dr. Henning Boecker and Prof. Dr. Tony Stöcker, particularly their comments on elaborating this thesis and their participation in the previous progress meetings and final examination.

I would also like to express my thanks to DZNE for providing a modern and comfortable place in which to work. I am also grateful to all the colleagues in the clinical research group of DZNE: Shumei, Marcel, Neeraj, Yilmaz, Hweeling and Sichu, with whom I enjoyed a fantastic working atmosphere, helpful discussions, social events and all the fun we shared inside and outside of the X. There is no way to express how much this meant to me.

To my friends in Germany: Xu, Dan and Ran. I am so happy to meet you at this special stage in my life. I cherish all the memories and time spent with you and cannot imagine what life would be without you.

To my best friend, Peijun: you make me want to be a better friend. We have been through a lot, up and down, happy and sad. I feel as if you are by my side, although we separated by thousands of miles.

I wish to thank my boyfriend, Chuyao, for being so supportive when I was working on my thesis, especially this difficult pandemic. You cooked for me when I missed the delicious food, you encouraged me when I felt down, you kept me company when I was alone, you made me feel the lyrics of the song ‘look at the stars, see how they shine for me’. You mean so much to me.

Last but not least, I am deeply grateful to my family for their love and support, especially my mum, for there is no one like her to connect with me, to cheer me up when I am down, to catch me when I am falling, to inspire me when I am upset.

I end with a song by Jonathan Lee, my favorite singer, whose voice got me through many nights. One lyrics may be translated as

‘Ever asking over and over again in the dark;

Only to know leading a leisure and simple life is true;

Looking back, suddenly like a dream;

Looking back, my heart will go on.’

Thank you all.